I. THERMODYNAMIC AND KINETIC BEHAVIOR OF AN ARGON PLASMA JET

II. DECOMPOSITION OF NITRIC OXIDE BETWEEN 1300 - 1750°K IN AN ARGON PLASMA

Thesis by

Satish Vithal Desai

In Partial Fulfillment of the Requirements

For the Degree of

Doctor of Philosophy

California Institute of Technology

Pasadena, California

1969

(Submitted May 8 , 1969)

ACKNOWLEDGMENT

I wish to express my gratitude to Professor W. H. Corcoran whose advice and encouragement has been useful during this work. I also appreciate the support provided for this work by the United States Public Health Service.

I would like to thank Dr. B. S. Malone for his help in the measurement of transition probabilities and to Dr. H. J. Astheimer for his enthusiastic cooperation in the measurement of temperatures and concentrations. My thanks are due to Mr. Erno Daniels for his help in the measurement of velocities and to Mr. Howard Tyler for his help in some experimental work. Thanks are also due to the staff of the chemical engineering shop and the glass-blowing shop for their prompt help in the construction of some apparatus. Thanks go to June Gray for the preparation of the figures in this thesis.

Finally, I appreciate my wife, Miyako, for typing the thesis, and for her help in many ways which I am unable to describe.

ABSTRACT

In the first part of the study, an RF coupled, atmospheric pressure, laminar plasma jet of argon was investigated for thermodynamic equilibrium and some rate processes.

Improved values of transition probabilities for 17 lines of argon I were developed from known values for 7 lines. The effect of inhomogeneity of the source was pointed out.

The temperatures, T, and the electron densities, n_e, were determined spectroscopically from the population densities of the higher excited states assuming the Saha-Boltzmann relationship to be valid for these states. The axial velocities, v_z, were measured by tracing the paths of particles of boron nitride using a three-dimentional mapping technique. The above quantities varied in the following ranges: $10^{12} < n_e < 10^{15}$ particles/cm^3, $3500 < T < 11000°K$, and $200 < v_z < 1200$ cm/sec.

The absence of excitation equilibrium for the lower excitation population including the ground state under certain conditions of T and n_e was established and the departure from equilibrium was examined quantitatively. The ground state was shown to be highly underpopulated for the decaying plasma.

Rates of recombination between electrons and ions were obtained by solving the steady-state equation of continuity for electrons. The observed rates were consistent with a

dissociative-molecular ion mechanism with a steady-state assumption for the molecular ions.

In the second part of the study, decomposition of NO was studied in the plasma at lower temperatures. The mole fractions of NO denoted by x_{NO} were determined gas-chromatographically and varied between $0.0012 < x_{NO} < 0.0055$. The temperatures were measured pyrometrically and varied between $1300 < T < 1750°K$. The observed rates of decomposition were orders of magnitude greater than those obtained by the previous workers under purely thermal reaction conditions. The overall activation energy was about 9 kcal/g mol which was considerably lower than the value under thermal conditions. The effect of excess nitrogen was to reduce the rate of decomposition of NO and to increase the order of the reaction with respect to NO from 1.33 to 1.85. The observed rates were consistent with a chain mechanism in which atomic nitrogen and oxygen act as chain carriers. The increased rates of decomposition and the reduced activation energy in the presence of the plasma could be explained on the basis of the observed large amount of atomic nitrogen which was probably formed as the result of reactions between excited atoms and ions of argon and the molecular nitrogen.

TABLE OF CONTENTS

TABLE OF CONTENTS (contd.)

LIST OF TABLES

LIST OF FIGURES

LIST OF FIGURES (contd.)

LIST OF FIGURES (contd.)

LIST OF FIGURES (contd.)

INTRODUCTION

The plasma jet is a versatile source of energy at very high temperatures, not easily attainable in the laboratory by chemical combustion processes, and as such offers exciting possibilities for studying chemical reactions and transport phenomena at very high temperatures. In addition, the effect of electronically excited species and free electrons on chemical reactions can be readily studied in a plasma jet.

A plasma may be defined in general terms as the ionized state of a gas in which the microscopic neutrality of the electrical charge is retained. The plasma state is characterized by the presence of atoms and molecules in their ground and excited states, ions in their ground and excited states, and free electrons.

When a stream of gas is subjected to a high degree of excitation by some external source such as a radio-frequency discharge, a plasma jet is formed. The plasma generator used in this study was similar to that described by Reed[1, 2]. An RF induction heated plasma was preferred over the arc type, because the RF method avoids the contamination arising from the electrodes and it has a stable operation over a long period. Argon was employed as the plasma gas because it forms plasma easily in the RF apparatus, it has a simple and well-defined atomic spectrum, and it is readily available in high purity.

The basic objective of this study was to investigate chemical reactions in the plasma. Decomposition of nitric oxide was chosen as the model reaction because this reaction is of great interest in the fixation of atmospheric nitrogen, and in the problem of air-pollution due to reactions occurring inside an internal combustion engine. A process for manufacturing nitric acid by fixation of the atmospheric nitrogen by means of an electric discharge was developed as long ago as 1900 A.D.[3]. The later developments in this process are reported by Timmins and Amman[4]. The reactions of compounds of nitrogen and oxygen are also of interest in the problem of re-entry of space vehicles in the terrestrial atmosphere.

It was necessary to make an inquiry into the thermodynamic state of the plasma in order to investigate the role of the plasma in the reaction under study. The term "state" denotes the composition of the various constituents of the plasma and the various equilibrium relationships between them. The scope of this inquiry was limited to the question of excitation equilibrium in a decaying plasma. Information regarding the basic atomic and electronic processes which establish the state of a plasma can be found in excellent references on this subject[5, 6, 7].

The process of decay of a plasma is characterized by the recombination of electrons with ions. It was found that the process of decay of the plasma had an influence on the rate of

decomposition of nitric oxide. Therefore the recombination of electrons with ions in the argon plasma was studied.

To obtain the rates of a reaction in a steady-state-flow system such as the plasma jet, it was necessary to know the velocity distribution in the reactor. A flow visualization technique was developed to obtain the velocity distribution in the plasma jet.

The diagnostic techniques for plasmas are described in references[8, 9]. Spectroscopy provided a powerful diagnostic technique in the determination of the excitation population, which was required in the characterization of the plasma in this study. An important quantity which enables determination of the population densities of the excitation levels from the spectroscopic observations is the Einstein transition probability. It was thought worthwhile to devote some effort to examine the values of the transition probabilities of argon reported in the literature and to improve them for their use in the spectroscopic studies.

A gas-chromatographic technique was developed for the quantitative determination of nitric oxide and nitrogen in the study of decomposition of nitric oxide. The range of temperatures from 1300 to 1750°K chosen for this study was sufficiently low to make the use of such a technique practical.

The sequence of the following material is based on the continuity of presentation rather than the scheme of work.

A number of publications related to the work are reported at the end of this presentation as appendices and they will be referred to frequently. In a few instances, the nomenclature for these appendices may be slightly different from that for the following presentation.

SECTION I

THERMODYNAMIC AND KINETIC BEHAVIOR OF THE ARGON PLASMA JET

1. Experimental Apparatus

A general photographic view of the experimental apparatus is shown in Figure I-1. The basic apparatus was described in a publication which is reproduced in Appendix A-4.

A plasma generated by induction heating with a radio-frequency unit similar to that described by Reed[1, 2] was the source of radiation. The plasma generator consisted of a high-voltage-power supply feeding d.c. power into a tuned-grid oscillator tube, the plate of which was presented with an inductive load by means of 3 turns of water-cooled copper tubing. The RF coil and the plasma-reactor assembly are shown in Figure I-2. The plasma gas which was argon, was introduced at a rate of 2.4 l/min into the inner quartz tube which was 25 mm in diameter, and was tapered to 20 mm diameter at its tip. The inner quartz tube extended right to the upper turn of the RF coil. The cooling gas, which was also argon, was introduced at a rate of 11.9 l/min into the annular gap between the inner quartz tube and a coaxial quartz tube which was 35.5 mm O.D. / 32.5 mm I.D. and 38 cm long. The outer tube extended 22 cm below the bottom turn of the RF coil.

The plasma was initiated by inserting a graphite rod. The electrical power output of the plasma generator could

be monitored by varying the supply voltage by means of a powerstat. The net power output to the plasma gas was calculated as 1.6 kw from the electrical power output under the operating conditions with and without the plasma. The oscillator current and the net power output to the plasma was quite sensitive to the composition of the plasma gas, and impurities as low as 100 ppm were found to affect the operation of the plasma generator (see Appendix A-2).

The flame extended approximately 18 cm below the bottom turn of the RF coil. A white glow was present at the open end of the outer quartz tube, which was spectroscopically analysed to be mainly N_2^+(1 -ve) and N_2(2 +ve) band radiation, possibly arising from the excitation of nitrogen present in the ambient air by the hot argon coming in contact at the open end of the tube.

The radiation from the plasma passed via an optical scanning system composed of seven front-surface mirrors and a quartz-lithium-fluoride achromatic, condensing lens into the spectrophotometric slit. Vertical and horizontal scanning of the plasma jet was achieved by means of moving platforms. The horizontal scanning could be synchronized, so that the intensities could be recorded as a function of lateral position in the plasma jet at a given axial position. The condensing lens had an aperture ratio of f:3.5 and the magnification factor for the image was 0.21.

The spectrophotometer was a 0.5-meter, Ebert-type unit

having a grating with 1180 grooves/mm which gave a dispersion of 16 Å/mm in the first order. Curved slits were used for maximum efficiency. The entrance slit was 60 microns x 1.5mm and the exit slit was 60 microns x 3mm. An RCA type 1P28 photomultiplier tube was used as the detector. The usable wavelength response of the detector was between 3000 - 7000 Å.

In order to increase the signal/noise ratio of the detecting system, a lock-in amplifier was used to amplify the electrical signal from the photomultiplier tube. A lock-in amplifier consists of a tuned-frequency amplifier, followed by a phase-sensitive detector and an RC filter. For further details of the lock-in technique, refer to the manufacturer's manual[10]. The optical signal was chopped at 1000 Hz by means of a mechanical chopper placed in front of the entrance slit of the spectrophotometer. The chopper simultaneously produced a reference signal at 1000 Hz required for the phase-sensitive-detector circuit in the amplifier. The low-pass filtering circuit in the amplifier in effect integrated the signal as the function of time. The noise being symmetric about zero, produced a null signal after integration, while the detector signal grew with time. Thus the signal/noise ratio was considerably improved, permitting detection of weak signals.

A record of the output from the lock-in amplifier was traced on a potentiometric chart recorder having a full-scale sensitivity of 1 mV. The recorder was fitted with an

electronic integrator which allowed a measure of the line intensity to be obtained immediately. A typical trace of the line intensity on the chart of the recorder is shown in Figure I-3. Figure I-4 shows a scan of the spectrum of argon I made by the spectrophotometer, between 3600 - 5700 Å. Some of the stronger and isolated lines of interest are identified. The peaks by no means represent the intensity of the lines, and no correction is made for the spectral response of the setup. The overall spectral response of the setup was obtained by the procedure described in Appendix A-1, and a correction for the spectral response was always applied in the measurement of intensities.

A study of the different spectroscopic methods of measurement of temperatures in the plasma jet required lateral scanning of intensities of two pre-selected spectral lines of argon. The additional equipment used for this purpose is shown in Figure I-5. A 1.5-m spectrograph of the grating type, covering the spectral range of 3700 - 7400 Å and having a dispersion of 15 Å/mm in the first order was used in addition to the wavelength-scanning spectrophotometer. A tilting mirror, as shown in Figure I-5 allowed the image of the plasma jet to be switched between the two instruments. The 1.5-m spectrograph was originally designed for a photographic analysis, and it was provided with a chamber for inserting a photographic film. Using the photographic record of the spectrum of argon as a guide, two narrow slits were cut for

each spectral line in a thin strip of metal which took place of the film holder. The function of the double slit was to make a correction for the continuum emission which was superimposed on the line radiation. The principle of correction for the background radiation was based on the operation of the lock-in amplifier which was sensitive to the time-varying component of the signal only. Essentially, one of the slits allowed the line plus the background radiation to pass, while the adjacent slit of equal dimensions allowed only the background radiation to pass through. The chopper placed between the slits and the detector was so designed that the two signals were 180° out of phase, so that the background radiation produced only a d.c. signal which was filtered out by the a.c. amplifier.

The description of the photographic setup used for the measurement of velocities in the plasma jet can be found in the publication reproduced in Appendix A-6. Figure I-6 shows a schematic diagram of the setup.

2. Transition Probabilities

The measurement of some transition probabilities of argon I constituted the initial part of this work. Two publications which discuss the method of measurement, the experimental apparatus and the results, are reproduced in Appendices A-4 and A-5. Appendix A-5 should be read as a suppliment to Appendix A-4. Table 2 of Appendix A-5 gives

the values of transition probabilities for 18 lines of argon I in the range of 5000 - 6500 Å, determined experimentally. The transition probability of the line at 3834.68 Å reported in Table 1 of Appendix A-4 was improved on the basis of the revised straight-line plot of $\log\frac{I_{nm}\,\lambda_{nm}}{g(n)A_{nm}}$ vs. E(n) shown in Figure 1 of Appendix A-5. The improved value was 5.6×10^{5} sec^{-1}.

A comparison of the transition probabilities reported in Table 1 of Appendix A-5 with those determined by other workers is given in Table I-1. The transition probabilities reported in this study were normalized on the absolute scale discussed and accepted in reference (1) of Appendix A-5.

3. Determination of Temperatures

An excellent review of the methods of temperature measurement in plasmas appears in reference (11). An attempt was made to compare the temperatures measured by the following three spectroscopic techniques.

The first technique was based on the slope of the plot of $\log\frac{I_{nm}\,\lambda_{nm}}{g(n)A_{nm}}$ vs. E(n), and is described in Appendix A-4. This technique will be referred to as the "slope method". The second technique was based on the ratio of two line intensities[12]. The following equation could be obtained by taking the ratio of intensities of two spectral lines, using equation (1) of Appendix A-4:

$$\frac{I_{pr}}{I_{qs}} = \frac{\lambda_{qs} A_{pr} g(p)}{\lambda_{pr} A_{qs} g(q)} e^{-\frac{E(p) - E(q)}{kT}} \qquad (I\text{-}1)$$

The temperature could be obtained from the above equation rearranged in the following form:

$$T = \frac{a}{b + \log \frac{I_{qs}}{I_{pr}}} \qquad (I\text{-}2)$$

where a and b were constants which could be evaluated from the known physical constants associated with the two lines. In the evaluation of the temperatures by this technique, referred to as the "ratio method", two lines of argon I at 4300 Å and 5739 Å were selected on the basis of their isolation from the rest of the spectrum, and their strong emission. The intensities of these two lines were monitored simultaneously by means of two RCA type 6199 photomultiplier tubes attached to the 1.5-m spectrograph as described above. The spectroscopic data related to the two lines are given below:

$\lambda_{pr} = 4300$ A	$\lambda_{qs} = 5739$ A
$A_{pr} = 3.9 \times 10^5 (sec)^{-1}$	$A_{qs} = 10 \times 10^5 (sec)^{-1}$
$g(p) = 5$	$g(q) = 5$
$E(p) = 116999.4 (cm)^{-1}$	$E(q) = 123505.5 (cm)^{-1}$

The intensities measured by the side-on observations

were converted to the radial intensities by the use of Abel-inversion procedure which is described in Appendix A-3. The radial distribution of temperatures in the plasma jet was then calculated in accord with equation (I-2).

The third technique which will be referred to as the "reference-temperature method" was based on the following form of equation (1) of Appendix A-4. The measured intensity of a given line at the required point in the plasma jet was compared with the intensity of the same line at the axis of the plasma jet where the temperature was previously determined by the "slope method". The pertinent equation for calculating the radial distribution of temperatures in the above manner was:

$$\frac{I}{I_{ref}} = \frac{T_{ref}}{T} e^{-\frac{E(n)}{kT}\left(\frac{1}{T} - \frac{1}{T_{ref}}\right)} \qquad (I-3)$$

The temperatures evaluated separately for the two lines mentioned above, agreed within 20°K at a given point. An average of the two values was taken at each point.

Figure I-7 gives a comparison between the radial distributions of temperatures obtained by the slope method, ratio method and the reference-temperature method, for a plane which was 4.7 cm below the leading edge of the RF coil.

In the cooler portion of the plasma, where the degree of excitation was low, a pyrometric technique based on

equation (A1-1) was used. Openings having a diameter of 1 mm were provided in the quartz tube through which a mullite tube which had a 0.8-mm O.D. could be inserted at known depths, and the brightness temperature at its tip could be read with an optical pyrometer located at a distance from the plasma jet. The emissivity of mullite was assumed to be 0.4, but the temperature was quite insensitive to the value of emissivity, as seen from equation (A1-1). Mullite, having a high softening point of 1900°K, and being relatively non-conductive of heat, was a suitable material for this technique. Corrections for the stagnation of gas and the formation of film around the probe were not considered. These sources might introduce an error of the order of -10°K in the measured temperatures. The pyrometric method yielded the kinetic temperatures of the gas while the spectroscopic methods discussed above gave the excitation temperatures. In Figure I-7, the temperature profile obtained by the slope method has been extended to the quartz wall, with help of the temperatures determined pyrometrically.

The uncertainty in the measurement of temperature by the ratio method was estimated as:

$$\frac{\Delta T}{T} \simeq 0.7\left[\frac{\Delta I_{pr}}{I_{pr}} + \frac{\Delta I_{qs}}{I_{qs}}\right] \qquad \text{at } 6000°K$$

Assuming the error in the relative intensity measurements to be ±5 per cent, the corresponding uncertainty in the measured

temperatures was ± 7 per cent. The uncertainty could be reduced by choosing the two lines with widely separated energy levels, but in that case, the assumption of equilibrium between these levels may be questionable.

For the reference-temperature method, the uncertainty in the temperature was:

$$\frac{\Delta T}{T} = 0.034\left[\frac{\Delta I}{I} + 29\,\frac{\Delta T_{ref}}{T_{ref}}\right] \qquad \text{at } 6000^{\circ}K$$

It is clear from the above equation that most of the uncertainty arose from the uncertainty in the reference temperature itself, which remained in the systematic form.

The slope method was the most reliable method studied, although it was more time-consuming. In a typical case, 7 experimental points were used to establish the slope, and a standard deviation of ±3 per cent was obtained for the slope. The error in the temperature was then about 3 per cent. Further, deviations from equilibrium could be easily detected from the plot of $\log\frac{I_{nm}\lambda_{nm}}{g(n)A_{nm}}$ vs. E(n). The reference temperature method should have yielded results close to the slope method, because the two methods had a common point of reference, which was the axis, but the temperatures obtained by the reference method were always higher than those obtained by the slope method, the discrepancy increasing towards the boundary. Examination of equation (1) of Appendix A-4, which was based on the assumption of a complete thermodynamic

equilibrium and was used in the reference-temperature method, reveals that the discrepancy could be an indication of the absence of complete thermodynamic equilibrium in the plasma. Therefore, the next step was to examine the question of equilibrium in the plasma jet under study.

4. Excitation Equilibrium

An important assumption made in this study was that the excitation temperature obtained by the slope method was equal to the kinetic temperature of the electrons and atoms. The kinetic energy levels of particles are almost continuously spaced and a large number of collisions are of the elastic type,so that one can safely assume a Maxwellian velocity distribution for each kind of particles in a plasma under atmospheric pressure. Inefficient transfer of energy between the particles of widely different masses may restrict the equilibrium between electrons and atoms, but in the plasma under investigation, the time for equilibration was of the order of 10^{-5} sec[13]. After this induction period, the same kinetic temperature would pressumably characterize both electrons and atoms.

The excitation levels of an atom are closely spaced near the ionization level, so that the Saha-Boltzmann relationship can be always assumed for the higher excited states. The lower energy levels are however, widely separated, due to which the condition of equilibrium may not prevail among

these states.

Bates and Kingston[14] proposed a collisive-radiative model for a hydrogen plasma in which they were able to prodict the departure from equilibrium of the lower excited states quantitatively. McWhirter and Hearn[15] extended their calculations to other hydrogen-like atoms. Some salient features of the collisive-radiative model are as follows:

1. The population density of a given excited state denoted by the principal quantum number p is maintained by the processes of excitation and de-excitation:

$$\frac{d\,n(p)}{d\,t} = (\text{rate of excitation}) - (\text{rate of de-excitation})$$

each rate being a sum over the different energy levels, written in the proper form.

2. The kinetic processes considered in the model are: excitation and de-excitation by electron impact, ionization and recombination by electron impact, and spontaneous radiative decay. Atom-atom collisions are neglected because they are infrequent and mostly of the elastic type.

3. All the energy levels above a certain cut-off quantum number (*) are assumed to be in partial equilibrium with each other and with the free electrons so that

the Saha-Boltzmann relationship is satisfied by these levels, together with the free electrons.

4. The relaxation-time constant of the ground state is orders of magnitude longer than that for the excited system of an atom. As a consequence, the changes in the excitation population may be regarded as instantaneous in comparison with the change in the ground-state population. This is the quasi-steady state assumption for the excitation population.

Deviations from comlete and partial thermodynamic equilibrium of inert-gas plasmas have been studied in both transient and steady-state discharges. Hinnov and Hirschberg [16] measured the instantaneous line intensities in a helium afterglow at low pressures and deduced that the excitation levels with a principal quantum number less than 3 were not in equilibrium at temperatures of the order of 2000°K. Hattenburg and Kostkowski[17] observed an off-axis peak in the intensity of a symmetrical helium plasma, which they attributed to the absence of equilibrium. Their data suggested that the radial distribution of electron temperature determined from the measured distribution of electron density was not consistent with the radial-intensity profiles. Simon and Rogers[18] claimed that the excitation temperature of 4800°K measured by them, using the relative distribution of intensity of line radiation from an arc plasma in helium

was much below that required to maintain the electron density of 1.2×10^{16} particles/cm^3 measured from the series limit of the resolvable lines. Bott[19] observed in an atmospheric helium arc that the temperatures calculated from the absolute line intensities were much higher than those obtained from the relative population densities, at low arc currents. His observations are supported by the conclusions drawn in this study, from the measurement of temperatures by different techniques. Bott's work on an argon arc plasma[20] gave clear evidence regarding non-equilibrium of the $2p_2$ level in argon I below 8000°K or so. Freeman[21] found that in an arc-heated argon plasma jet, the composition of electrons, ions, ground-state atoms and metastable atoms was consistent with a complete thermodynamic equilibrium. Scholz and Anderson[22] investigated the central core of an RF-heated-argon-plasma jet at different pressures and concluded that deviations from equilibrium set in near the $3p_6$ level of AI at pressures below 0.1 atm. Brewer and McGregor[23] observed that the line radiation from an argon-plasma jet was much higher than its equilibrium value. They proposed the existence of an equilibrium system of excited atoms with the long-lived-metastable state as their ground level. Assuming that the interaction between the normal excited system and the metastable system to be negligible, they obtained an expression for the population density of any excited state, which can be written with an additional assumption that $n_t \approx n(1)$ as:

$$n(p) = \left(\frac{g(p)}{Z} e^{-\frac{E(p)}{kT}} \right) n(1) + \left(\frac{g(p)}{Z_m} e^{-\frac{E(p) - E(2)}{kT}} - \frac{g(p)}{Z} e^{-\frac{E(p)}{kT}} \right) n(2) \qquad \text{(I-4)}$$

In the light of the collisive-radiative model for plasmas, the metastable atoms may have some influence on the excitation population, but the hypothesis of a metastable-equilibrium system having distinguishable atoms in the same energy level is not reasonable, and not necessary.

An a priori assumption of a complete thermodynamic equilibrium has sometimes led to erroneous conclusions. For example, Chu and Gottschlich[24] measured the temperatures in an alkali seeded argon plasma by both pyrometric and the absolute-line-intensity methods and concluded that the electron temperature was much higher than the atom temperature assuming that the absolute-line-intensity method gave the electron temperature. They excluded the possibility that the degree of excitation was much greater than its thermodynamic-equilibrium value, in which case equation (1) of Appencix A-4 would yield higher excitation temperature than its actual value.

Experimental

Side-on observations were made for the seven different lines of the spectrum of argon I for which the spectroscopic data are given in Table I-2. In each of the observations, the selected line was scanned at a rate of 2 Å/min for at least three times, and an average value of the integrated intensity was taken. A preliminary scan across the plasma jet indicated that the intensity profile was quite symmetrical about the axis; hence only one side of the plasma jet was considered. The test zone was divided into 5 planes located at 4.267, 6.172, 8.077, 9.982 and 11.89 cm measured below the bottom turn of the RF coil. At each plane, the line intensities were measured at five transverse positions, starting from the center, and 10 values at equal intervals were interpolated. The reproducibility of the intensities was ± 3 per cent. The measured line intensities were converted to the radial intensities by the use of numerical Abel-inversion described in Appendix A-3. Population densities of the upper-excitation levels giving rise to the observed lines were calculated from the absolute intensities, using the following equation:

$$I_{nm} = \frac{hc}{\lambda_{nm}} A_{nm} n(n) \qquad \text{(I-5)}$$

The energy levels which were in equilibrium with each other should fall on a straight line given by the following equation which is based on the Boltzmann distribution:

The intercepts of the straight lines shown in Figure 1 of Appendix A-7 on the vertical axis gave $n_E(1)$, which was the hypothetical ground-state population in equilibrium with the higher excited states, and according to the partial equilibrium model, with the free electrons. The equilibrium-ground-state population therefore, represents the degree of excitation of the higher energy levels and the degree of ionization in the plasma, at a given temperature.

The actual ground-state population was calculated from the kinetic theory of ideal gases according to the equation:

$$n(1) \approx n_t = \frac{P}{kT} = \frac{0.734 \times 10^{22} P}{T} \text{ (particles)(cm)}^{-3}$$

The assumption that the ground-state population was numerically equal to the total particle population holds good, because over 99% of the atoms were in the ground state. The ground-state population was expressed as a fraction of the equilibrium-ground-state population:

$$\rho(1) = \frac{n(1)}{n_E(1)} \qquad \text{(I-7)}$$

Figure I-9 shows the ground-state population as the function of the parameter $\frac{1}{2.303kT}$.

The free-electron density was calculated from the equilibrium-ground-state population and the excitation temperature by applying the Saha-Boltzmann relationship to the first stage of ionization:

$$\log\frac{n(p)}{g(p)} = \log\frac{n_E(1)}{g(1)} - \frac{E(p)}{kT} \qquad \text{(I-6)}$$

Figures I-8A through I-8D show the radial distribution of intensities at the first four axial positions. The fifth axial position is omitted because there, the intensities could be measured only at a short radius. The plots of the excitation population as a function of the energy level are shown in Figures 1A through 1E of Appendix A-7. The plots of $\log \frac{n(n)}{g(n)}$ vs. E(n) are shown for 11 radial positions for the 7 energy levels for the first four axial positions, and only at the center for the fifth axial position. It can be seen that the higher energy levels fall on a straight line meaning that these levels were in partial equilibrium, while the lower energy levels show marked deviations from equilibrium under certain conditions. Even the higher energy levels do not fall on a straight line, near the boundary of the plasma. In this case, the temperatures measured pyrometrically by the method described above served as a guideline to determine the slopes of the straight lines.

The slopes of the straight lines passing through the higher excited states gave the excitation temperatures in accord with equation (I-6). The radial distributions of temperatures for the 5 experimental planes are shown in Figure 2 of Appendix A-7. The temperatures at the lowest plane beyond a short radius are extrapolated values.

$$n_e^2 = 2\left(\frac{2\pi m_e kT}{h^2}\right)^{\frac{3}{2}} Z^+ \frac{n_E(1)}{g(1)} e^{-\frac{E^+}{kT}} \qquad \text{(I-8)}$$

The radial distributions of electron density are shown in Figure 3 of Appendix A-7.

Discussion

The experimental error in the absolute-intensity measurements, including the reproducibility, was ±8 per cent. Added to this, was the error in Abel-inversion, which was ±5 per cent or so. Thus, the total error in the intensity measurements could be ±13 per cent. The error in the absolute-transition probabilities was ±18 per cent, which placed the error in the population densities at ±31 per cent. The slope method gave excitation temperatures within ±3 per cent in most cases, but the error could be considerably larger when deviations from equilibrium were severe. The experimental error in the electron densities was ±34 per cent. The error in the equilibrium-ground-state population was ±60 per cent.

Figure I-9 illustrates that the ground state was overpopulated at higher temperatures and tended to be rapidly underpopulated at lower temperatures. In other words, the degree of excitation and ionization in the plasma was much lower at higher temperatures and was much higher at lower temperatures than its value under complete thermodynamic equilibrium. In Figure I-9, the experimental data points

representing the experimental planes are shown with different symbols. The spread of these points from a smooth curve shows to some extent, the effect of deexcitation due to electron recombination. The process of recombination between electrons and ions being quite slow, its influence on the equilibrium-ground-state population is not exhibited clearly in Figure I-9.

The equilibrium-ground-state population can be represented by means of an equation of the form:

$$\rho(1) = \frac{g(*)n(1)}{g(1)n(*)} e^{-\frac{E(*)}{kT}}$$

where $E(*)$ is the slope and $\log \frac{g(*)n(1)}{g(1)n(*)}$ is the intercept of the tangent to the curve representing the equilibrium ground-state population, at a given temperature and electron density. The relationship between the population density of some excited state p and the state denoted by $(*)$ can be written as:

$$\frac{n(p)}{n(*)} = \frac{n(p)}{n_E(1)} \times \frac{n_E(1)}{n(*)} = \left(\frac{n(p)/g(p)}{n_E(1)/g(1)} e^{\frac{E(p)}{kT}}\right)\left(\frac{g(p)}{g(*)} e^{-\frac{E(p)-E(*)}{kT}}\right)$$

It may be seen that the term in the first bracket becomes unity if the state p belongs to the partial-equilibrium population, and that $(*)$ denotes the lowest excited state belonging to the partial equilibrium population. The state

(*) may be called the critical state at the given temperature, and the corresponding energy level may be called the critical energy level. For illustration, a straight line representing the critical state (*) is shown in Figure IV-4 at a fixed electron density of 8×10^{12} particles/cm^3. The value of E(*) from the slope of this straight line at the lower end of temperatures is 126000 cm^{-1}, which is close to the first ionization level in argon (127110 cm^{-1}), meaning that the partial equilibrium model breaks down at lower temperatures. At much higher temperatures, E(*) tends to vanish, meaning that the partial equilibrium can be extended down to the ground state. It should be noted that the value of $\rho(1)$ by itself does not denote the state of equilibrium in the plasma. At about 6500°K, the value of $\rho(1)$ is unity, but the value of E(*) is close to the metastable level (93143 cm^{-1}). Therefore at this temperature, a partial equilibrium exists among the entire excitation population and the degree of excitation coincides with its thermodynamic value. This should not be confused with the condition of complete thermodynamic equilibrium because the latter requires the partial equilibrium to exist down to the ground level. In a highly decaying plasma, such as the plasma jet, thermal lagging of the excitation population behind the processes of energy loss results in rapid underpopulation of the ground state. On the other hand, when the plasma is

being excited, the ground state will be overpopulated. A stable, complete thermodynamic equilibrium can be attained probably in a plasma, in which the temperature gradients are small, and the electron densities are high[21]. An enclosed arc comes close to these requirements[19].

In Figure 1 of Appendix A-7, the critical energy level is the point of departure of the plot of $\log \frac{n(p)}{g(p)}$ vs. E(p) from the straight line depicting equilibrium. The fractional departure from equilibrium expressed as the ratio of the experimental value of n(p) to the value of $n_E(p)$ corresponding to the straight line was calculated for the 7 energy levels listed in Table I-2. The results were correlated to the temperature and electron density in the plasma by means of an equation of the form:

$$\rho(p) = \frac{n(p)}{n_E(p)} = 1 - AT^B n_e^C \qquad \text{(I-9)}$$

using a least-squares fit. Table I-2 gives the values of constants A, B and C in equation (I-9) for 4 energy levels. The higher energy levels were omitted because their fractional departure from partial equilibrium was close to unity under the experimental conditions. The constants listed in Table I-2 are purely empirical, and they hold good only in the limited range of conditions encountered in the experiment. They do point out that the effect of higher electron

density is to bring the excitation population closer to equilibrium and that the effect of temperature is very small.

McWhirter and Hearn[15] expressed the results of their calculations for hydrogen-like plasmas in the form of the following equation:

$$\rho(p) = r_o(p) + r_1(p)\rho(1) \qquad \text{(I-10)}$$

where $r_o(p)$ and $r_1(p)$ are coefficients which are functions of temperature and electron density. In the present case, excitation from the ground state could be neglected because of the low ground-state population, so that $\rho(p) \approx r_o(p)$. To compare the argon plasma with the hydrogen-like plasmas, the following approximations were introduced. The effective nuclear charge seen by the electrons in the field of argon ions was assumed to be unity. An effective principal quantum number p_{eff} defined by the following relationship:

$$\frac{z_{eff}^2 \times 109737}{p_{eff}^2} = 127110 - E(p) \qquad \text{(I-11)}$$

was substituted for the required energy level in argon. For the purpose of comparison of the experimental results with the calculations of McWhirter and Hearn, the following temperature and electron-density conditions were assumed:

$$T = 8000°K \qquad n_e = 10^{14}(\text{particles})(\text{cm})^{-3}$$

The calculated values of p_{eff} are listed in Table I-2. Figure I-10 shows a comparison between the values of $r_o(p)$ from McWhirter and Hearn's theoretical work and the experimental values of $\rho(p)$ for argon for the given values of T and n_e. Considering the approximations involved in the comparison and considering the great sensitivity of $\rho(p)$ to the values of z_{eff} and p_{eff}, the agreement is reasonably good. It can be however noticed that the experimental values of $\rho(p)$ are always greater than the theoretical values of $r_o(p)$. To resolve this discrepancy, one must look into the assumptions made in the collisive-radiative model in the derivation of equation (I-10). Because of their long lifetime, a metastable level can influence the excitation population in a manner similar to the ground state. The effect of metastable level can be accounted for, by including a term corresponding to excitation from the metastable level in equation (I-10) [25].

$$\rho(p) = r_o(p) + r_1(p)\rho(1) + r_2(p)\rho(2) \qquad \text{(I-12)}$$

where $\rho(2)$ is the fractional departure from equilibrium of the metastable density, and $r_2(p)$ is a coefficient which is also a function of the temperature and electron density. Although the limited number of experimental data did not allow evaluation of the coefficient $r_2(p)$, Figure I-10 points out that the effect of the low-lying-metastable level

is to bring the excitation population closer to equilibrium.

Although the form of equation (I-12) bears some resemblance with equation (I-4) proposed by Brewer and McGregor [23], their derivation and interpretation of the equation are entirely different. In fact, their assumption that the excitation population is always in equilibrium with the metastable level does not seem to be consistent with the present results.

The analysis presented here was limited to the quasi-steady-state-population densities of a few excited levels of argon. The temperature and the electron density were treated as independent variables, although in principle, they could be obtained as a function of the position in the reactor, by solving the macroscopic energy-balance equation in conjunction with the equations representing the microscopic rate processes, knowing the initial conditions and the boundary conditions in the reactor. This was however, not the aim of the present investigation.

5. Velocity distribution

The velocity distribution in the plasma jet being studied was required in order to calculate the rates of reactions. A three dimentional mapping technique for the flow pattern was developed for the measurement of velocities, in which the paths of particles of boron nitride were traced photographically. The details of this technique and the experimental

results are given in the publication which is reproduced in Appendix A-6. The experimentally determined velocities are reported in Table I-3. The third-order-polynomial fit to these data points, as shown in Figure 2 of Appendix A-6 holds good only within the experimental boundaries which were $6 < z < 18$ cm and $0 < r < 1.3$ cm, where z denotes the axial distance measured from the leading edge of the RF coil and r denotes the radial distance.

A material balance on argon made in the plasma jet enabled the experimentally determined velocity distribution to be improved. The flow rates of argon in the plasma stream and the cooling stream were measured with two calibrated rotameters. The calibration of the rotameters was accomplished by clocking the volume of water displaced by the gas flowing through the rotameters. The water was contained in an inverted cylinder. A correction for the vapor pressure of water at the prevailing temperature was applied. No correction was applied for the effect of the small head of water in the jar. The pressure of the gas at the outlet of the rotameter was 14.2 psia for the plasma gas and 17.0 psia for the cooling gas. A corresponding correction was applied in calculating the total mass-flow rate of argon. Ideal gas law was assumed. The total feed rate of argon to the reactor was then calculated as the sum of the feed rates to the plasma and the cooling streams in the following manner:

$$\dot{m} = \frac{(P_c\dot{V}_c + P_p\dot{V}_p)M}{RT} = 0.407 \quad g/sec$$

where P_c and P_p were the pressures of cooling and plasma gases respectively at the delivery side of the meters, $\dot{V}_c$ and $\dot{V}_p$ were the corresponding volumetric flow rates; M, the molecular weight of argon; R, the gas constant and T, the ambient temperature.

The equation of continuity for argon, with the assumption of an ideal gas, no angular or radial flow and of a constant pressure was written as:

$$v_z \equiv f(r) \times T \qquad (I-13)$$

The total flow rate of argon at any given plane was calculated by integrating the mass flux over the cross-sectional area of the tube.

$$\int_0^{r_o} 2\pi r(\rho v_z)dr = \dot{m}$$

By the use of the relationships:

$$\rho = \frac{PM}{RT}$$

$$v_z = f(r) \times T$$

the above integral equation became:

$$\int_0^{r_o} r \times f(r)dr = \frac{R\dot{m}}{2\pi PM} = 0.149 \qquad (I-14)$$

Equation (I-13) states that the velocity is proportional to the temperature at a given radial position irrespective of the axial position. The form of f(r) is a characteristic of the flow pattern in the reactor and should be invariant with respect to changes in temperatures. Thus, the function f(r) provides the means of calculating the velocity distribution from the known temperature distribution in the reactor. Numerical values of f(r) obtained by dividing the measured velocities by the temperatures shown in Figure 2 of Appendix A-7 are shown in Figure I-11 upto the radius of 1.3 cm for four axial positions. The axial position at 4.267 cm was omitted because the velocities were not measured at this height in the reactor. The spread in f(r) at a given radial position is within the limits of experimental error. The cause for the pronounced hump in f(r) at $r \approx 1$ cm was the uncertainty due to large temperature gradients present in this region. The bold curve indicates averaged values of f(r) which were represented by the equation:

$$f(r) = 0.113166 - 0.0362068r + 0.1275032r^2 - 0.0801974r^3 \quad \text{(cm)/(sec)(°K)} \qquad \text{(I-15)}$$

Further, it can be seen from Figure I-11 that the function f(r) may be approximated by a constant value of 0.117 (cm)/(sec)(°K) without significant loss of precision, upto the radius of 1.3 cm.

With the form of f(r) given by equation (I-15), the

left-hand side of equation (I-14) was evaluated and had a value of 0.134 which is seen to agree quite well with the right-hand side of the same equation based on the measured flow rate of argon.

The refined velocity distribution computed from the above f(r), and the temperature distribution shown in Figure 2 of Appendix A-7, is shown in Figure I-12.

Energy Balance

The equation of energy balance in the plasma jet was solved after knowing the temperature and the velocity profiles. The radiated power of argon was obtained as the result. The following assumptions were made in solving the equation of energy balance for the configuration of the plasma jet. The plasma jet was assumed to be isobaric. The viscous dissipation of energy was neglected. The heat capacity of argon was assumed to be constant, and not influenced by the absence of microscopic equilibrium. This assumption was good because the amount of the excitation energy in argon was quite small. The plasma was assumed to be transparent to its own radiation. The ideal gas law was assumed. Under these assumptions, the steady-state equation of energy was written as:

$$\rho C_p \underline{v} \cdot \nabla T + \nabla \cdot \underline{q} + \mathcal{E} = 0 \qquad \text{(I-16)}$$

where $\mathcal{E}$ was the radiated power of argon expressed as the energy radiated per unit time per unit volume. The conductive transport of energy was described by the Fourier's law:

$$\underline{q} = -K \nabla T$$

The thermal conductivity of argon at high temperatures was investigated by several workers[26, 27, 28, 29], and their results agreed well within 7 per cent. In the present analysis, the following equation given by Collins and Menard [27], was used:

$$K = 3.2 \times 10^{-6} \times T^{0.703} \qquad \text{(watts)/(cm)(°K)}$$

The value of heat capacity was assumed to be 20.8 (Joules)/(g mol)(°K). Substitution of the numerical values, resolution of equation (I-16) into cylindrical coordinates and assuming no angular flux of energy:

$$\mathcal{E} = 3.2 \times 10^{-6} \left\{ T^{0.703} \left[\frac{\partial^2 T}{\partial r^2} + \frac{\partial^2 T}{\partial z^2} + \frac{1}{r} \frac{\partial T}{\partial r} \right] + 0.703 T^{-0.297} \left[\left(\frac{\partial T}{\partial r} \right)^2 + \left(\frac{\partial T}{\partial z} \right)^2 \right] \right\} - 0.246 f(r) \frac{\partial T}{\partial z} \qquad \text{(I-17)}$$

It can be noted in equation (I-17) that the radiated power has been expressed as an explicit function of the temperature distribution in the reactor.

The numerical solution of equation (I-17) was obtained by dividing the region of interest into 15 radial and 17 axial increments. The radiated power, $\mathcal{E}$, was obtained as a point function in the reactor. The order of magnitude of $\mathcal{E}$ was the same as that of the conductive and the convective terms in equation (I-16). The values of $\mathcal{E}$ are shown for some typical points in Table I-4. The radiated power was correlated to the temperature and the electron density by means of a least-squares fit. The resulting relationship showed very little dependence of $\mathcal{E}$ on the electron density. The relationship between $\mathcal{E}$ and T was:

$$\mathcal{E} = 2.14 \times 10^{-8} \times T^{2.25} \qquad \text{watts/cm}^3 \qquad \text{(I-18)}$$

The accuracy of this technique of evaluating the radiated power was poor because of the second-order-partial derivatives and their squares occurring in equation (I-17). The error in $\mathcal{E}$ given by equation (I-18) could be as large as a factor of three. In spite of the poor accuracy, the present technique made it possible to evaluate small amounts of the radiated power from the known conductive and the convective terms of energy transport.

Electron-Ion Recombination

The experimental method for the determination of the rates of recombination comprised of solving the steady-state equation of continuity for the electrons:

$$\nabla.(n_e \underline{v}) + \nabla.(D_a \nabla n_e) + R_e = 0 \qquad \text{(I-19)}$$

where D_a was the ambipolar diffusion coefficient for the electrons and ions. With the assumption of no angular variation of fluxes, the above equation was written in the cylindrical coordinates as:

$$\frac{1}{r}\frac{\partial(rN_r)}{\partial r} + \frac{\partial N_z}{\partial z} + R_e = 0$$

$$N_r = -D_a \frac{\partial n_e}{\partial r}$$

$$N_z = -D_a \frac{\partial n_e}{\partial z} + v_z n_e \qquad \text{(I-20)}$$

The radial component of the velocity of the gas was neglected. The ambipolar diffusion coefficient was expressed as a function of temperature in the following form, based on the work of Beaty[30] and Biondi and Brown[31]:

$$D_a = 8.69 \times 10^{-7} T^2 \qquad \text{cm}^2/\text{sec} \qquad \text{(I-21)}$$

equations (I-20) and (I-21) were solved numerically in the region of interest in the plasma jet, in conjunction with the profiles of the temperature, electron density and the velocity obtained previously. As the result of the detailed solution of the equations, it was determined that the ambipolar diffusion velocity of the electron-ion pairs was less than 10 cm/sec in either the radial or the axial direction. In

consequence, the contribution of the ambipolar diffusion to the decay of electron density was neglected in comparison with the recombination effect. The above conclusion was independently verified by solving the equation of continuity without considering the effect of diffusional flux of electrons. The results agreed within $\pm$10 per cent at most points with the case in which the diffusional effect was considered. The discrepancy of $\pm$10 per cent could easily arise in the numerical solution of the second-order-partial-differential equation.

A discussion of the results and the comparison of this work with the previous studies on recombination in inert gases is given in a publication reproduced in Appendix A-7. An important conclusion drawn in Appendix A-7 is that the observed rates of recombination were consistent with a dissociative-molecular-ion model. The pertinent molecular ion in pure argon was A_2^+. The molecular ions of bimolecular gases such as N_2^+, increased the rates of recombination significantly. For this reason, and for the purpose of reproducibility of the results, the gas used in the study of recombination in pure argon was purified to remove the traces of impurities by the method described in Appendix A-2.

The effect of introducing nitrogen as an impurity in argon was to quench the line radiation from argon. A typical intensity profile for the line radiation of argon I at 5572 Å as a function of the axial position is shown in Figure I-13.

An explanation of the quenching effect on the basis of the dissociative-molecular-ion mechanism is given in Appendix A-7.

An important consequence of the dissociative-molecular-ion mechanism on the chemical reactions was the formation of atomic species from the molecular gases. For example:

$$N_2^+ + e \longrightarrow N + N^*$$

would yield a large amount of atomic nitrogen in a highly excited plasma. It was pointed out by Bates and Massey[32] that the large amount of nitric oxide in the upper ionosphere could be explained on the basis of the presence of atomic species formed as the result of the recombination of electrons with the dissociative-molecular ions. The effect of atomic nitrogen on the decomposition of nitric oxide will be discussed in the next section.

Table I-1

Experimental Transition Probabilities of Argon I

Wavelength Å	E(n) (cm^{-1})	g(n)	$A_{nm} \times 10^{-5}$ sec^{-1} (present work)	$A_{nm} \times 10^{-5}$ sec^{-1} (Ref.1,App.5)
5118	125113.48	5	6.2	2.8
5162.4	123468.03	3	16.6	19.8
5177.6	124771.67	5	3.7	2.5
5187.3	123372.98	5	14.4	13.8
5373.6	124692.02	5	3.2	2.8
5421.4	123903.30	5	7.5	6.2
5495.9	123653.24	9	17.7	17.6
5506.4	123773.92	7	5.0	3.7
5606	121932.91	3	21.3	22.9
5739.7	123505.54	5	10.0	9.1
5888.7	122440.11	5	14.9	13.4
5912.1	121011.98	3	12.4	10.5
6032.1	122036.13	9	24.3	24.6
6043.2*	122160.22	7	14.4	15.3
	123832.50	7	18.6	
6052.7	120619.08	5	1.8	2.0
6059.3	120600.94	5	3.7	4.2
6145.4	123557.46	7	6.4	7.9
6416.3	119683.11	5	18.0	12.1

* Arises from two transitions having almost equal differences between the upper and the lower energy levels. The reported value of A_{nm} is based on the total measured intensity.

Table I-2

Spectroscopic Data for The Observed Lines

and The Corresponding Energy Levels

Wavelength Å	Upper Energy Level E(p) (Paschen)	Term Value of E(p) cm^{-1}	Statistical Weight of p g(p)=(2J+1)	Transition Probability for The Line x 10^{-5} $(sec)^{-1}$	Equivalent Principal Quantum Number p_{eff}	Equation I-9 Values of Constants Determined by Least Squares A	B	C
6965	$2p_2$	107496.463	3	67.0	2.18	8.5×10^3	0.122	-0.344
4251.2	$3p_{10}$	116660.054	3	1.13	3.0	3.2×10^6	0	-0.54
4300	$3p_8$	116999.389	5	3.94	3.06	5.2×10^4	0	-0.414
4345.2	$3p_4$	118407.494	3	3.13	3.29	2.8×10^6	-0.1	-0.52
3834.7	$4p_5$	121470.304	1	5.6	4.08	-	-	-
5558.6	$5d_3$	122086.974	5	14.8	4.34	-	-	-
5572.6	$5s_1'''$	123557.459	7	6.9	5.15	-	-	-

Table I-3

Raw velocity data obtained by the use of particles of boron nitride. 1.84 cm should be added to the axial distance in order to make the zero of the axial coordinate coincide with the leading edge of the RF coil.

RADIAL POSITION (CM)	AXIAL POSITION (CM)	VELOCITY (M/SEC)	RADIAL POSITION (CM)	AXIAL POSITION (CM)	VELOCITY (M/SEC)	RADIAL POSITION (CM)	AXIAL POSITION (CM)	VELOCITY (M/SEC)
0.831	4.597	8.077	1.288	5.639	3.607	0.869	5.690	7.188
0.673	5.918	7.722	0.317	6.325	7.899	0.663	6.883	7.925
1.173	8.026	3.785	1.097	8.992	3.607	0.965	11.303	3.505
0.841	10.617	6.299	1.069	9.195	4.140	1.151	11.201	3.607
1.125	11.481	3.404	0.820	11.862	3.861	0.881	11.862	5.842
0.427	11.963	5.486	0.627	12.344	5.563	1.031	12.446	4.496
0.427	14.275	5.486	1.011	9.373	4.394	0.945	4.394	4.674
1.090	4.115	4.496	0.843	4.369	6.655	0.155	4.369	8.331
0.155	4.496	9.804	0.315	6.071	8.230	0.526	12.979	8.128
0.787	14.199	5.207	1.377	13.640	5.207	0.622	13.411	6.045
0.417	13.081	6.147	0.892	12.421	5.740	0.163	11.989	6.452
0.869	11.303	4.801	0.833	11.201	4.699	0.389	11.100	5.207
0.660	5.537	7.493	0.566	5.207	8.331	0.705	3.886	8.128
0.889	9.093	6.248	0.691	9.754	6.248	0.782	8.433	6.248
0.678	8.763	6.045	0.493	10.871	6.248	0.127	8.992	6.756
0.371	8.204	7.823	0.036	11.989	7.188	0.378	15.189	6.147
0.691	10.516	5.740	1.234	15.291	5.410	0.513	11.989	5.309
0.439	11.405	7.087	0.363	11.303	6.553	0.952	10.414	5.004
0.884	10.871	4.699	0.988	9.093	4.166	1.074	8.763	4.064
1.034	8.534	4.166	1.059	8.103	4.267	0.404	5.944	6.299
1.275	9.601	3.099	1.166	10.465	3.099	0.437	11.963	4.089
1.090	13.106	3.683	0.810	13.360	4.267	0.810	13.792	4.597
0.757	16.586	4.750	0.262	10.033	6.553	0.818	13.716	4.343
0.892	5.232	6.375	0.086	12.827	6.629	0.744	16.053	4.496
0.714	16.408	4.902	0.772	13.183	6.147	0.825	16.231	4.013
0.617	16.586	4.267	0.556	10.846	5.740	0.330	10.744	6.147
1.057	9.957	6.375	0.483	8.915	5.893	0.165	8.458	6.629
1.430	3.378	3.175	0.417	8.382	6.706	0.544	7.849	6.375
0.190	6.807	7.112	0.462	13.614	5.410	0.544	15.900	4.166
0.447	11.709	6.553	0.879	11.354	4.750	0.127	11.354	5.893
0.330	9.957	5.969	0.190	8.992	6.629	0.411	4.089	8.941
0.531	4.978	6.706	0.427	6.375	7.620	0.475	6.121	7.366
1.346	3.759	3.607	1.257	6.731	3.937	0.859	7.772	5.893
1.100	8.026	4.267	1.125	8.280	4.267	1.143	9.246	3.683
0.099	10.312	8.026	0.127	11.709	7.290	0.643	13.284	5.740
0.991	13.183	4.496	0.361	12.294	6.553	0.673	8.026	5.740
0.968	9.246	4.572	0.658	10.211	4.674	0.493	12.395	5.740
0.765	13.437	4.826	0.831	6.706	6.706	0.467	11.709	7.518
0.704	14.148	5.893	0.556	13.614	5.969	0.317	15.977	5.893
0.820	6.426	7.696	1.333	5.766	3.327	0.823	6.325	7.010
1.359	7.087	3.505	0.800	13.716	6.121	1.151	12.294	5.436
0.968	12.217	5.436	1.128	11.735	5.232	0.577	15.545	6.045
1.059	14.249	4.013	1.140	14.554	3.505	1.090	12.116	4.547
1.125	6.477	5.690	0.696	15.646	5.944	0.351	14.529	6.553
1.082	12.978	5.690	1.227	13.335	3.683	1.052	8.763	5.944
0.836	7.925	6.553	0.366	12.649	6.198	0.198	11.379	6.121
0.254	11.100	6.655	0.178	9.703	7.010	0.653	10.236	6.121
0.744	3.454	6.883	0.732	3.886	7.214	0.622	6.045	7.366
0.229	5.182	8.687	0.378	5.004	8.179	0.605	8.966	6.299
0.975	10.262	5.258	1.125	3.200	6.071	0.450	4.826	9.652
1.143	6.299	4.039	0.086	9.144	8.103	0.302	9.068	7.112
0.754	8.280	5.817	0.838	8.458	5.588	1.587	11.303	2.845
0.145	15.113	5.893	0.650	14.656	6.147	0.927	9.500	5.105
1.173	8.534	4.445	0.846	8.357	6.807	0.648	8.026	6.477
0.643	7.671	6.883	0.434	8.103	5.512	1.003	10.084	4.039
0.818	12.243	5.029	1.044	13.818	3.810	0.597	15.291	5.029
0.391	16.485	4.775	0.046	13.030	6.477	0.478	9.068	6.299
0.856	7.671	4.928	0.775	7.595	5.664	0.720	7.061	6.147
1.074	6.909	4.445	0.345	14.249	6.477	0.138	13.970	6.477
0.102	7.239	7.849	0.698	5.613	6.071	0.317	11.811	5.383
1.021	13.691	4.445	0.058	11.379	7.696	0.678	10.414	6.528
0.696	7.823	7.239	0.734	13.792	5.436	0.894	13.614	4.978
1.052	15.240	3.353	1.212	9.169	3.429	1.097	9.652	4.521
1.191	10.516	4.064	0.577	7.518	7.417	0.617	6.375	7.417
0.427	5.893	8.153	0.986	5.105	7.239	0.772	4.140	7.239

Table I-4

Radiated power of argon evaluated from the pointwise energy balance in the plasma jet. The numbers following the letter E are powers of 10 to be multiplied.

Temperature °K	Electron Density particles/cm^3	Radiated Power Watts/cm^3
10483	7.8E 14	28.0
10417	7.6E 14	27.0
10350	7.3E 14	26.0
10215	6.8E 14	20.0
10021	6.3E 14	10.0
9364	4.3E 14	22.0
9207	4.1E 14	19.5
8965	3.7E 14	11.4
8607	3.3E 14	5.0
8218	2.6E 14	19.5
8000	2.3E 14	19.0
7728	2.1E 14	12.4
3377	1.8E 14	1.0
7088	1.6E 14	15.5
6810	1.3E 14	16.5
6530	1.1E 14	14.0
6363	9.6E 13	6.5
6060	7.7E 13	8.2
5772	6.0E 13	8.7

Figure I-1 A photographic view of the experimental setup.

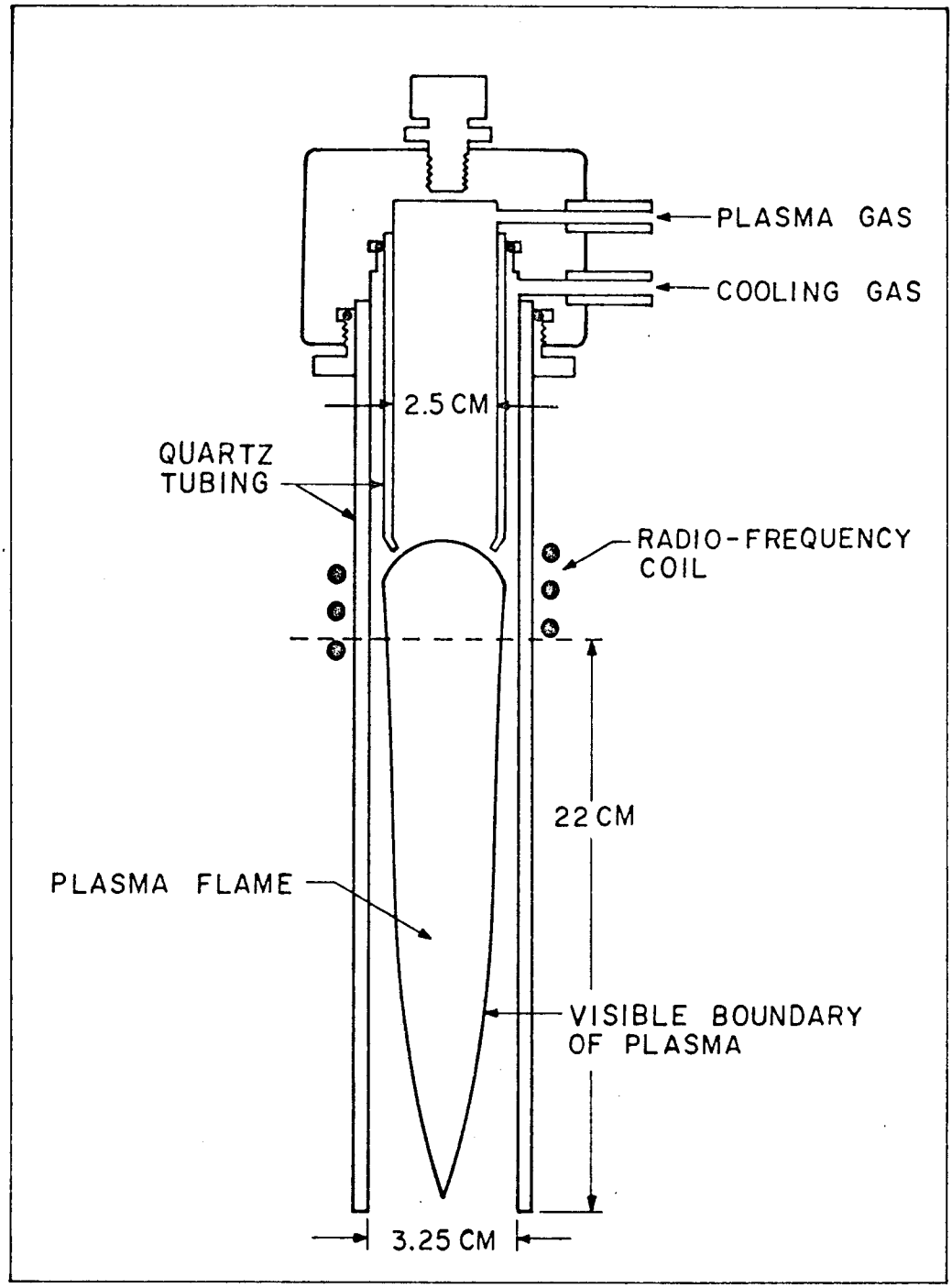

Figure I-2

Reactor assembly used for spectroscopic study of the plasma jet.

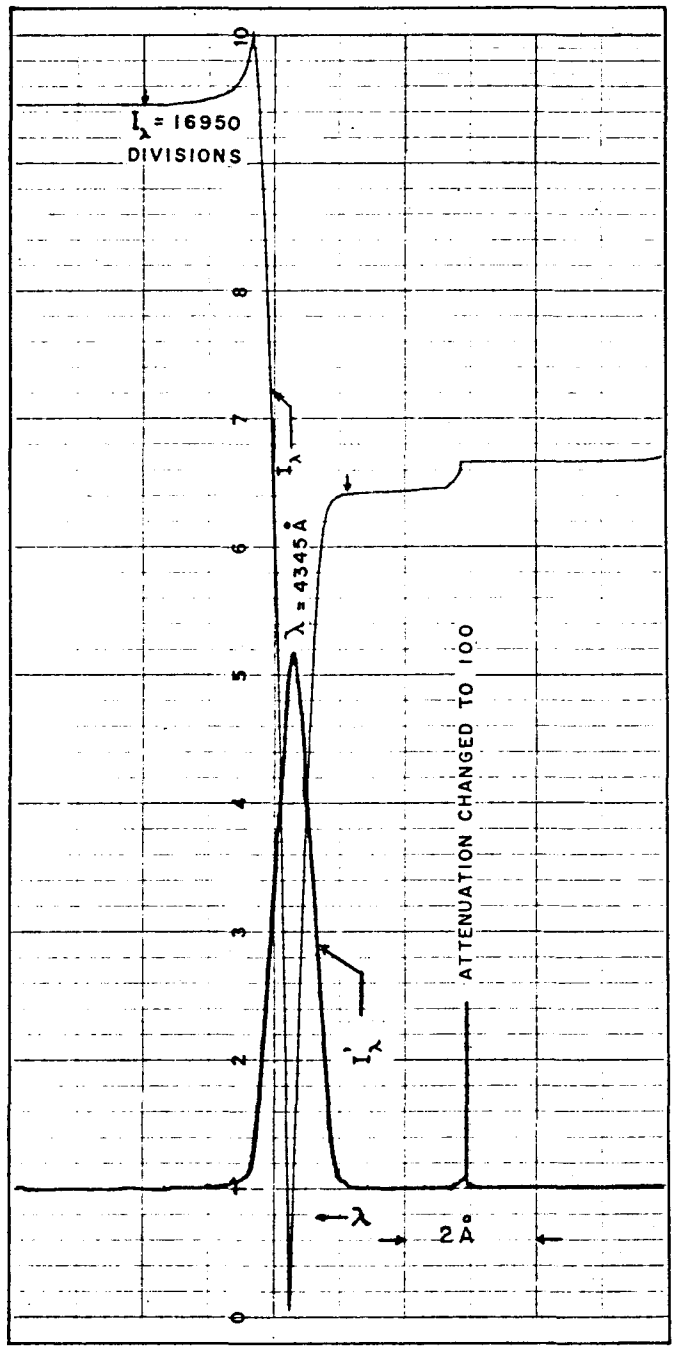

Figure I-3

A typical measurement of spectral intensity with 1P28 photomultiplier tube. The bold line shows shape of the intensity curve and the thin line shows electronically integrated value of the intensity.

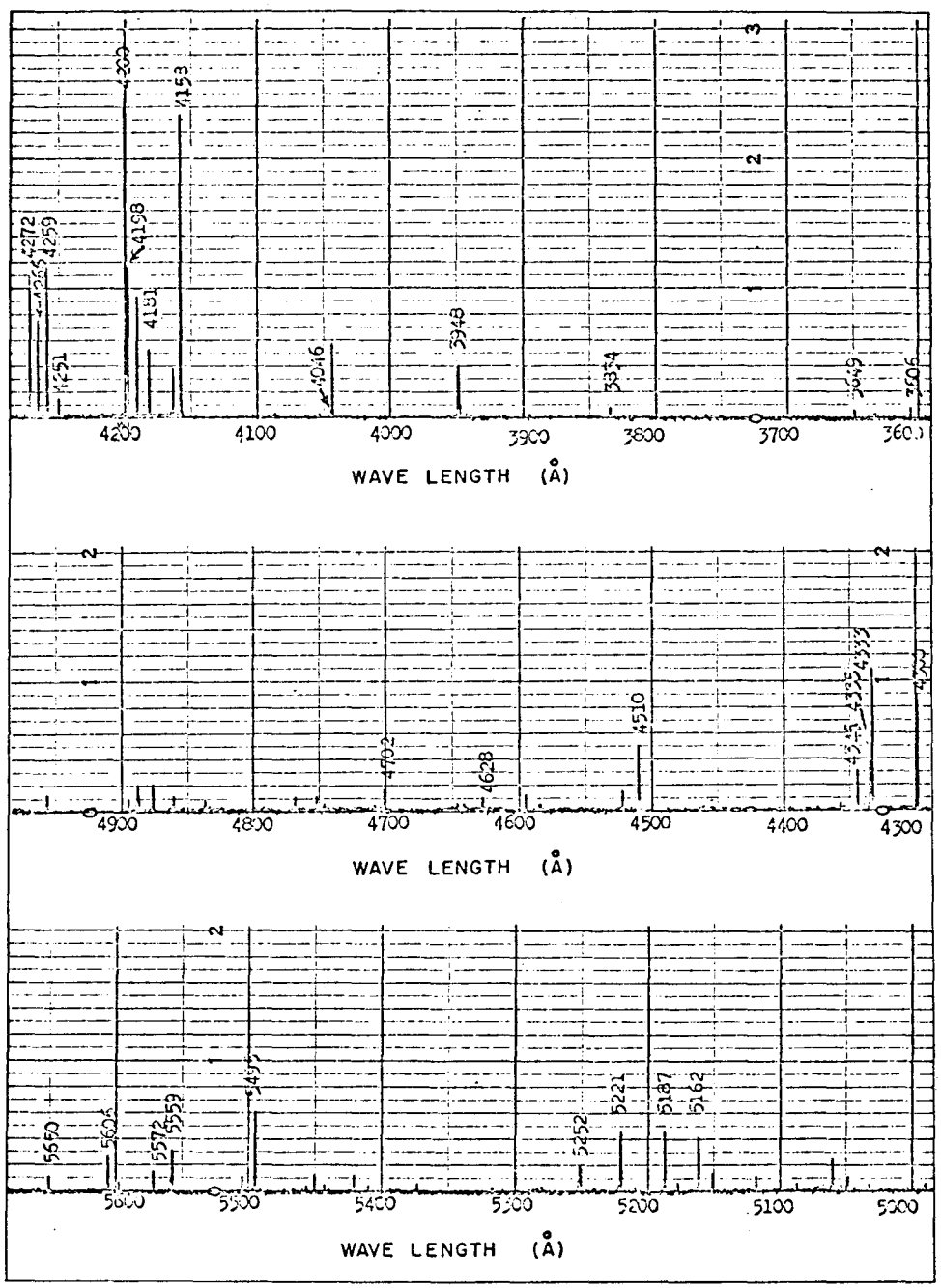

Figure I-4

A spectrophotometric scan of spectrum of argon I between 3600 - 5700Å, for the purpose of identification of lines.

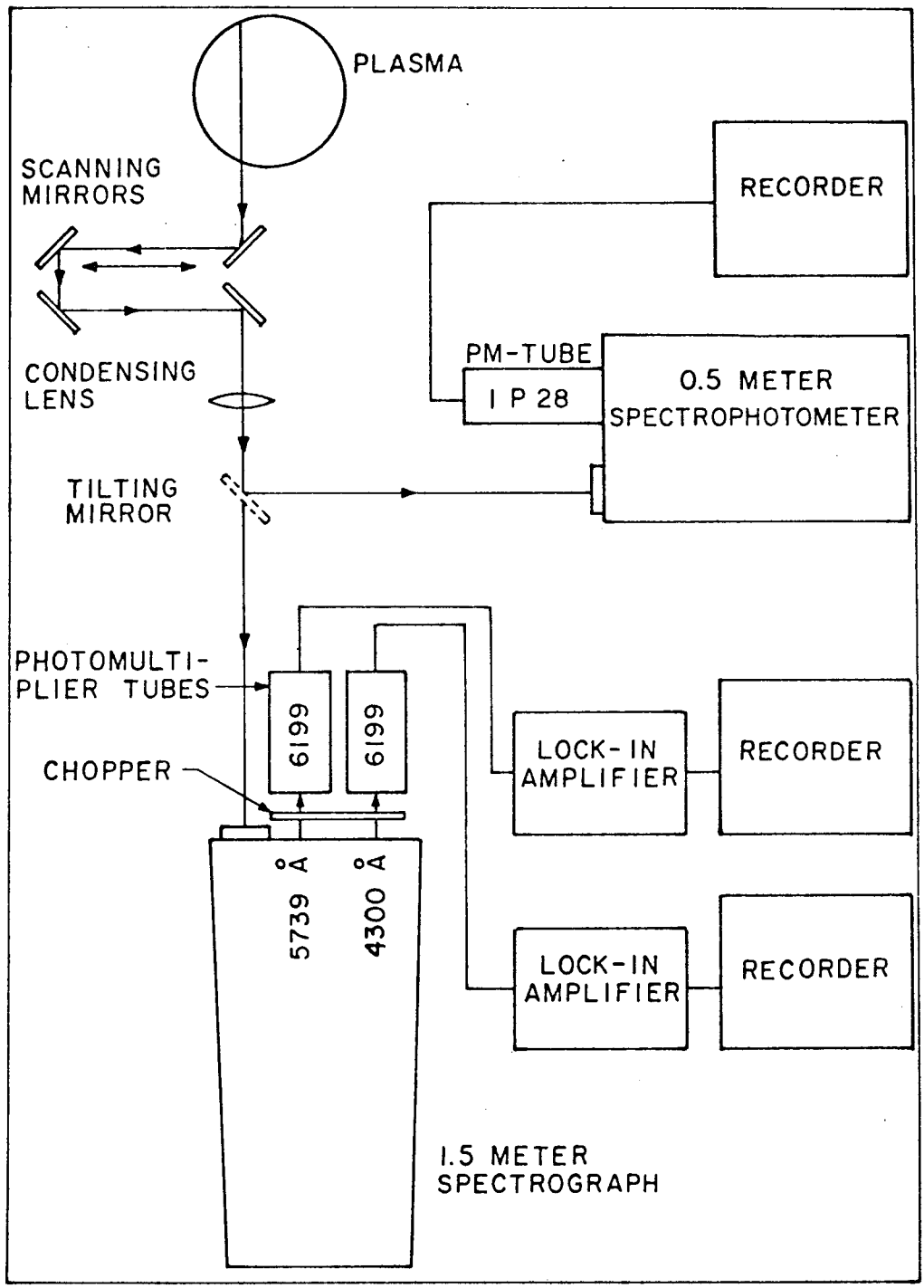

Figure I-5

Schematic diagram of the experimental setup for the comparison of the spectroscopic methods for measurement of temperature in the plasma jet.

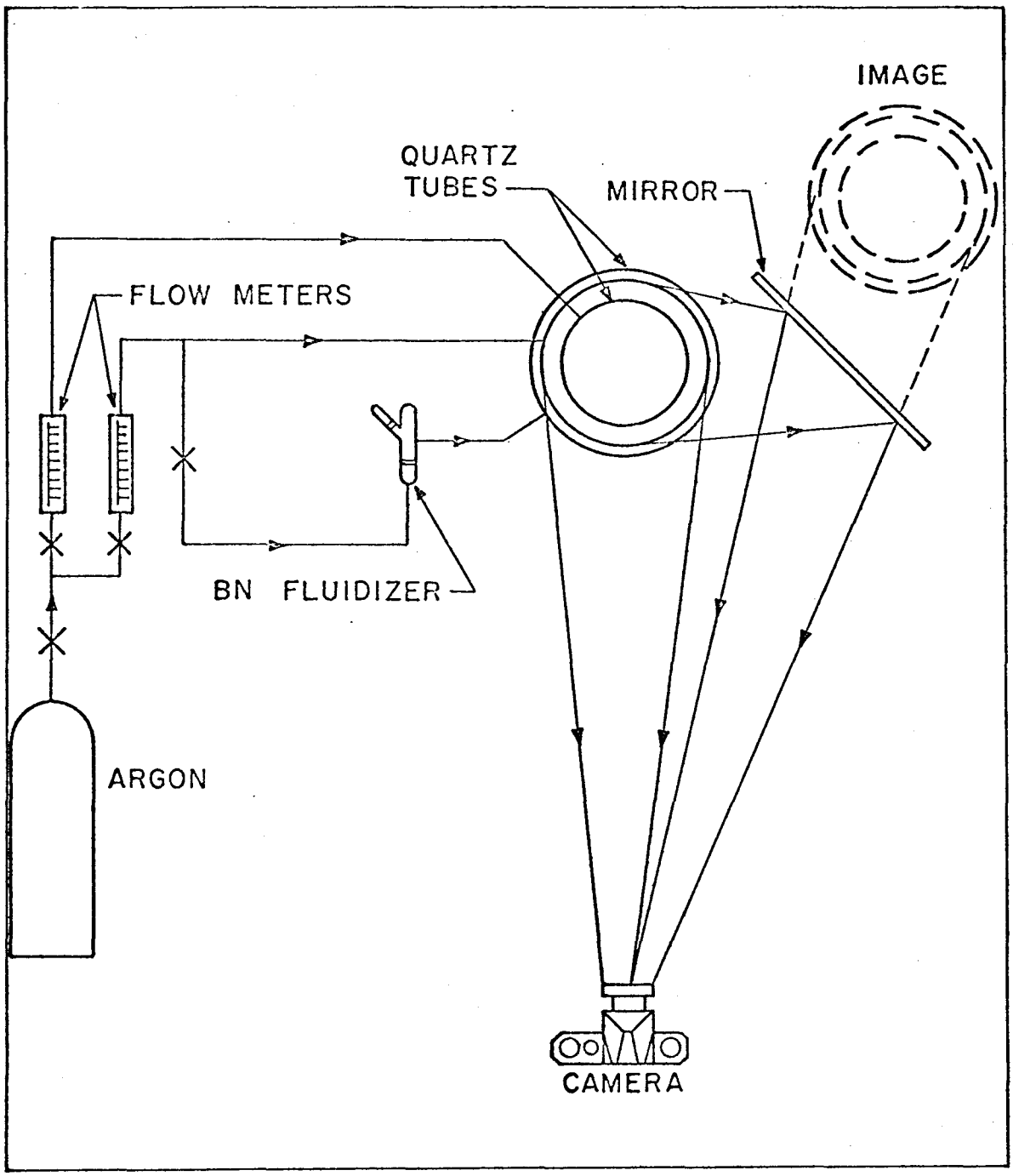

Figure I-6

Schematic diagram of the apparatus used for the measurement of velocities in the plasma jet by the use of particles of boron nitride.

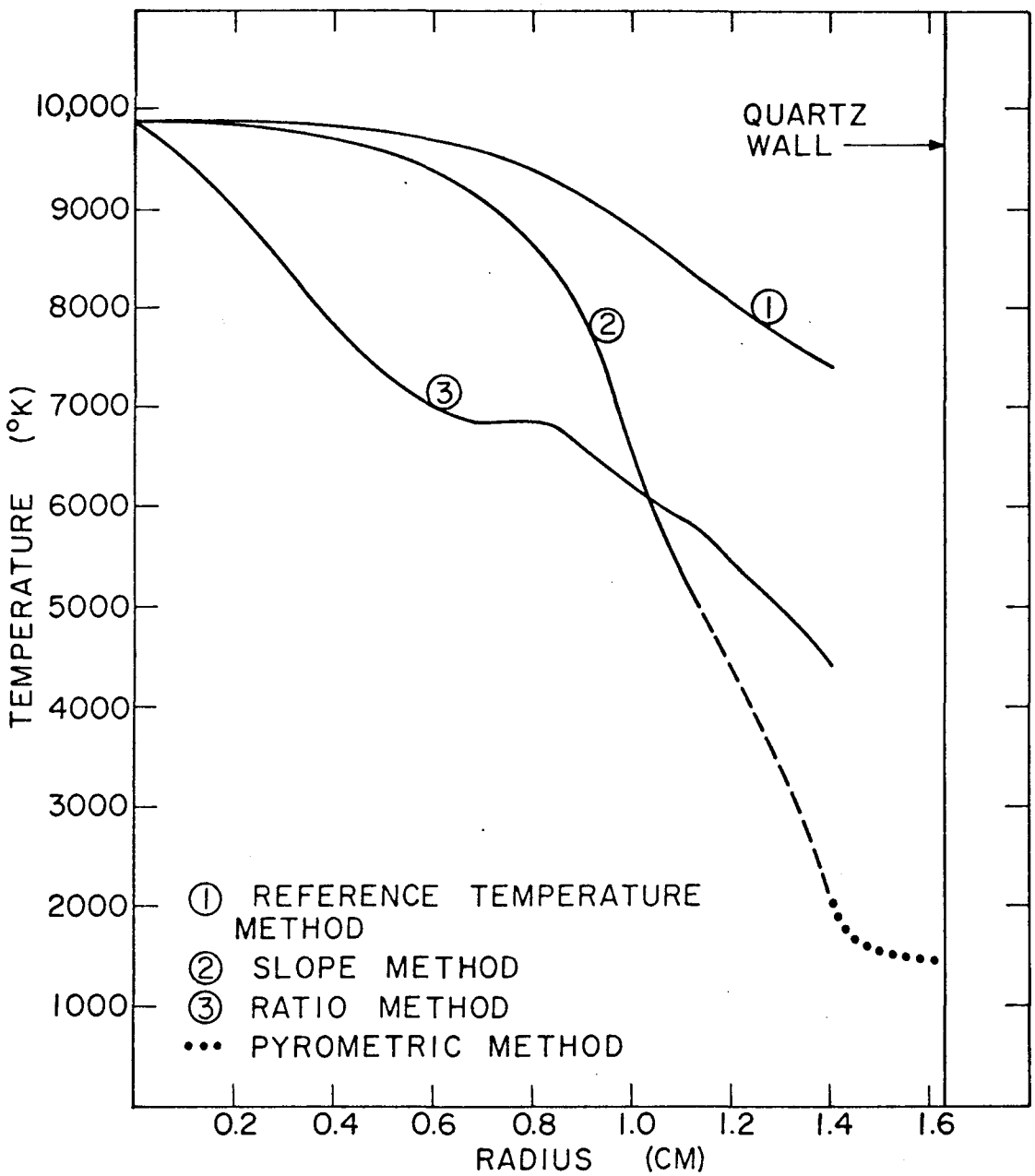

Figure I-7

Comparison between temperatures measured by different spectroscopic techniques.

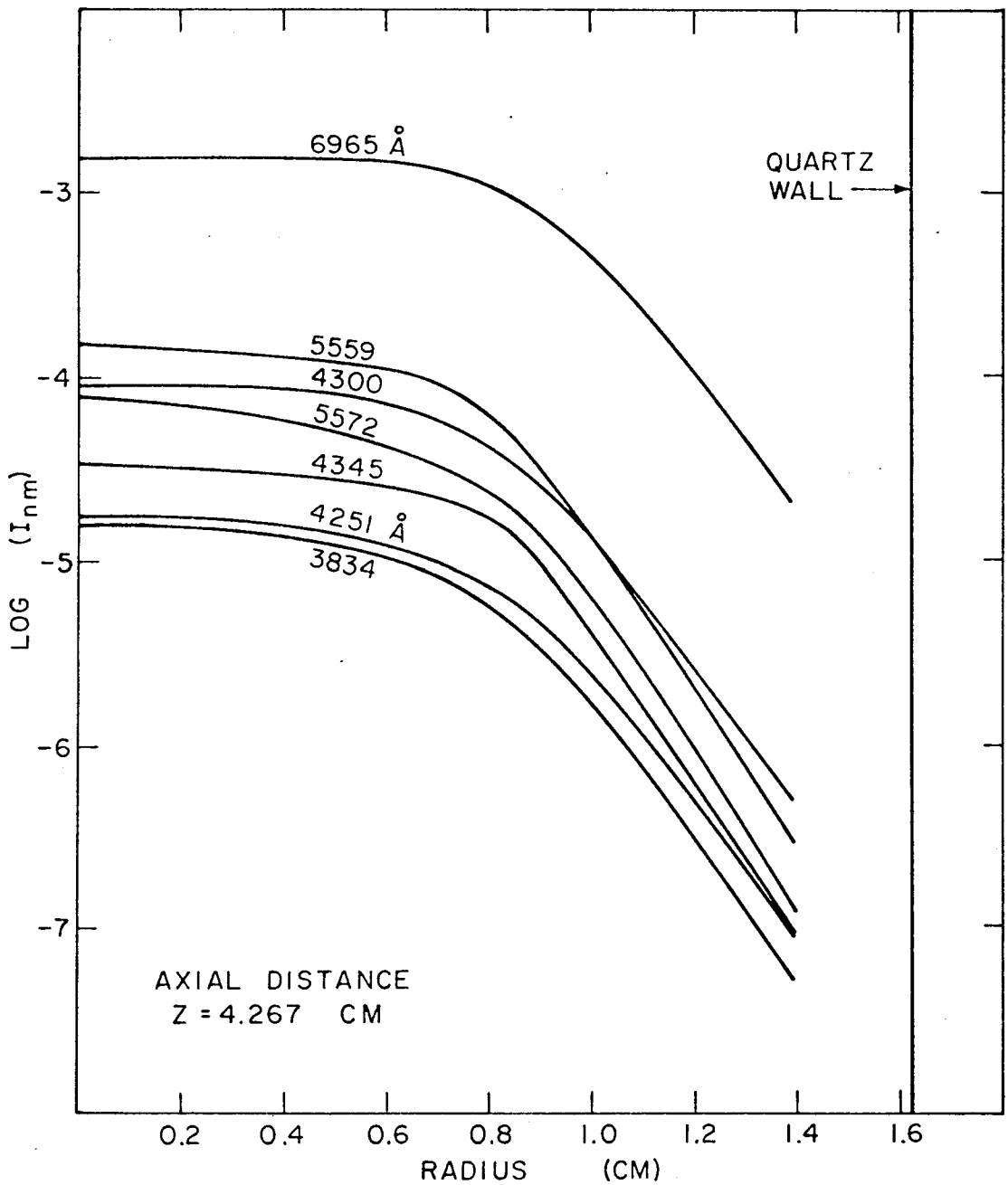

Figure I-8A

Radial intensity distributions for 7 lines of argon I. Intensity is expressed in absolute units as watts/cm^3. The axial distance is measured below the leading edge of the RF coil.

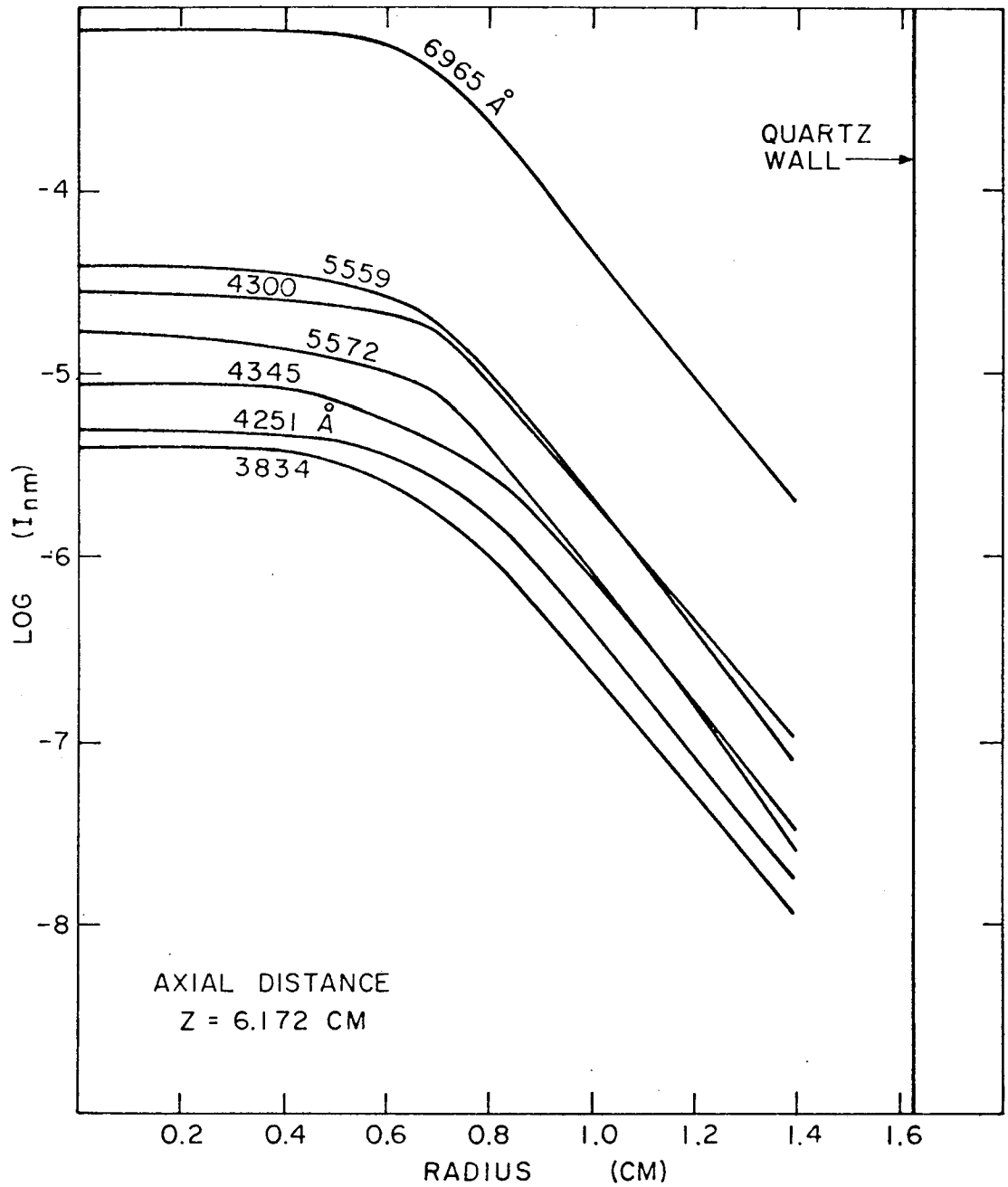

Figure I-8B

Radial intensity distributions for 7 lines of argon I. Intensity is expressed in absolute units as watts/cm^3. The axial distance is measured below the leading edge of the RF coil.

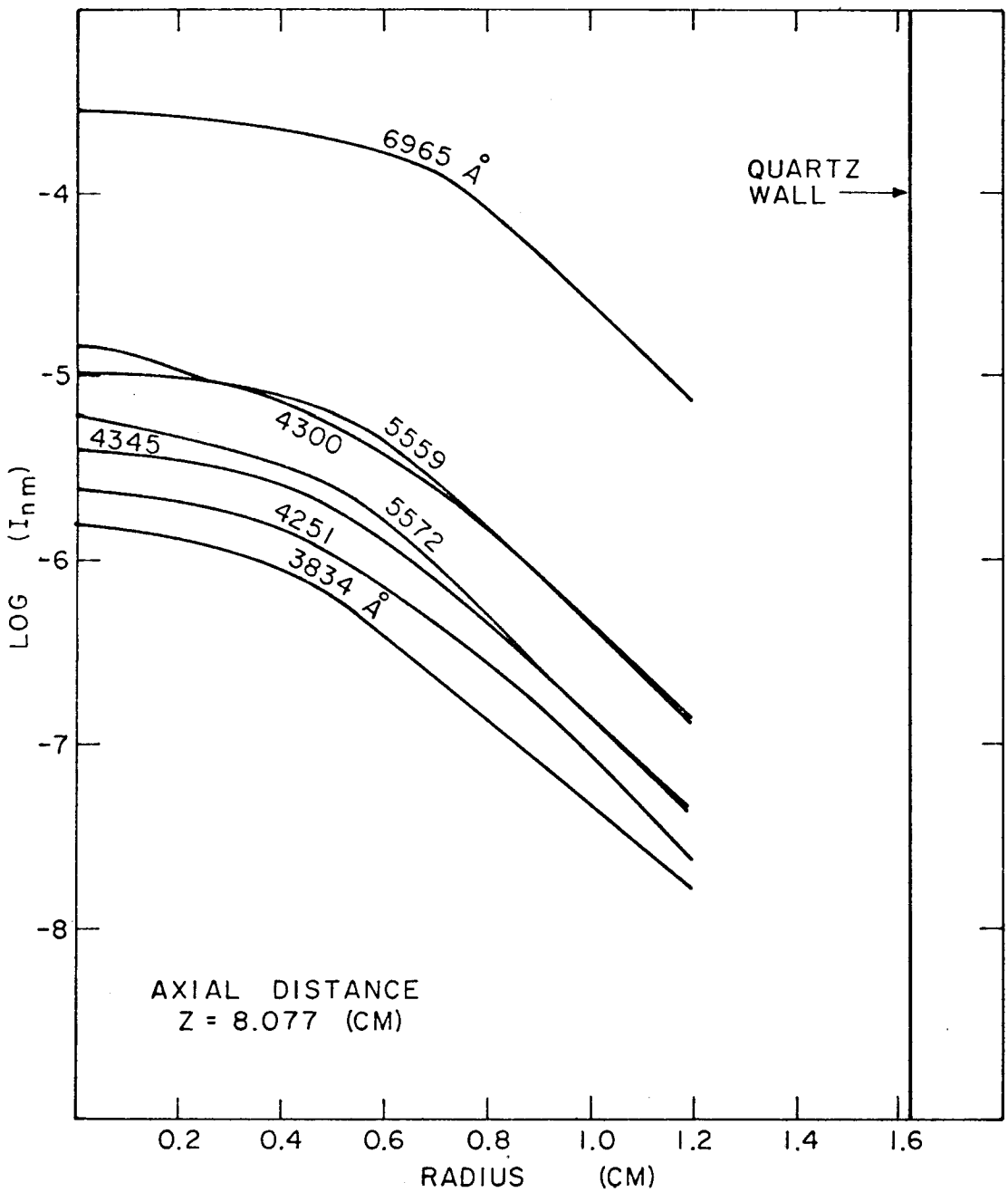

Figure I-8C

Radial intensity distributions for 7 lines of argon I. Intensity is expressed in absolute units as watts/cm^3. The axial distance is measured below the leading edge of the RF coil.

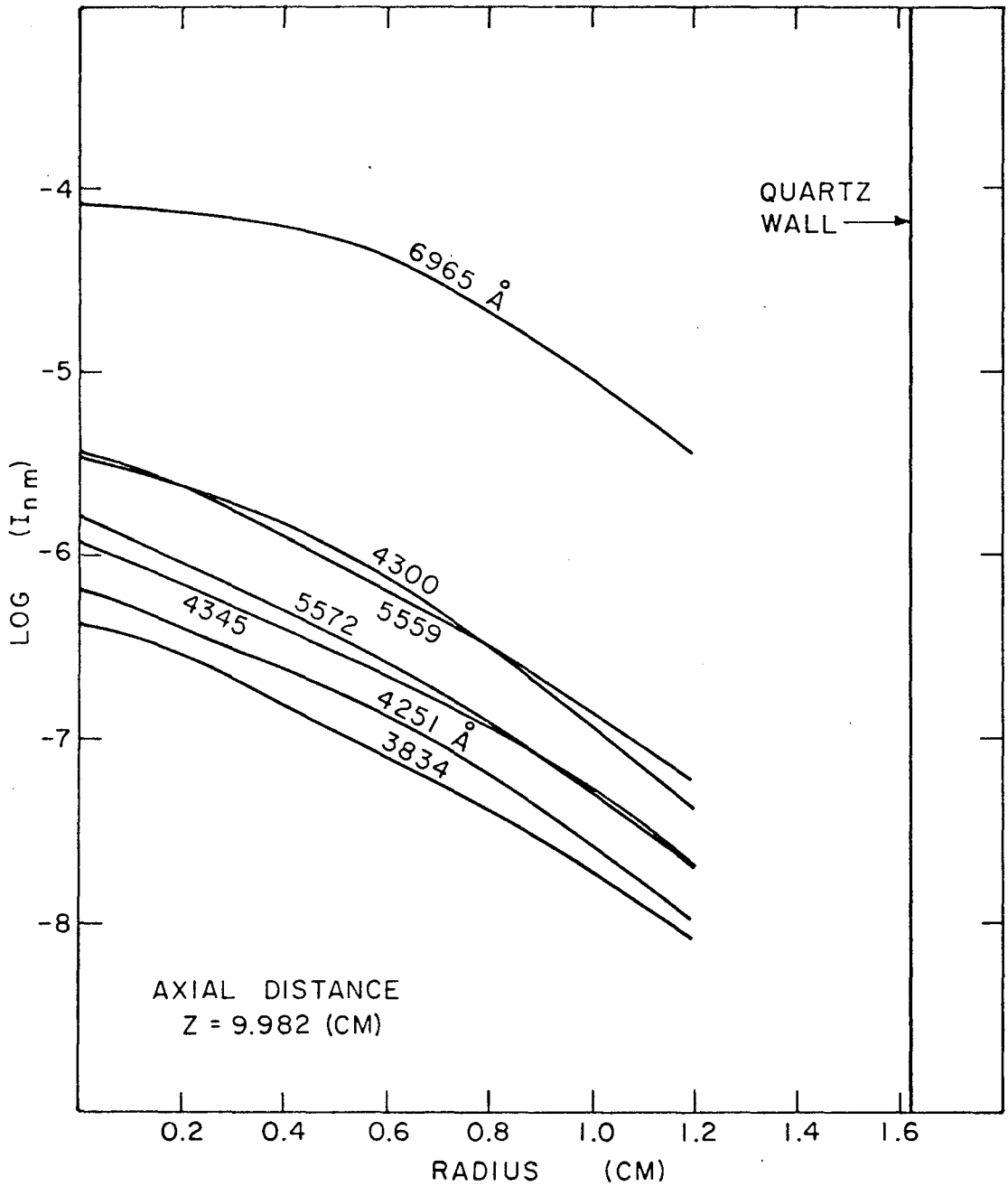

Figure I-8D

Radial intensity distributions for 7 lines of argon I. Intensity is expressed in absolute units as watts/cm^3. The axial distance is measured below the leading edge of the RF coil.

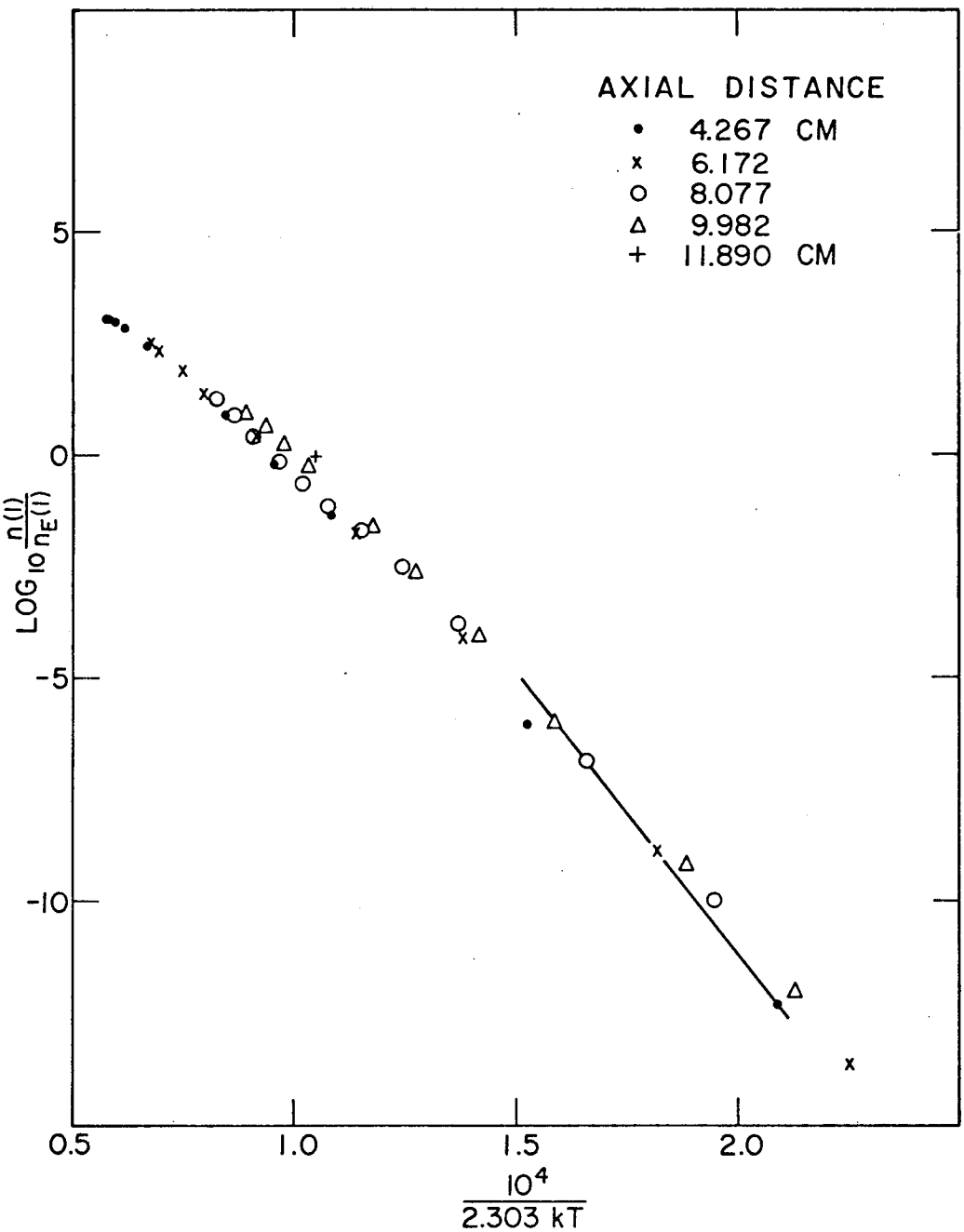

Figure I-9

Fractional departure of the ground state population from equilibrium expressed as a function of the parameter $\frac{10^4}{2.303kT}$. Axial distance is measured below the leading edge of the RF coil. The straight line shown indicates slope of the curve for a fixed electron density of 8×10^{12} particles/cm^3. Value of k is 0.69502 (cm)$^{-1}$(°K)$^{-1}$.

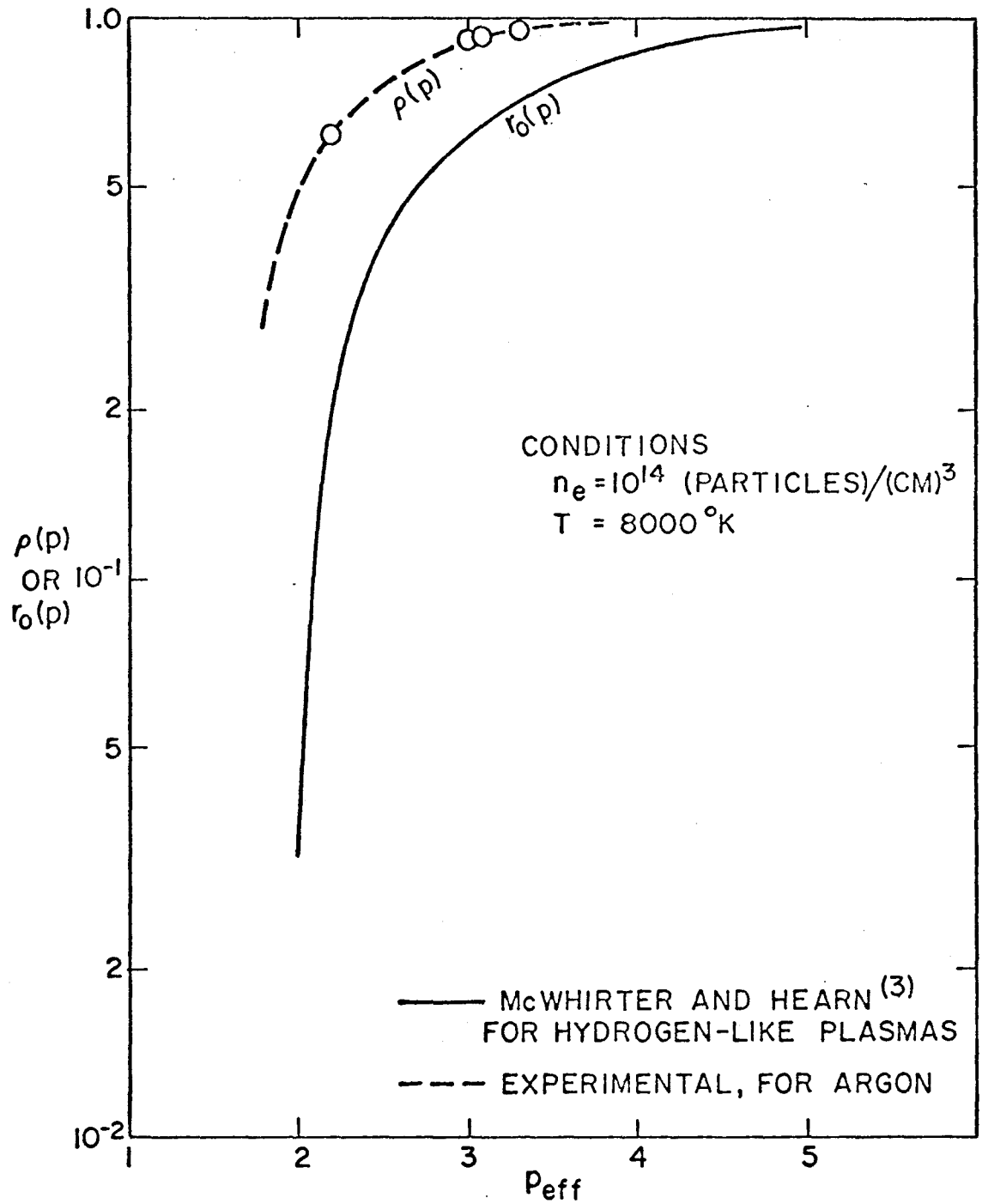

Figure I-10

Comparison between the experimentally determined fractional deviations from equilibrium for different effective principal quantum numbers and the collisive-radiative model adapted for argon.

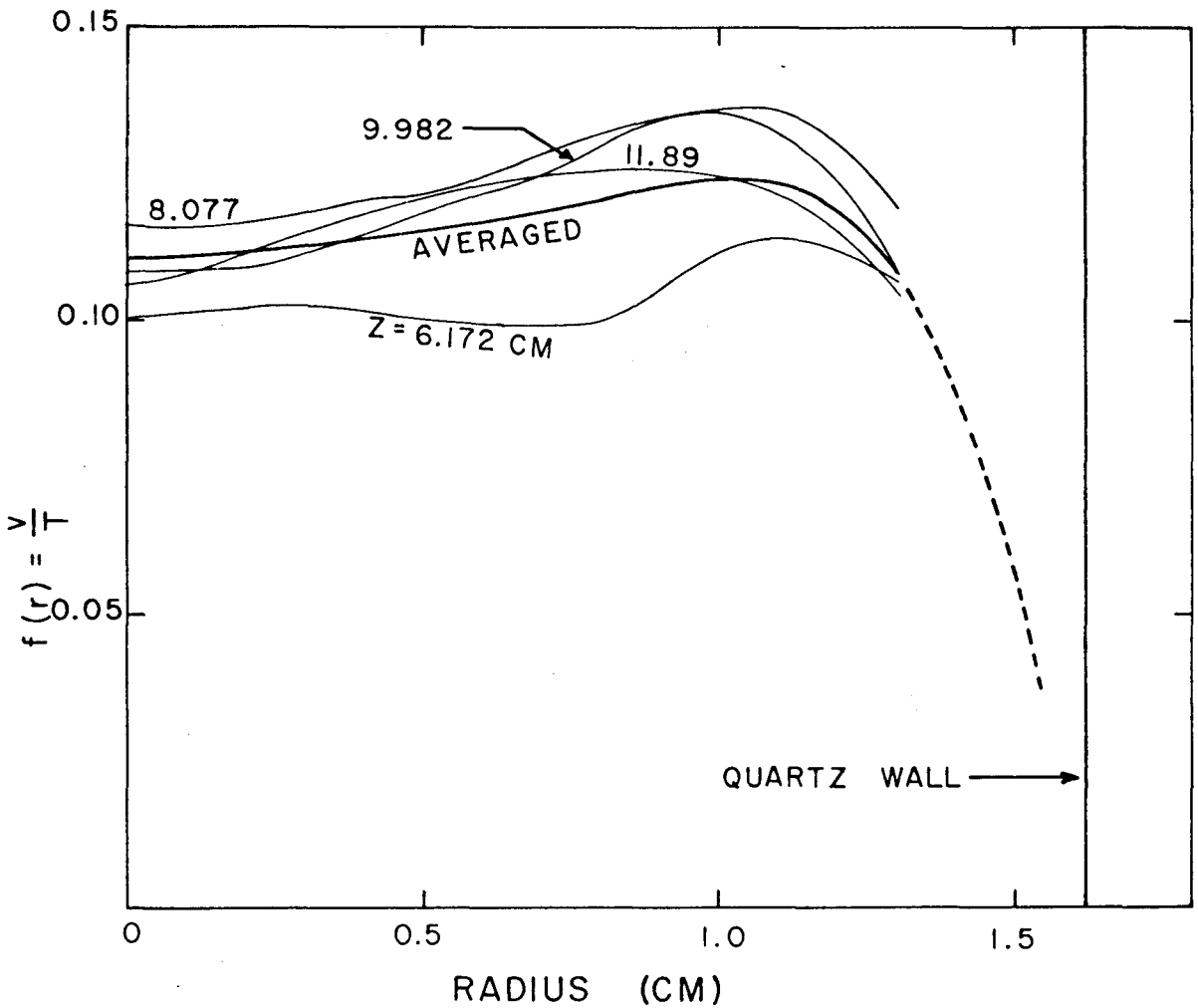

Figure I-11 Function f(r) calculated for different axial positions in the plasma jet.

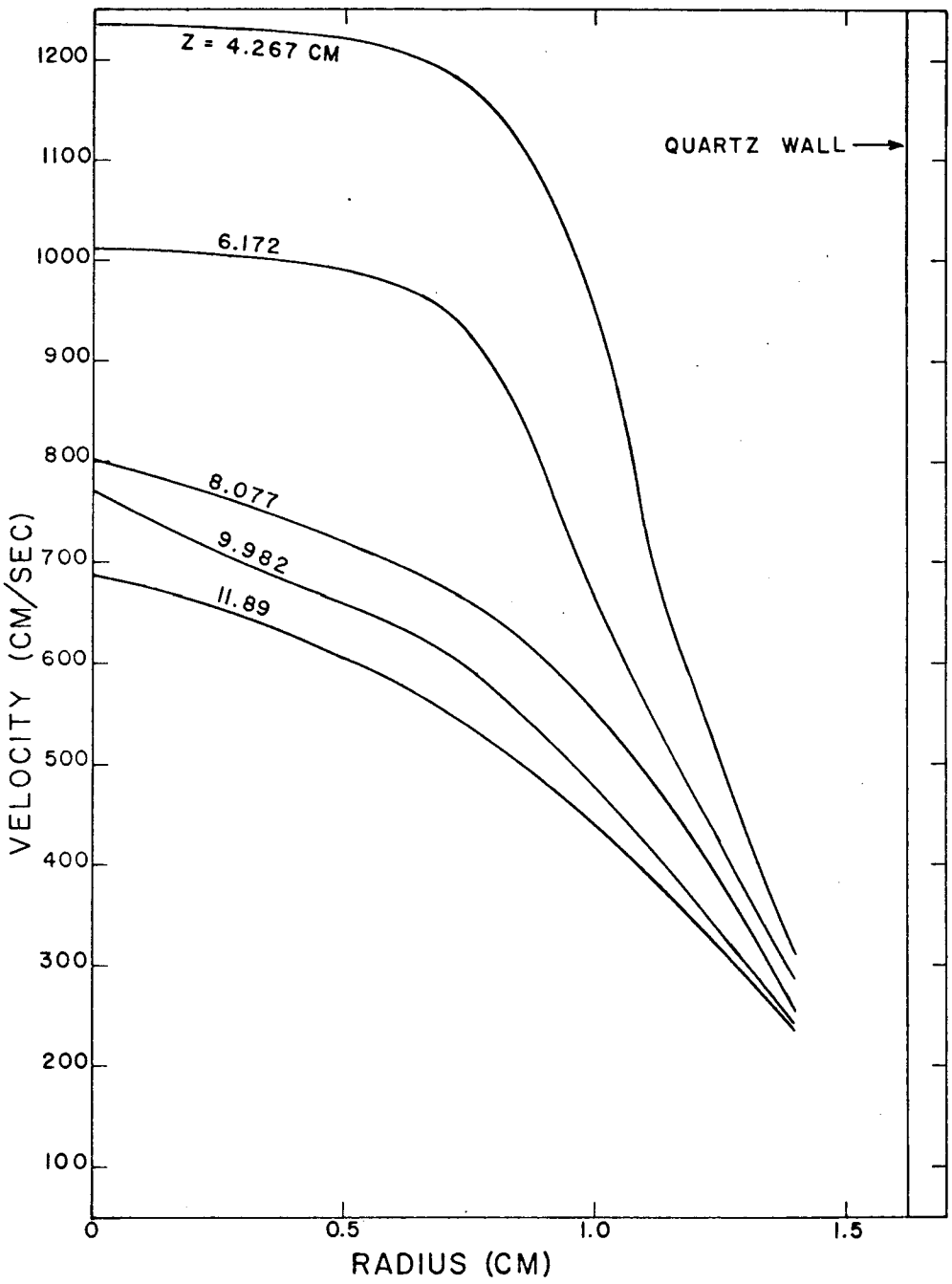

Figure I-12

Improved velocity distribution in the plasma jet obtained by the use of function f(r).

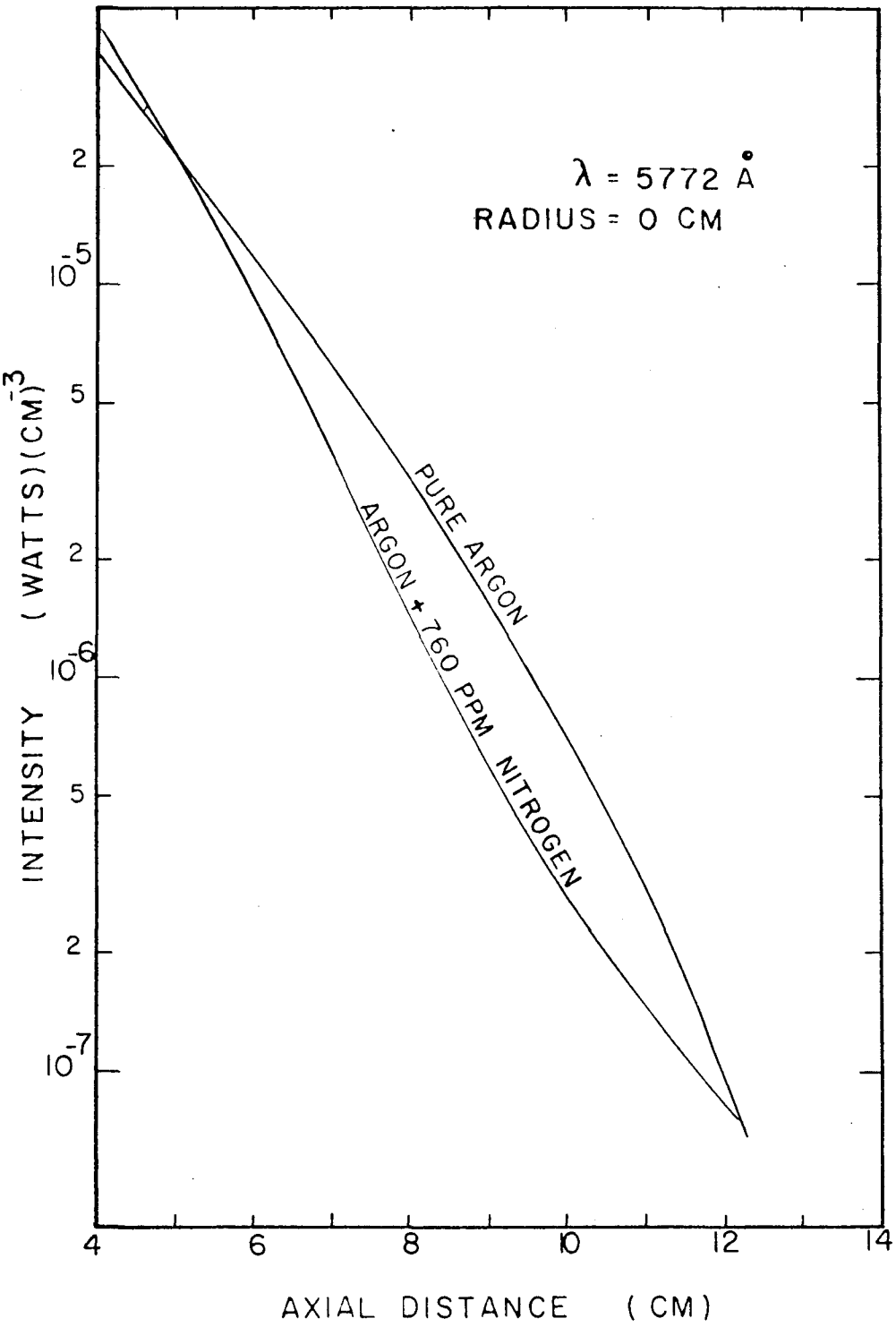

Figure I-13 Effect of impurity in argon on the line radiation from the plasma jet. The axial distance is measured below the leading edge of the RF coil.

SECTION II

DECOMPOSITION OF NO BETWEEN 1300 - 1750°K IN AN ARGON PLASMA

1. Introduction

The reaction under investigation was the decomposition of nitric oxide, represented by the equation:

$$2NO \underset{}{\overset{k'}{\rightleftharpoons}} N_2 + O_2$$

$$\Delta H_f^\circ = 21.6 \text{ kcal/g mol} \qquad \text{(II-1)}$$

in the presence of the argon plasma. The reverse reaction of formation of nitric oxide from nitrogen and oxygen is shown in equation (II-1), because the mechanisms of the two reactions were coupled. An important property of the decaying argon plasma was found in the previous section to be the presence of the excited species whose concentration was far above the value which would be obtained in the case of a complete thermodynamic equilibrium. On this basis, a distinction can be made between reaction (II-1) occurring under purely thermal conditions and the same reaction occurring in a plasma. Examples of the thermal reaction are: explosion processes, combustion processes and the initial reactions in a shock tube. On the other hand, the reactions occurring in the atmosphere struck by a thunderbolt, and the reactions of air used as an oxidant in an internal-combustion engine in

which an electric spark is used to ignite the fuel, are the cases of the plasma reaction.

The study of the kinetics of reaction (II-1) at higher temperatures began comparatively recently. In most cases, the reaction was studied under nearly thermal conditions, and yet, considerable discrepancy exists in the literature regarding the rates of the reaction. One of the earliest studies on the formation of nitric oxide was made by Haber and Coates[33] in a CO flame. They observed that the yields of NO were quite high compared with the thermodynamic-equilibrium value. They concluded that the reaction could not be explained on the basis of a thermal mechanism and that the electrons and the ions which were known to exist in the flame must have played roles in the reaction. Zeldovich[34] studied the reaction represented by equation (II-1) in explosions created by means of rapid combustion of hydrocarbons with air, in the range of temperatures between 2000 - 3000°K. He refuted Haber's claim of the non-thermal character of the reaction of formation of NO, by proposing a chain mechanism involving atoms of oxygen and nitrogen as follows:

$$N_2 + O \rightleftharpoons NO + N \quad - 47 \text{ kcal/g mol}$$

$$O_2 + N \rightleftharpoons NO + O \quad + 4 \text{ kcal/g mol}$$

He assumed that the nitrogen and oxygen atoms were in steady state, and the oxygen atoms were in equilibrium with the oxygen molecules. His results showed that the decomposition of nitric oxide was apparently second order in NO, and the apparent activation energy was 86 kcal/g mol. Vetter[35] studied the decomposition reaction in a flow tube between 1500 - 1900°K, and he obtained results which were second order with respect to NO. He considered a total of 10 reactions including the four (forward and backward) proposed by Zeldovich. He showed that excess O_2 decreased the rate of decomposition of NO. In his analysis however, he neglected the temperature and concentration gradients within the flow reactor. Kaufman and Decker[36] also studied reaction (II-1) in the presence of oxygen at about 1600°K. Wise and French[37] studied reaction (II-1) in a static flask between 872 - 1275°K and pointed out that the reaction is heterogeneous with an activation energy of 12 kcal/g mol at temperatures below 1000°K and above 1600°K, it was homogeneous and second order with respect to NO, having an activation energy of 82 kcal/g mol. Kaufman and Kelso[38] studied the reaction by a static method between 1170 - 1530 °K. They gave the value of the activation energy for the second order decomposition of NO as 63.8 kcal/g mol. They found no effect of addition of a four-fold excess of nitrogen on the rate of the reaction.

Freedman and Daiber[39] studied reaction (II-1) in the

presence of argon in a shock-tube between 3000 - 4400°K. They concluded that the initial rate of decomposition of NO proceeds according to the sum of the following two steps:

$$NO + A \longrightarrow N + O + A \qquad \text{(II-2)}$$

$$2NO \longrightarrow N_2 + O_2 \qquad \text{(II-3)}$$

After the steady-state concentrations of the atoms have been established, the Zeldovich chain mechanism would prevail. Wray[40] studied reaction (II-1) for NO-A mixtures rich in NO in a shock-tube between 3000 - 8000°K. His data suggested that Kaufman and Kelso's values for k' were lower by a factor of 10, when extrapolated to higher temperatures. Wray[41] has made a critical survey of the reactions involving nitrogen and oxygen at high temperatures.

The method of concentration measurement in the previous studies has been either chemical or that based on absorption spectroscopy. In either case, NO was measured by converting it to NO_2 with excess oxygen and then analysing the amount of NO_2. The present study differed from the previous studies in the following manner:

a. A flow method was used and the gradients of concentration and temperature were accounted for.
b. The method of concentration measurement was based on a direct analysis of NO by gas-chromatography.
c. Concentrations of NO below 0.5 per cent were used. A

gas-chromatographic method of analysing the composition of the products enabled low concentrations of NO to be determined accurately.

d. The effect of N_2 on decomposition of NO was evaluated.

e. Electrons, ions and excited atoms of argon were present in the reactor. The effect of these constituents of a plasma on chemical reactions has not been studied before.

2. Experimental Apparatus

The main experimental apparatus has been described in Section I. Changes were made in the quartz tube containing the argon plasma to enable injection of the reactants into the plasma stream. Figure II-1 shows a picture of the reactor assembly. A quartz jacket surrounded the main tube, which extended 31.5 cm below the leading edge of the RF coil, the jacket being 12.5 cm below the coil. The gas was injected through 8 orifices 0.3 mm in diameter and equally spaced within the jacket on the periphery of the main tube. The number, size and position of the orifices were governed by the required velocity of the jets of the injection gas.

A mixing manifold was constructed for the injection gas. Rotameters were used for measuring the flow rates of the reactants. These rotameters were calibrated using a bubble flowmeter for flows upto 300 ml/min and an inverted cylinder filled with water for higher flow rates. A correction was applied for the saturated vapor pressure of water at

the prevailing temperature. The mixing system is shown in Figure II-2.

The NO used in this study was obtained from the Matheson Company and was stated to be 99.5 per cent pure by the suppliers. The major impurities were N_2 and N_2O, and their presence was not expected to affect the results. The argon gas was obtained from the Linde Corporation and had stated impurities of 40 ppm which were further reduced by the process described in Appendix A-2.

Sampling of the gas was done on a continuous-flow basis. A mullite tube, which was 1/32 in O. D./0.02 in I. D. was inserted into the reactor through slightly oversize holes at locations which were 2.064, 4.128, 6.102, 7.883 and 9.863 cm below the plane of the injection holes. Mullite was chosen because of its high softening point (1900°K) and low reactivity with oxygen. Insertion of the probe was measured with previously made markings at 2.5 mm intervals. The sampling holes not in use were plugged with quartz rods with round tips which were carefully ground to prevent leakage of the atmospheric air into the reactor. Details of the sampling section of the reactor can be seen in Figure II-1.

The sample gas was carried to the gas-chromatographic analyzer by means of 1/16 in O. D. stainless-steel tubing, 22 ft. long. A 4 in piece of Teflon tubing provided flexible connection between the stainless-steel tubing and the probe. In order to fill the sample loop of the

chromatograph with the sample gas, a steady suction was created by means of a water-jet ejector. The pressure at the sample loop was measured to 0.1 in Hg with a mercury manometer, and a correction for the same was applied in calculating the concentrations. Typically, a negative pressure of 2 in of mercury was required to maintain a flow rate of 25 ml/min through the sampling system. A schematic diagram of the sampling system is shown in Figure II-3.

3. Gas-Chromatographic Analysis

It was necessary to separate N_2 and NO from argon in the course of analysis of the products of decomposition of NO. A basic problem associated with the analysis of NO by gas chromatography was the tailing of the NO peak which reduced the sensitivity of the instrument and made a quantitative analysis difficult. Sakaida et al[42] carried out the separation of NO from N_2 on a silica-gel column with a limited success. Trowell[43] reported a good separation on 13X-molecular sieve, but the life of the column was limited to a few months. Dietz[44] eliminated the tailing of the NO peak by using 5A-molecular sieve. In all the above attempts, an extremely careful pretreatment of the column before its use was essential, and the reproducibility of the performance of the column was poor. The pretreatment varied from a rapid flushing of the column with a stream of helium at 250°C[43] to passing NO and O_2 for an extended time[44].

Hollis[45] could separate NO from a mixture containing O_2, A, N_2 and NO with some success on microporous polymer beads, commercially known as Porapak-Q. Improved results were obtained by the use of a longer column[46], but the resolution between NO, A, N_2 and O_2 was not satisfactory.

Experiments were done with Porapak types P, Q, R, S and T which have different degrees of polarity. It was found that Porapak-T gave the best results in the separation of NO-A-N_2-O_2 mixture. Oxygen was however unresolved from argon.

Initial experiments with a chromatograph constructed in the laboratory using a standard thermal-conductivity detector confirmed the observations of Wilhite and Hollis[46] that the dead space within the instrument was responsible for the loss of resolution between the peaks. A Carle model 8000 chromatographic unit with a thermistor type, micro-thermal-conductivity detector and a micro-sampling valve which had a very low internal volume proved satisfactory in this application.

The column was a 23-ft length of stainless-steel tubing having an I. D. of 0.1 in. The tube was washed with reagent-grade acetone and dried with air before packing, to remove residual oil and grease. The tube was packed with 35 ml of 80 - 100 mesh Porapak-T and the two ends were plugged with short lengths of glass wool.

No pretreatment of the column was necessary. On the contrary, heating the column above 120°C for more than 2 hr under a stream of helium seemed to deteriorate the separation of NO. Excessive tailing of the NO peak was the result. Helium having 99.998-per-cent purity was used as the carrier gas. Further drying of the carrier gas did not improve the performance of the instrument. The flow rate of the carrier gas was maintained at 30 ml/min requiring a pressure drop of 50 psia. The flow rate of helium thrcugh the reference channel of the instrument was limited to 50 ml/min by means of a dummy column. The imbalance of flow rates between the two sections of the detector did not seem to affect the base line of the output, which was more sensitive to the changes in the ambient temperature. The output of the bridge circuit associated with the detector was recorded on a potentiometric recorder which had a full-scale sensitivity of 1 mV.

The size of the sample was 0.2 ml. The column was operated at 30°C, but the inlet section was designed to operate approximately 15°C higher than the column. The detector operated at 165°C which assured the optimum performance from the detector.

Calibration of the chromatograph was done by the use of the mixing manifold shown in Figure II-2. Mixtures having concentrations as low as 200 ppm could be prepared with an

accuracy of 4 per cent. The peak height was used as the measure of concentration resulting in nearly linear relationship between the peak height and the concentration, because the shape of the peak remained almost triangular.

A sample chromatogram for the NO-N_2-A system is shown in Figure II-4A and that of N_2-O_2 system is shown in Figure II-4B. The calibration curves for NO and N_2 are shown in Figures II-5 and II-6 respectively. Calibration was repeated once in a week for three weeks and a standard deviation of less than 4 per cent was obtained.

The limit of detection for NO was 60 ppm based on 1/2 division of the chart and for N_2, it was 25 ppm.

4. Experimental Procedure

Two separate experiments were carried out. In the first experiment, the flow of the injection gas consisted of 75 ml/min of NO + 820 ml/min of A measured at S. T. P. In the second experiment, the aim was to evaluate the effect of excess N_2 on decomposition of NO. The flow of the injection gas consisted of 75 ml/min NO + 400 ml/min N_2 + 420 ml/min of A. By maintaining the total flow rate constant, the same flow conditions in the reactor were maintained. There could be some change in the flow conditions in the case of excess N_2 because of diffusion of N_2, but this effect was small and did not affect the validity of the results. Due to the highly laminar nature of the plasma jet, mixing between

the injection stream and the plasma stream was not complete. The purpose of argon in the injection gas was to maintain sufficient linear velocity of the jets through the orifices to reach the axis of the plasma stream.

In both experiments, samples of the reaction mixture were taken at radial increments of 2.5 mm starting from the axis and going upto 12.5 mm from the axis. The procedure was repeated three times at each axial position, and the results at a given position agreed within ±4 per cent in most cases. Measurements on concentrations of N_2 and NO were taken at 5 axial positions in the above manner.

The temperatures in the reactor were measured by the pyrometric technique described in Section I. The flow of the gas in the mullite probe was stopped during the temperature measurements to avoid errors due to cooling of the probe. Temperatures were measured at the same points in the reactor as for the concentration measurements. A blank run without any injection was also taken for calculating velocities.

The atmospheric pressure was 74.0 ± 0.05 cm Hg and the ambient temperature was 22 ± 1°C during the experiments.

5. Analysis of Data

The measured peak heights for N_2 and NO were converted to mole fractions with an assumption of ideal behavior of the gases. Figures II-7 and II-8 show the distribution of mole fraction of NO and N_2 for the two experiments,

respectively. The results are shown as smooth curves drawn through the experimental data points.

The measured brightness temperatures of the mullite tube were converted to absolute temperatures, assuming $\epsilon_{\lambda T}$ = 0.44 and τ_{λ} = 0.9 (see Appendix A-1). The temperature distributions in the reactor for the two experiments are shown in Figures II-9 and II-10 respectively. The temperature distribution without injection of any gas is shown in Figure II-11.

The velocity distribution required to resolve the concentrations as a function of time was obtained by the use of function f(r) as described in Section I, using the temperature distribution shown in Figure II-11.

To obtain the rates of decomposition as a point function, the equation of continuity for NO was solved in a manner described in Section I in connection with recombination of electrons. For example, n_e and D_a in equation (I-20) were replaced by (NO) and D_{NO} respectively. The diffusion coefficient for NO was expressed as:

$$D_{NO} = 2.11 \times 10^{-5} T^{1.667} \text{ cm}^2/\text{sec}$$

using the Chapman-Enskog theory[47]. As the result of detailed calculations including the effect of diffusion, it was determined that the diffusional mass flux of NO never exceeded 2 per cent of the bulk transport of NO in the axial

direction upto a radius of 1 cm in the reaction zone. Therefore, the diffusional term in the equation of continuity was disregarded. The analysis of the data was limited upto the radius of 1 cm. Validity of the results was independently verified by comparing the final rate constants with the case which included diffusion. It was found that the diffusional term only increased the R. M. S. error of the rate constants without improvement in the accuracy of the results. This was mainly because of the second order partial differential coefficients involved in the diffusional term which gives rise to numerical noise.

6. Results and Discussion

In the sampling procedure described above, an important assumption was embedded. The reactions were assumed to be "frozen" at the time of sampling. Extensive calculations of Amman and Timmins[48] indicated that the composition of the sample would not alter significantly if the initial temperature was below 3000°K. The quenching rate in the present experiment was at least 10^5 °K/sec which would assure freezing of the reactions that are fast at higher temperatures.

A possible reaction which could be appreciable at near room temperature was:

$$NO + 1/2\ O_2 \longrightarrow NO_2$$

Calculations based on the rate data presented by Morrison et

al[49] showed that the decrease in NO concentration by the above reaction would be less than 5 per cent in 2.5 min if the initial concentration of NO were held below 0.55 per cent. The time lag between the reactor and the gas chromatograph was less than 10 sec, and the estimated time for the separation of NO from the O_2 formed as the result of decomposition was 1.5 min. Therefore the effect of the above reaction can be safely neglected in the present experiment. Based on the standard deviation in the calibration and in the samples, the error in the concentration measurements was estimated at ±5 per cent.

In the measurement of temperatures, a systematic error of about 5 °K could arise from uncertainty in the value of the emissivity of mullite. Formation of a gas film on the probe would slightly lower the values of the measured temperatures, but error due to this effect was not expected to be larger than 10 °K. We may therefore place the maximum error in temperatures at 15 °K.

Slight error in the velocities could arise due to cooling of the plasma by the injected gas. The injection was less than 6 per cent on the overall basis and the cooling effect was compensated for by the use of the function f(r) in conjunction with the temperature profiles without injection. The velocities were known within ±10 per cent, the maximum error being near the point of injection.

The leakage of air from the surroundings into the reactor through the gap between the probe and the hole in the quartz wall was about 300 ppm. This leakage did not influence the validity of the final results in appreciable manner, because the total amount of N_2 was measured at every point.

In the first analysis, the measured rates of decomposition of NO were correlated to the concentrations of NO and the temperatures by means of a least-squares fit in the following form:

$$-\frac{d(NO)}{dt} = A\, e^{-\frac{E}{RT}} (NO)^n \qquad \text{(II-4)}$$

the values of the parameters being:

		Experiment No.1	Experiment No.2
A	$cm^3/(g\ mol)(sec)$	1.9×10^5	1.07×10^9
E	cal	8453	9807
n		1.33	1.85

Thus the order of the reaction with respect to NO was always less than 2, but greater than unity. This observation immediately ruled out reactions II-2 or II-3 as the possible mechanism of decomposition of NO. That the effect of nitrogen was to reduce the rate of decomposition of NO could be seen by comparing the concentration profiles of NO in the presence and absence of excess N_2, as seen in Figures II-7A and

II-7B. The increase in the value of n from 1.33 to 1.85 with increase in the concentration of N_2 intuitively suggested a rate expression of the form:

$$-\frac{d(NO)}{dt} = \frac{a(NO)^2}{b(N_2) + (NO)} \qquad \text{(II-5)}$$

where a and b are functions of the temperature only. It is to be noted at first that the rates of decomposition of NO obtained in the argon plasma were higher by approximately 5×10^4 than the rates obtained with pure NO or NO diluted in argon[41]. This observation substantiates Haber's hypothesis of non-thermal character of the reaction in the presence of electrons and ions. It remains to be seen in which manner the electrons and ions may influence the reaction rates.

Following Zeldovich, the chain propagation steps were written as:

$$NO + N \underset{k_{-1}}{\overset{k_1}{\rightleftharpoons}} O + N_2 \qquad \text{(II-6)}$$

$$NO + O \underset{k_{-2}}{\overset{k_2}{\rightleftharpoons}} N + O_2 \qquad \text{(II-7)}$$

Assuming (N) and (O) to be in the steady state, from equations (II-6) and (II-7):

$$-\frac{d(NO)}{dt} = \frac{2(N)}{k_{-1}(N_2) + k_2(NO)} \left\{ k_1 k_2 (NO)^2 - k_{-1} k_{-2} (O_2)(N_2) \right\} \qquad \text{(II-8)}$$

The concentration of NO in the present experiment was at least 40 times its equilibrium value[50], so that one can neglect the rate of the reverse reaction shown in equation (II-8). In that case, equation (II-8) reduces to:

$$-\frac{d(NO)}{dt} = \frac{2k_1(N)(NO)^2}{(k_{-1}/k_2)(N_2) + (NO)} \qquad \text{(II-9)}$$

Consistent with the assumption of steady state for (N), the form of equation (II-9) is identical to that of equation (II-5)

A non-linear-least-squares fit to the data encompassing both the experiments (i. e. with and without excess N_2) gave the following best values of the parameters in equation (II-9):

$$(N)k_1 = 1.73(\pm 0.2) \times 10^3 \, e^{-\frac{13900(\pm 700)}{RT}} \qquad \text{(II-10)}$$

$$\frac{k_{-1}}{k_2} = 2.26(\pm 0.17) e^{-\frac{4325(\pm 300)}{RT}} \qquad \text{(II-11)}$$

The experimental data covered the following conditions:

$$1.2 \times 10^{-3} < x_{NO} < 5.5 \times 10^{-3}$$

$$6.0 \times 10^{-4} < x_{N_2} < 2.7 \times 10^{-2}$$

$$1300°K < T < 1750°K$$

The indicated limits of error were obtained from the standard deviation of the non-linear-least-squares fit, for a

95-per-cent-confidence level. The standard error of the fit was ±28 per cent.

7. The Role of Atomic Nitrogen

It may be observed in equation (II-9) that the rate of decomposition of NO is directly proportional to the concentration of atomic nitrogen which appears as an independent variable. In general, the concentration of atomic nitrogen which acts as a chain carrier can be written as[51]:

$$(N) = \left(\frac{r_i}{r_b}\right)^{\frac{1}{w}}$$

where r_i and r_b are the rates of chain initiation and chain breaking steps in which the term (N) has been excluded and w is the order of the chain breaking step with respect to (N). The apparent activation energy for the chain propagation reaction can be expressed as:

$$E = E_p + \frac{1}{w}(E_i - E_b)$$

where E_p, E_i, E_b are the activation energies of the chain propagation, chain initiation and chain breaking steps respectively. The most likely mechanism of chain breaking is three-body-atomic recombination, $N + N + M \longrightarrow N_2 + M$ in which case E_b will be close to zero, and w will be equal to 2, so that:

$$(N) = \sqrt{\frac{r_i}{r_b}} \qquad \text{(II-12)}$$

$$E = E_p + \tfrac{1}{2}E_i \qquad \text{(II-13)}$$

Zeldovich[34] considered the effect of (O) for which similar equations can be developed. Let the activation energies corresponding to k_1, k_{-1} etc. be denoted by E_1, E_{-1} etc. Taking the value of the overall activation energy for reaction (II-1) to be 64 kcal/g mol as quoted by Kaufman and Kelso[38] and the activation energy for the formation of atomic oxygen to be 59 kcal/g mol, it can be deduced from Zeldovich's analysis that $E_1 + E_2 - E_{-2} = 64 - 59 = 5$ kcal/g mol. Assuming the principle of microscopic reversibility for reaction (II-7), $E_2 - E_{-2} = 4$ kcal/g mol, so that $E_1 = 1$ kcal/g mol. After consideration of equations (II-10) and (II-12), one can conclude that the activation energy for the chain initiation reaction for the nitrogen atoms in the present experiment must have been close to 13 kcal/g mol. This value of E_i is far less than the heat of formation of atomic nitrogen which is 112.5 kcal/g mol. In that case, a large rate of formation of atomic nitrogen and corresponding to equation (II-12), a large steady-state concentration of atomic nitrogen can be expected.

The small value of E_i in the plasma can be explained on the basis of the non-thermal character of the chain-

initiation reaction. In the argon plasma, the rate of formation of nitrogen atoms by means of super-elastic collisions with excited atoms which are present in a supersaturated state will supersede the mechanism of activated collisions in which only a minute fraction of the atoms and molecules possess the requisite kinetic energy to break the molecular bond. The energy of excitation of the argon atoms and ions is between 11 - 15.5 eV which far exceeds the activation energy for the formation of atoms from molecules.

It was noted in Section I that the decaying plasma contains a supersaturated system of excitation population and electron population. According to Figure I-9, the degree of excitation in the argon plasma was approximately 10^{15} times its thermodynamic equilibrium value at about 2000°K, and the corresponding value of electron density was about 10^{9} - 10^{10} particles/cm^3. The decay of the excitation population in argon was noted in Section I to be coupled with the recombination of electrons with ions. It was concluded in that section that an important process of recombination of electrons in the presence of molecular gases was the dissociative-molecular-ion mechanism such as:

$$N_2 + A^+ \longrightarrow N_2^+ + A$$

$$N_2^+ + e \longrightarrow N^* + N \qquad \text{(II-14)}$$

In addition, the large population of the lower excited

states close to the metastable level in argon might also cause reactions of the type:

$$N_2(X^1\Sigma_g^+) + A(1s_5) \longrightarrow N\ (C^3\Pi) + A(1p_o)$$

$$N_2(C^3\Pi) + A(1p_o) + KE \longrightarrow N(4S^o) + N(^2D^o) + A(1p_o) \qquad \text{(II-15)}$$

An evidence for the effect of the N_2^+ ions on the decay of the plasma was presented. The presence of $N_2(C^3\Pi)$ molecules in quantity above its equilibrium value could be deduced from the selective nature of the $N_2(2\ +ve)$ radiation for which a spectroscopic evidence will be presented below. Reactions (II-14) and (II-15) would yield atomic nitrogen in quantity far above its equilibrium value, due to the effectiveness of the collisions of the excited atoms of argon.

Spectroscopic evidence for the presence of a large amount of atomic nitrogen above its equilibrium value supported the above hypothesis. Spectrograms of the reaction mixture taken with a grating type 1.5 m spectrograph on Kodak 2475 film are shown in Figures II-12A through II-12C. Figure II-12A shows a spectrum of argon I for reference, taken at some bright region of the plasma. Figures II-12B and II-12C are the spectra of the reaction mixture for experiment numbers 1 and 2 respectively. The time of exposure was 2 hr, and the film was processed at an equivalent ASA speed of 2000 for Figures II-12B and II-12C. The position in

the reactor shown in the slides was approximately the same for both slides, which was from 2 cm to 6.8 cm below the plane of injection and on the center line of the jet. Some strong lines of argon I are marked in Figure II-12A. In Figures II-12B and II-12C, a fairly strong line of nitrogen I at 6708 Å which arises from the $4d^4$ level is visible. Another line at 6740 Å from the same level was detected but it was quite weak. No other lines of the spectrum of nitrogen I were detected, including the usually strong lines at 4100, 4110 and 4935 Å. A series of bands of N_2(2 +ve) radiation, starting at 3804.9 Å are also visible. These molecular bands arise from the upper excited state of $C^3\Pi$ as mentioned previously. These bands seemed to be quite weak in Figure II-12C where excess nitrogen was present. The reason for this discrepancy was not clear. A comparison of the intensity of the line of nitrogen at 6708 Å with that of argon at 6965 Å, with help of the spectrophotometer, at a point where the concentration of the $2p_2$ level giving rise to the argon line was known, gave an estimation of the population density of the $4d^4$ level of nitrogen which was of the order of $10^3 - 10^4$ particles/cm^3 at around 2000°K. According to the thermodynamic calculations of Burhorn and Wienecke[50], the equilibrium concentration of (N) under the conditions of the experiment should be less than 10^7 particles/cm^3 at 2000°K. The excitation energy for the $4d^4$ state is 13.7 eV. Then,

it is not possible to account for the observed concentration of the $4d^4$ excited level of nitrogen if one assumes thermodynamic equilibrium in nitrogen, such as that expressed in equation (1) of Appendix A-4. The conclusion is that either the ground-state population of the nitrogen atoms was too high compared with its equilibrium value, and gave rise to a higher amount of excitation population, or the population of the $4d^4$ level was much higher than its equilibrium value. The first argument can be withdrawn because no important lines of nitrogen were observed. The selective excitation of the $4d^4$ level therefore, supports the argument that the population of this level was above its equilibrium value. This case does not preclude the case in which the ground-state population of nitrogen was also high, but in any case, excitation from the ground state was negligible. It was not possible to estimate the ground-state population of nitrogen directly. The likely mechanisms for the production of nitrogen atoms in their ground state and excited states were discussed earlier. The spectroscopic observations support the non-thermal character of the production of atoms of nitrogen which take place in the reaction of decomposition of nitric oxide, as chain carriers.

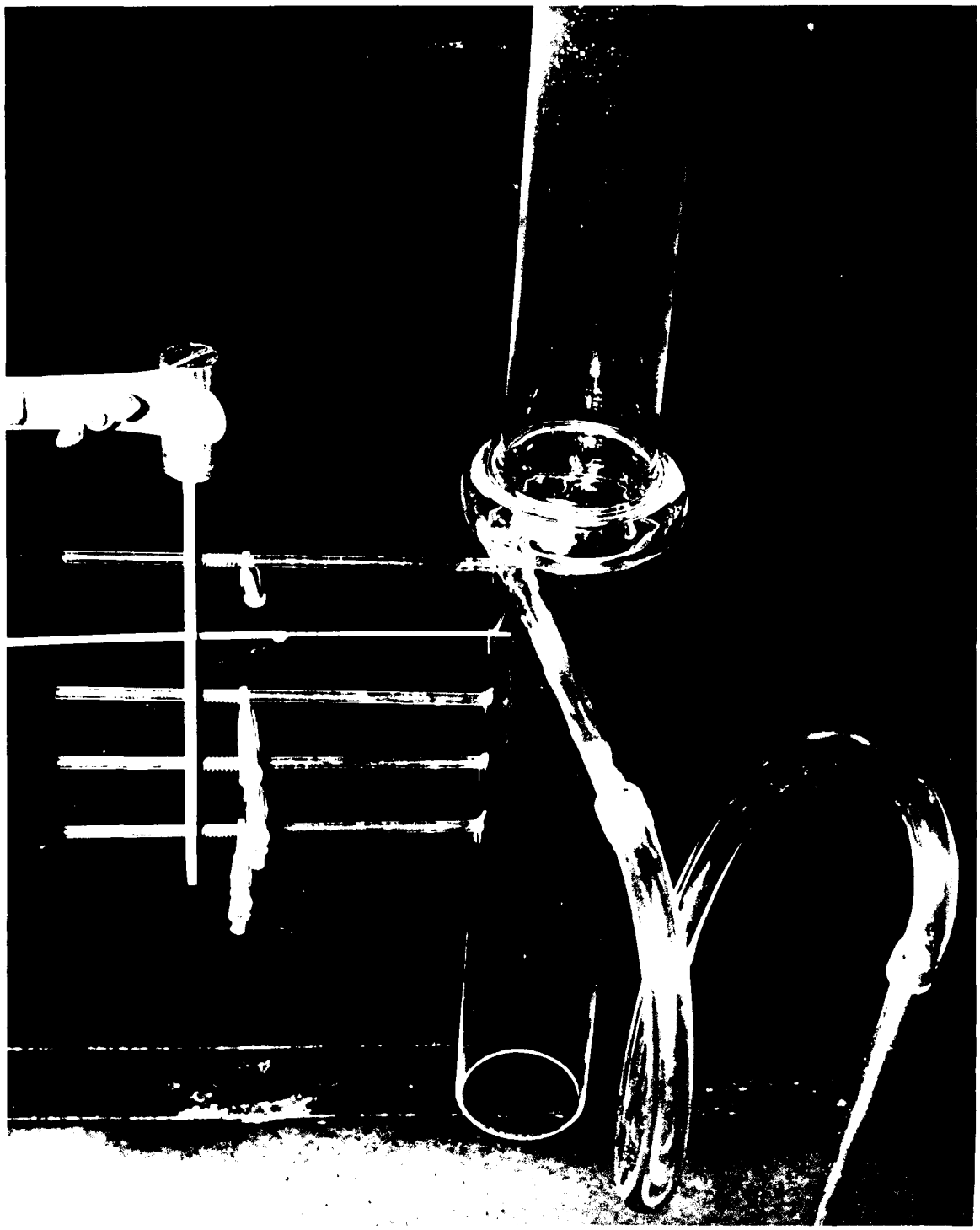

Figure II-1 A photographic view of the reactor assembly used for studying decomposition of nitric oxide. The sampling probe is inserted into the second hole counted from the top.

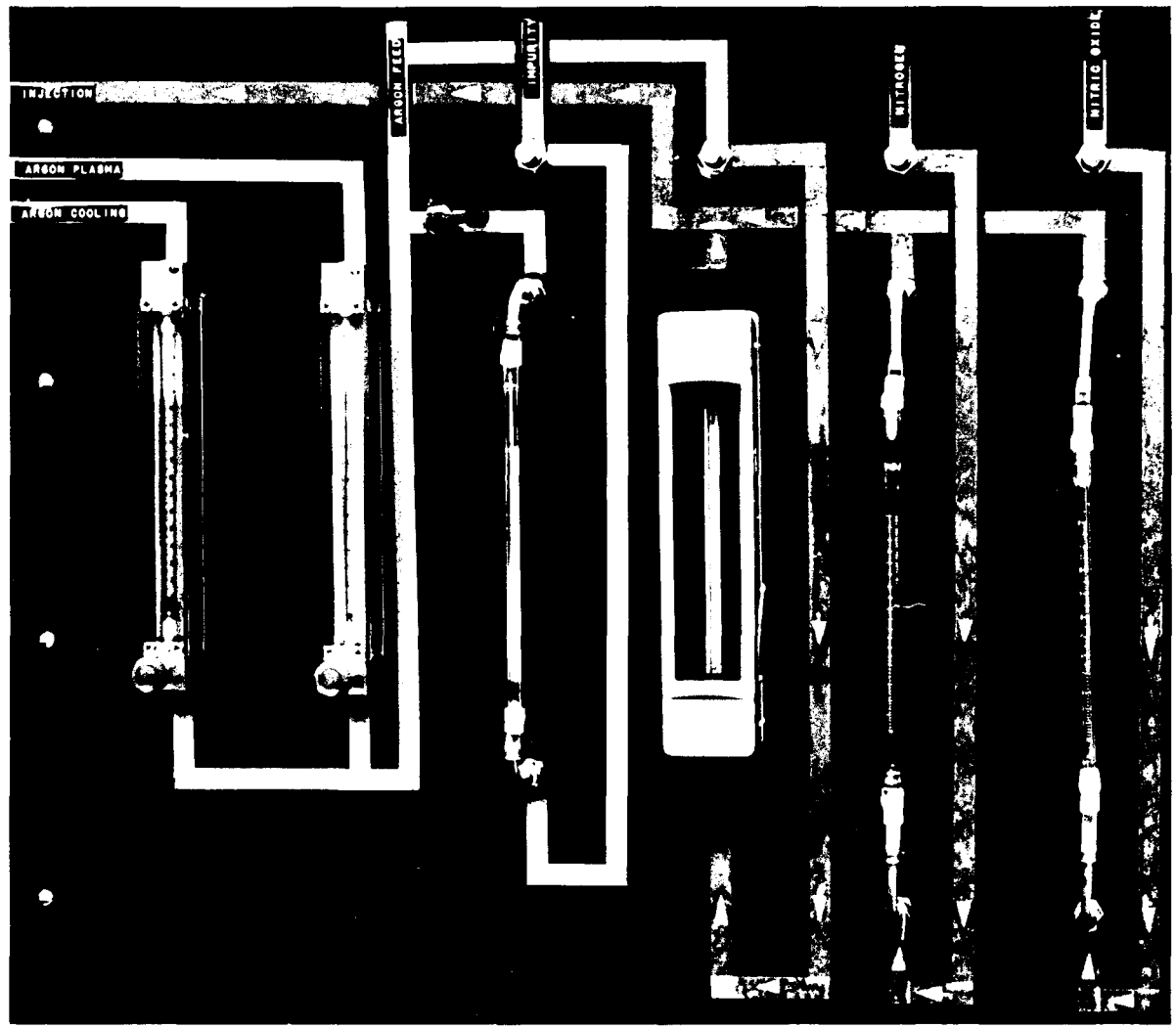

Figure II-2 A photographic view of the mixing system used for the reactants.

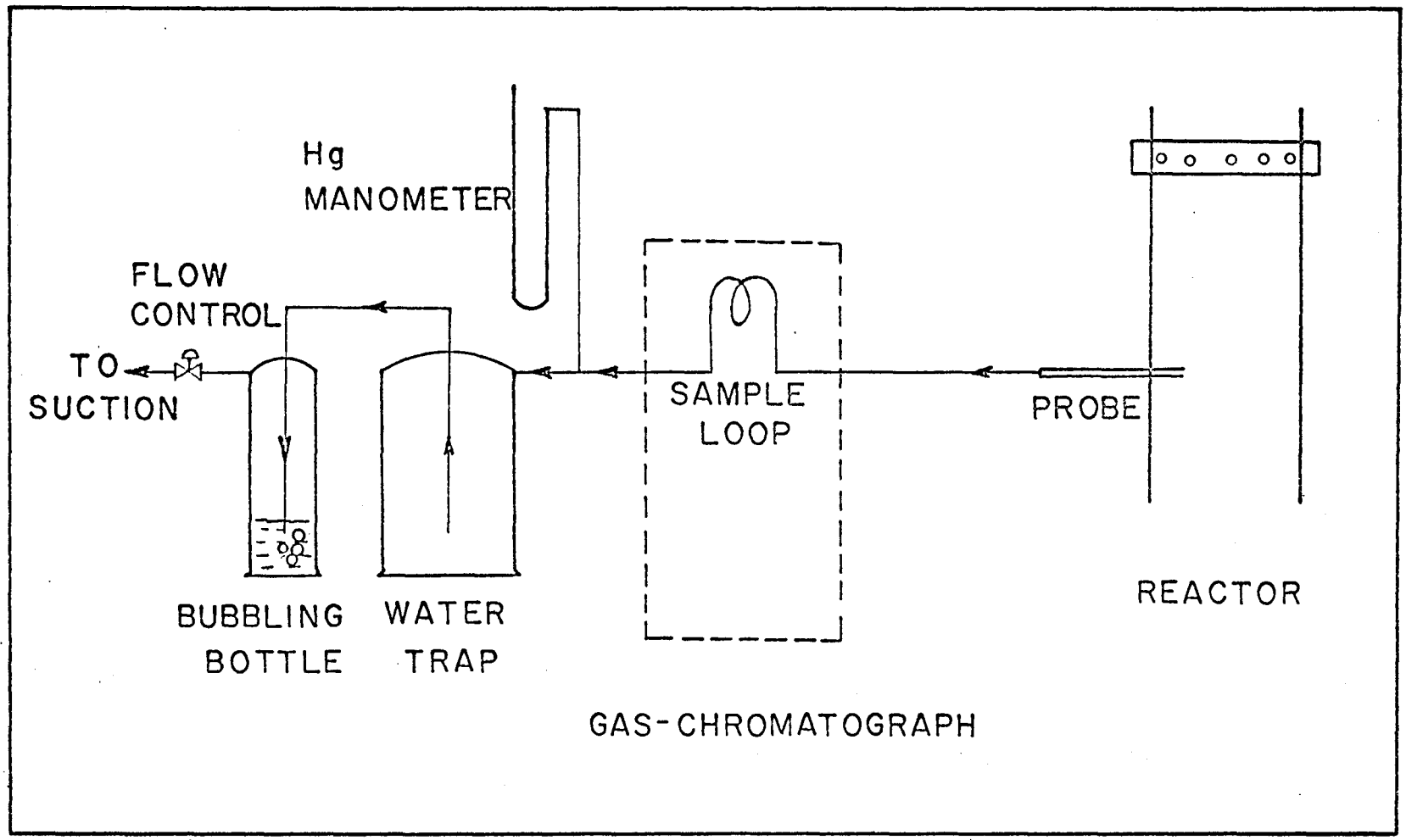

Figure II-3 Sampling system used to carry the sample gas from the plasma jet to the gas-chromatographic analyser.

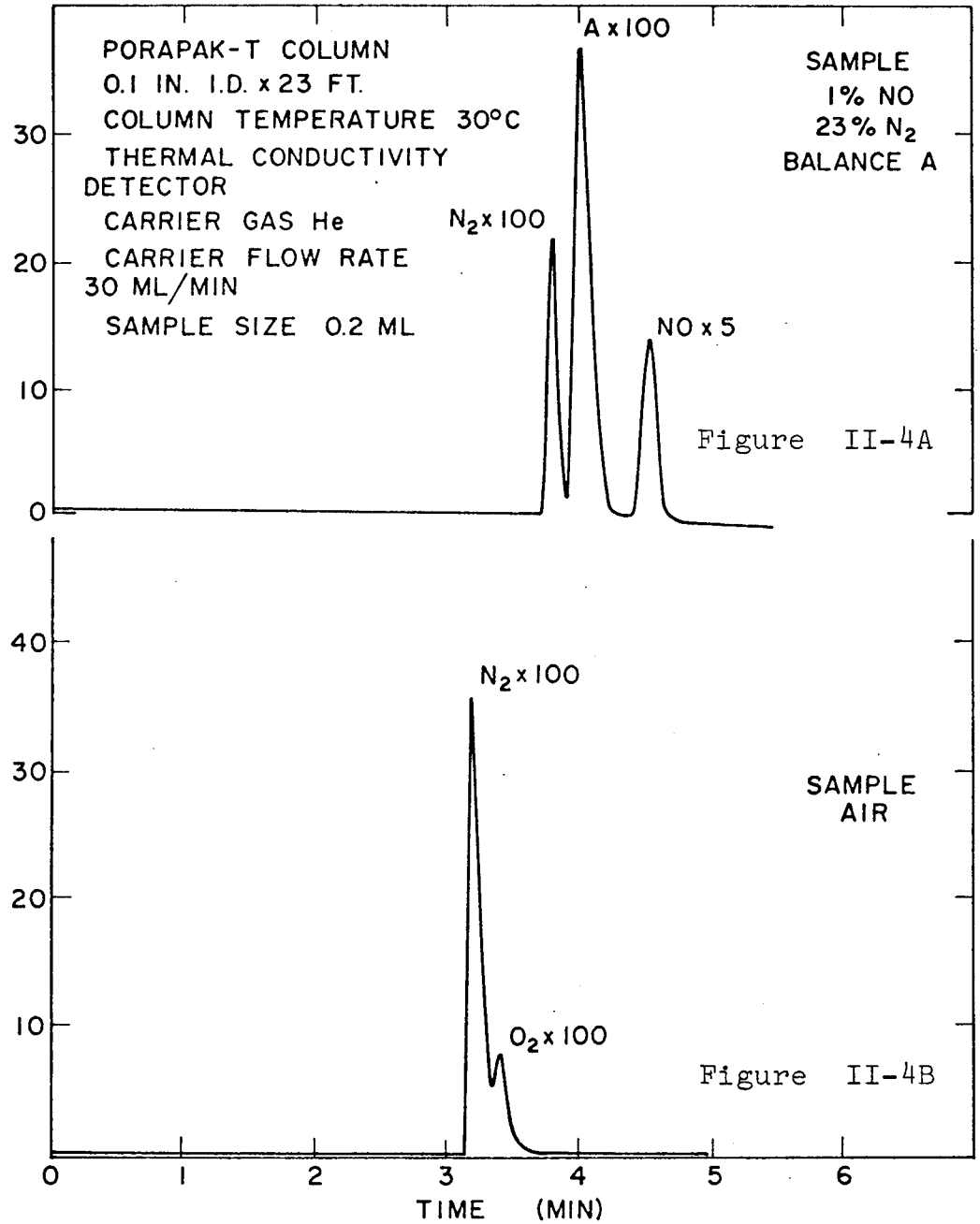

Figure II-4A
Figure II-4B

Typical chromatograms of NO-N_2-A and N_2-O_2 systems. Attenuation factors are shown near the peaks.

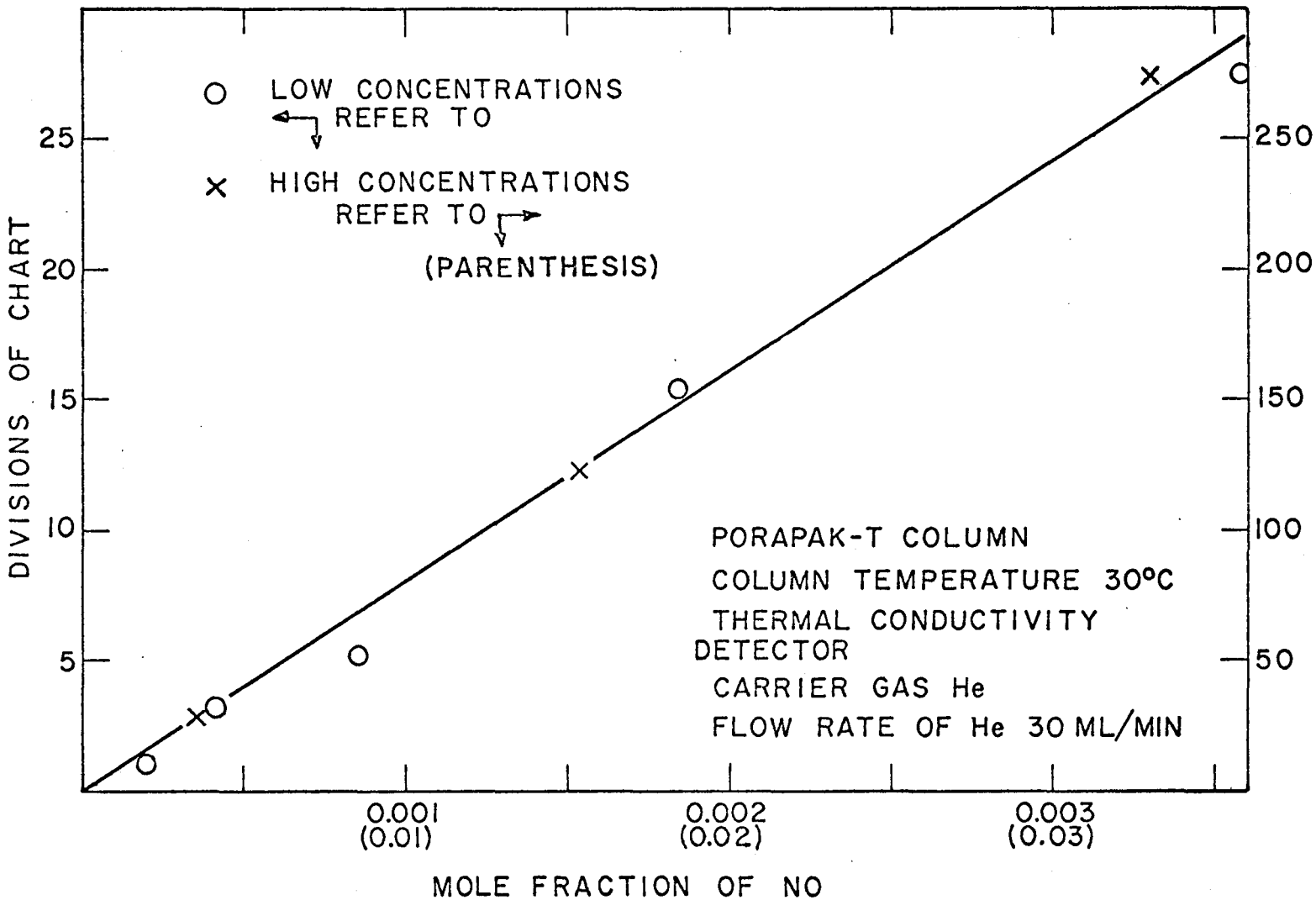

Figure II-5 Calibration of gas-chromatograph for the measurement of concentration of NO. Linear relationship between the peak height and the concentration was obtained upto 0.03 mole fraction.

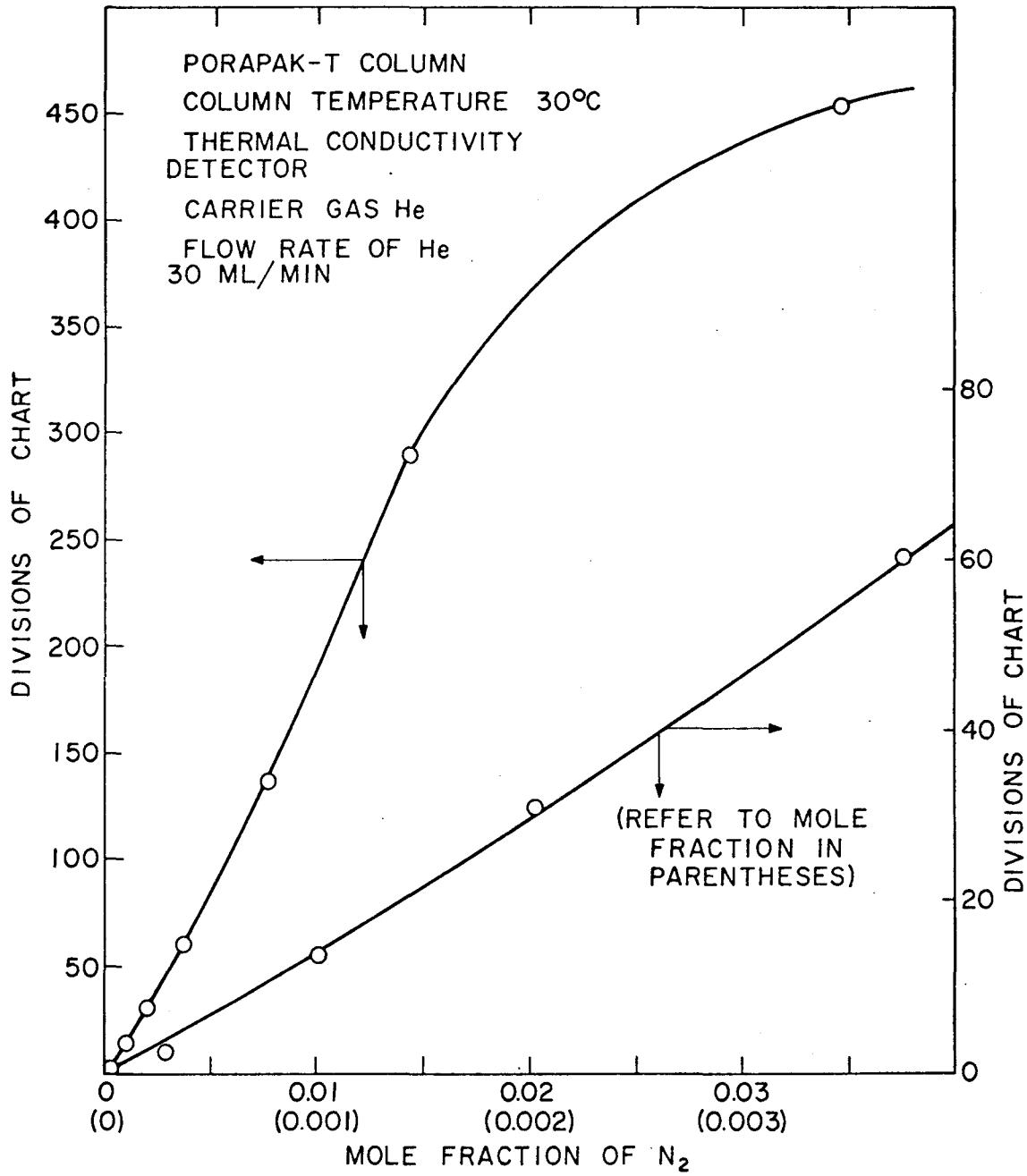

Figure II-6

Calibration of gas-chromatograph for the measurement of concentration of nitrogen. Divisions of chart record peak-heights.

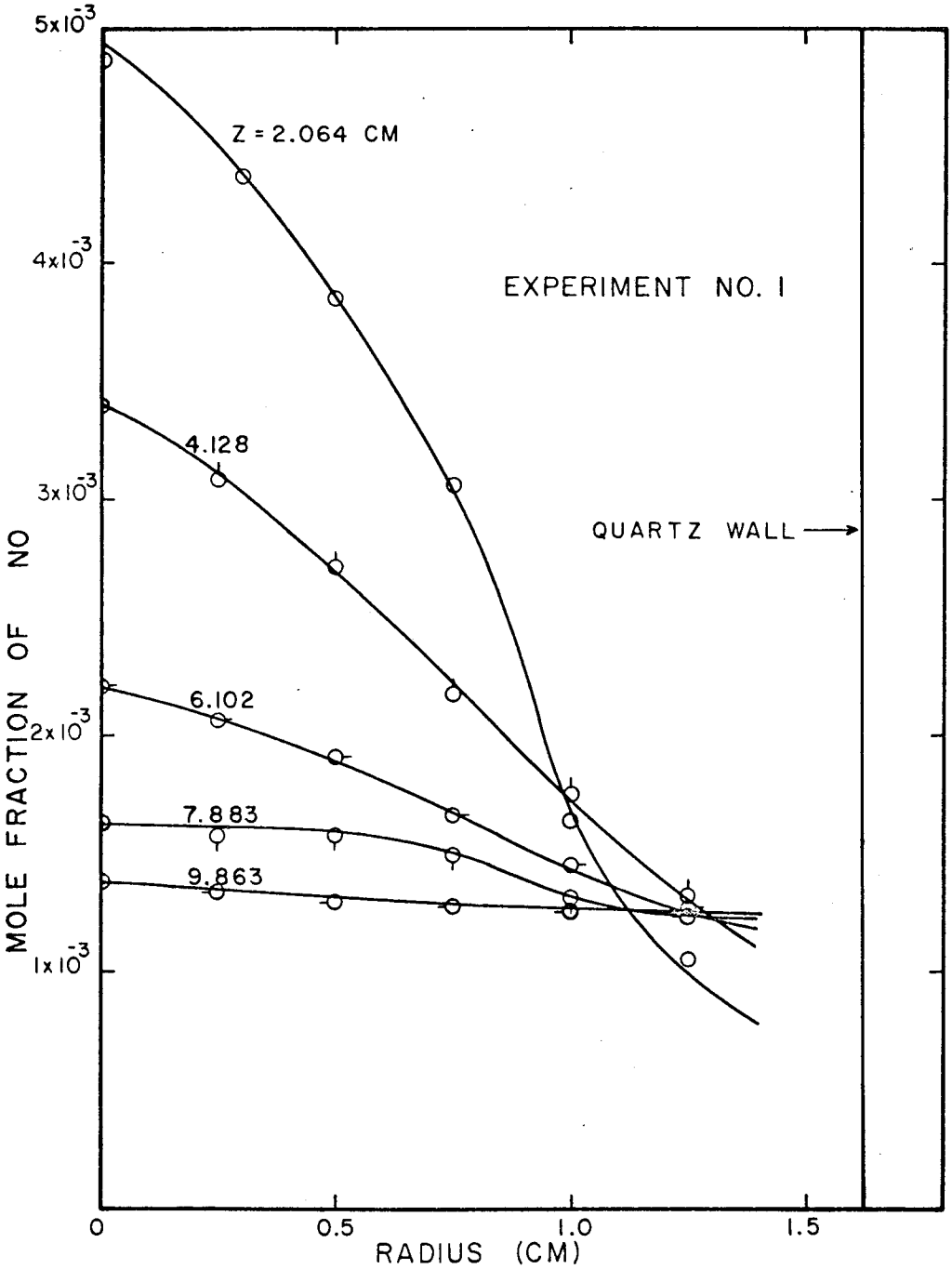

Figure II-7A

Concentration distribution of NO in the reactor for the case in which no excess N_2 was premixed. z denotes axial distance measured below the injection plane.

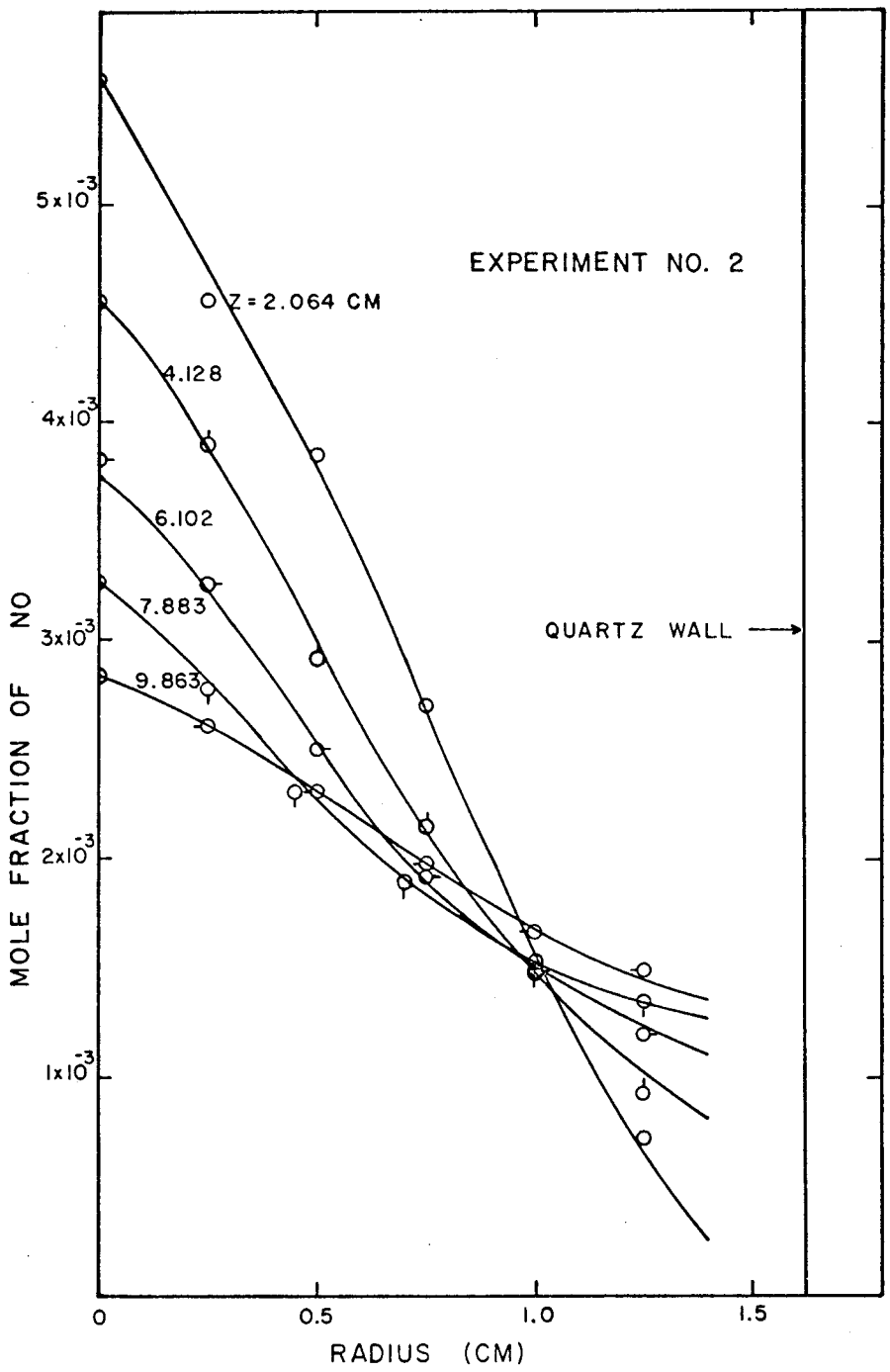

Figure II-7B

Concentration distribution of NO in the reactor for the case in which excess N_2 was premixed. z denotes axial distance measured below the injection plane.

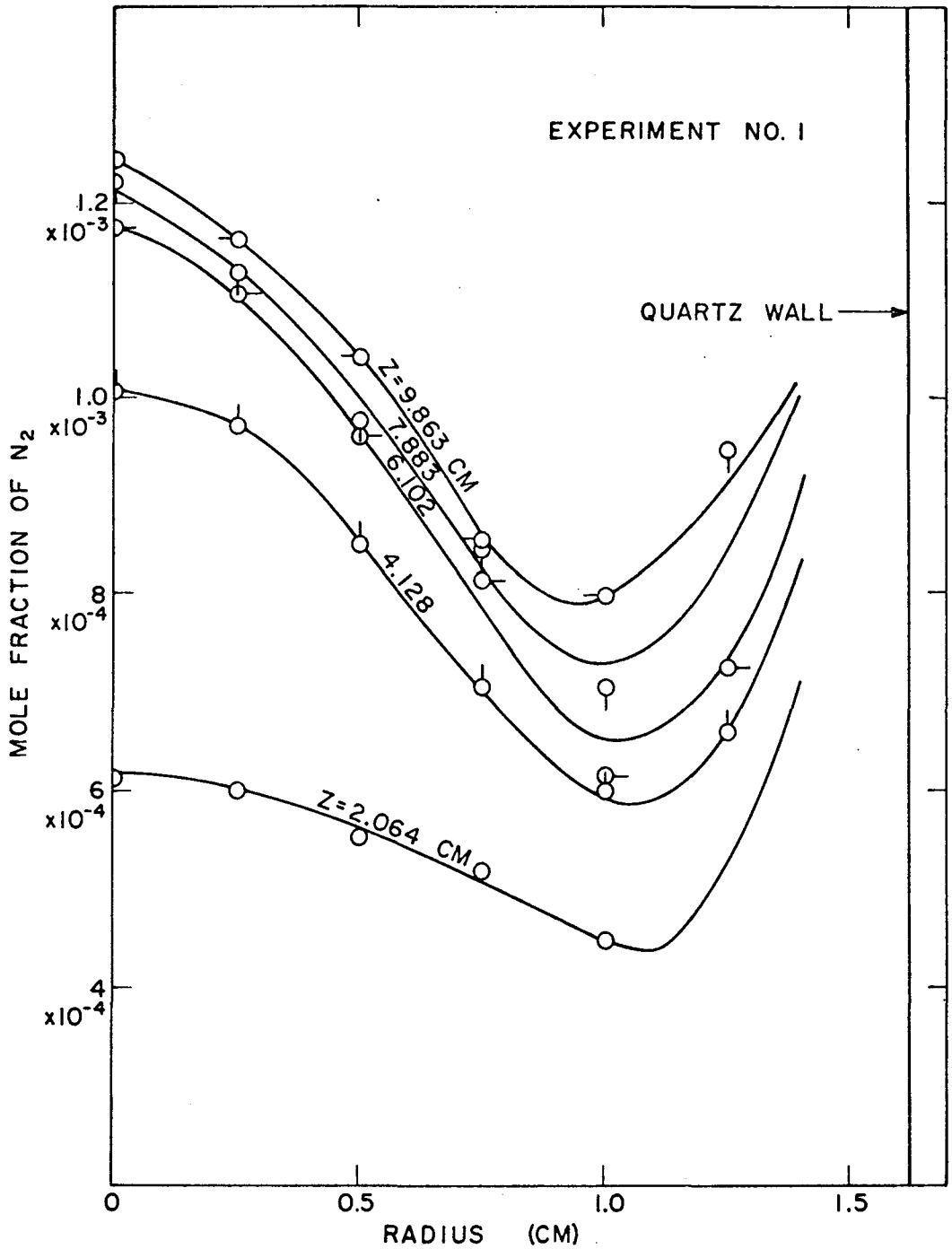

Figure II-8A

Concentration distribution of N_2 in the reactor for the case in which no excess N_2 was premixed. z denotes axial distance measured below the injection plane.

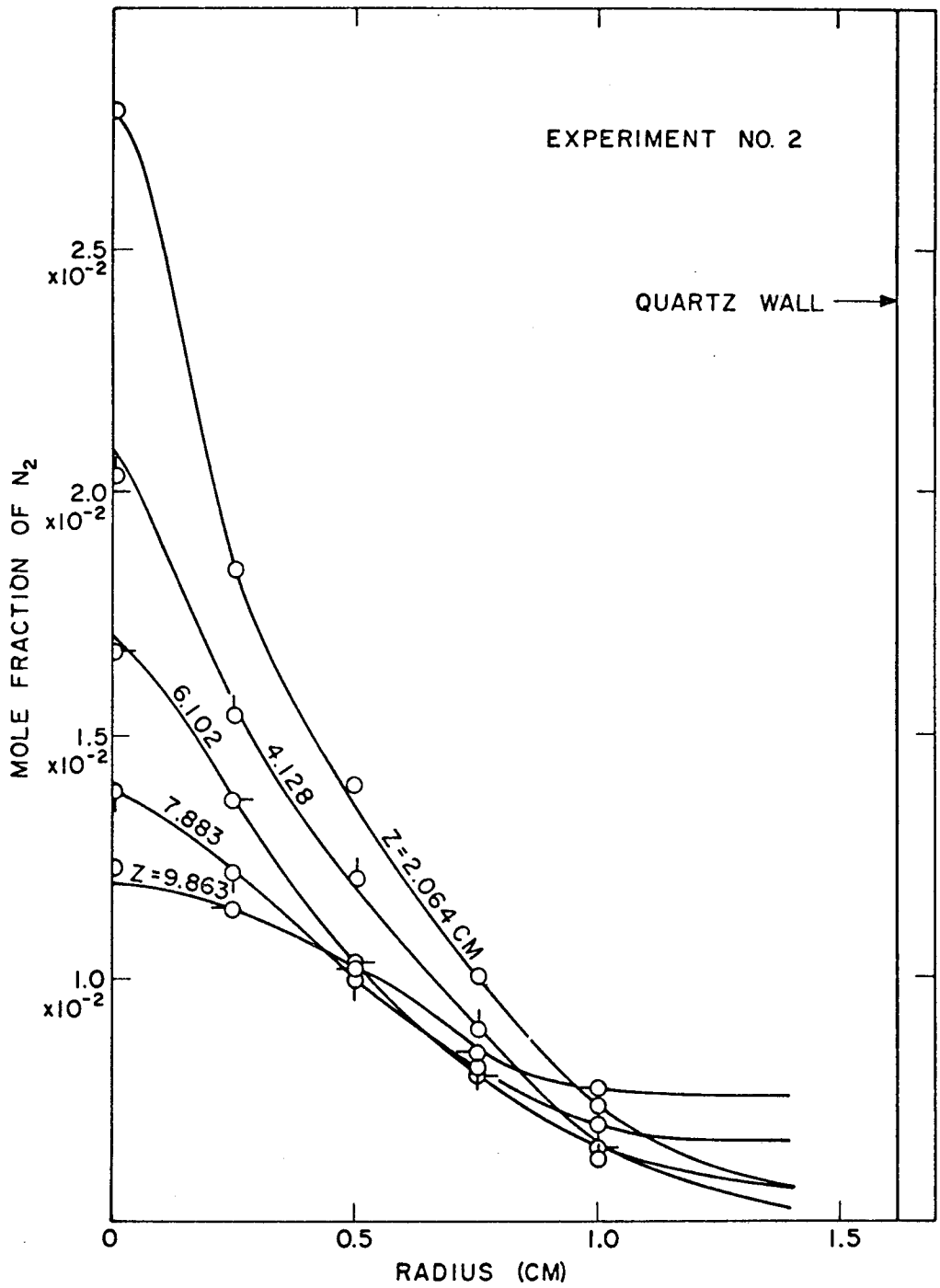

Figure II-8B

Concentration distribution of N_2 in the reactor for the case in which excess N_2 was premixed. z denotes axial distance measured below the injection plane.

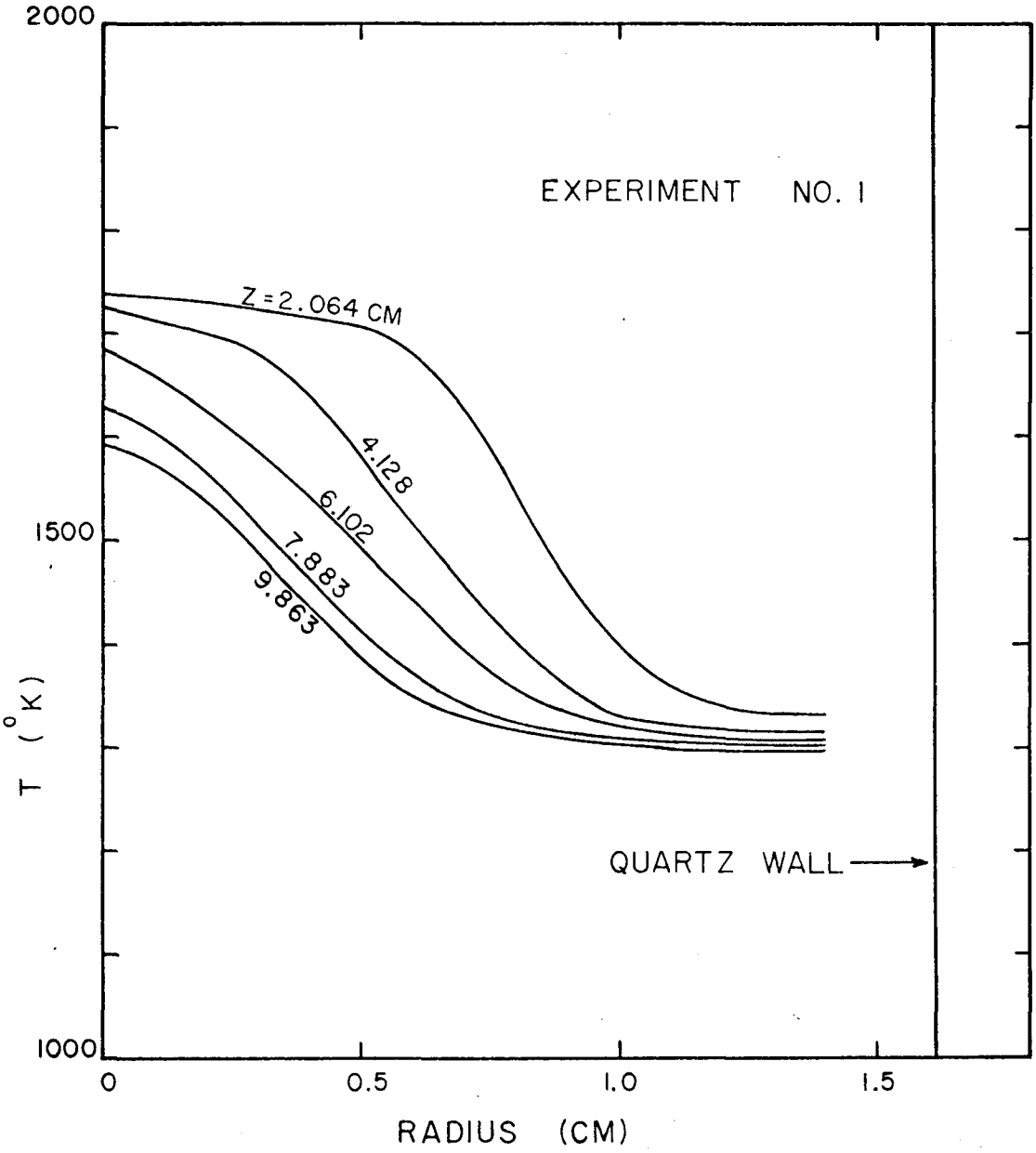

Figure II-9

Temperature distribution in the reactor when only nitric oxide as the reactant was introduced in the plasma jet. The temperatures shown are absolute temperatures. Scattering of the experimental data points was within ±5°K from the curves. z denotes axial distance measured below the injection plane.

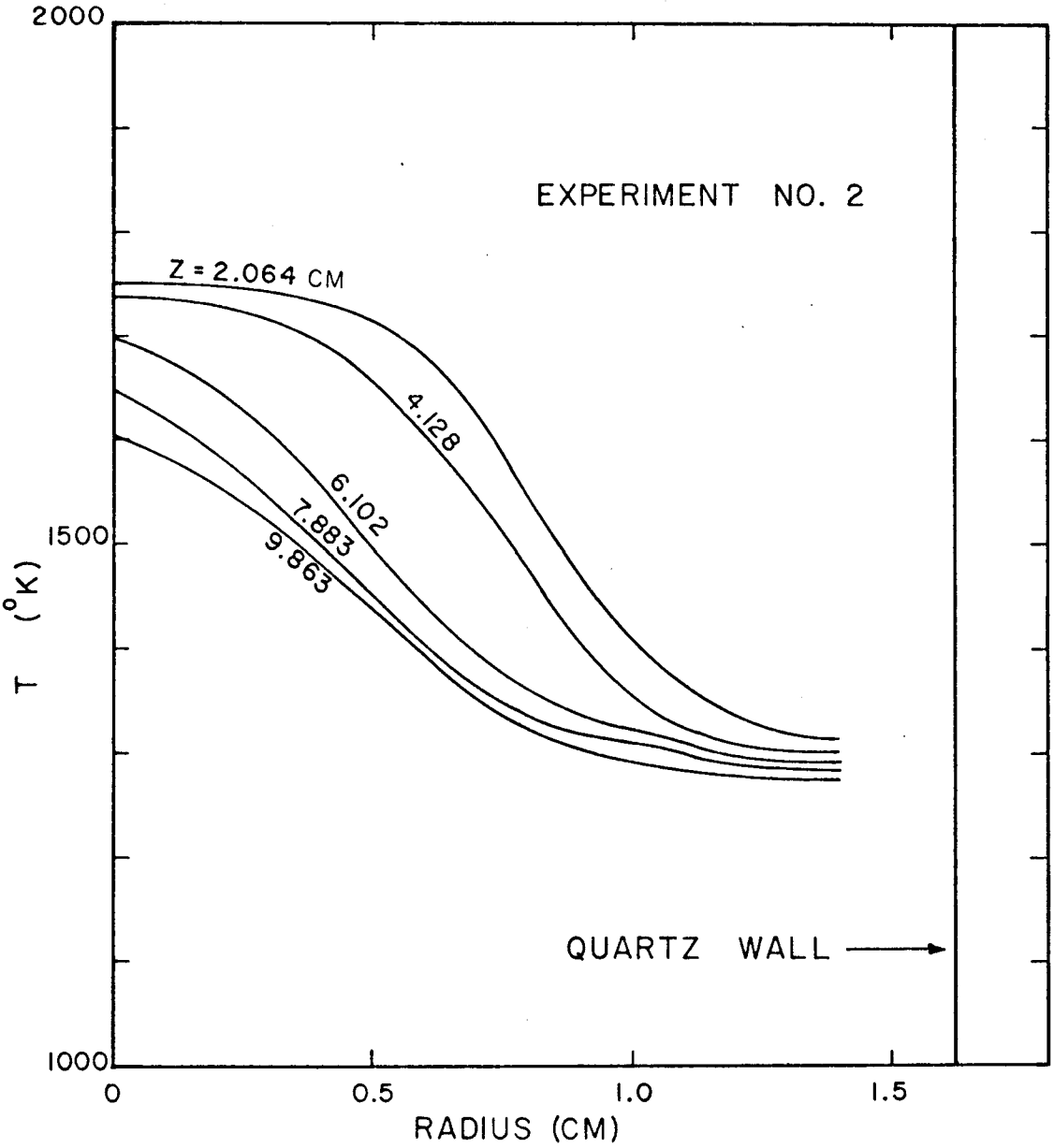

Figure II-10

Temperature distribution in the reactor when excess nitrogen was premixed with nitric oxide. The temperatures shown are absolute temperatures. Scattering of the experimental data points was within ±5°K from the curves. z denotes axial distance measured below the injection plane.

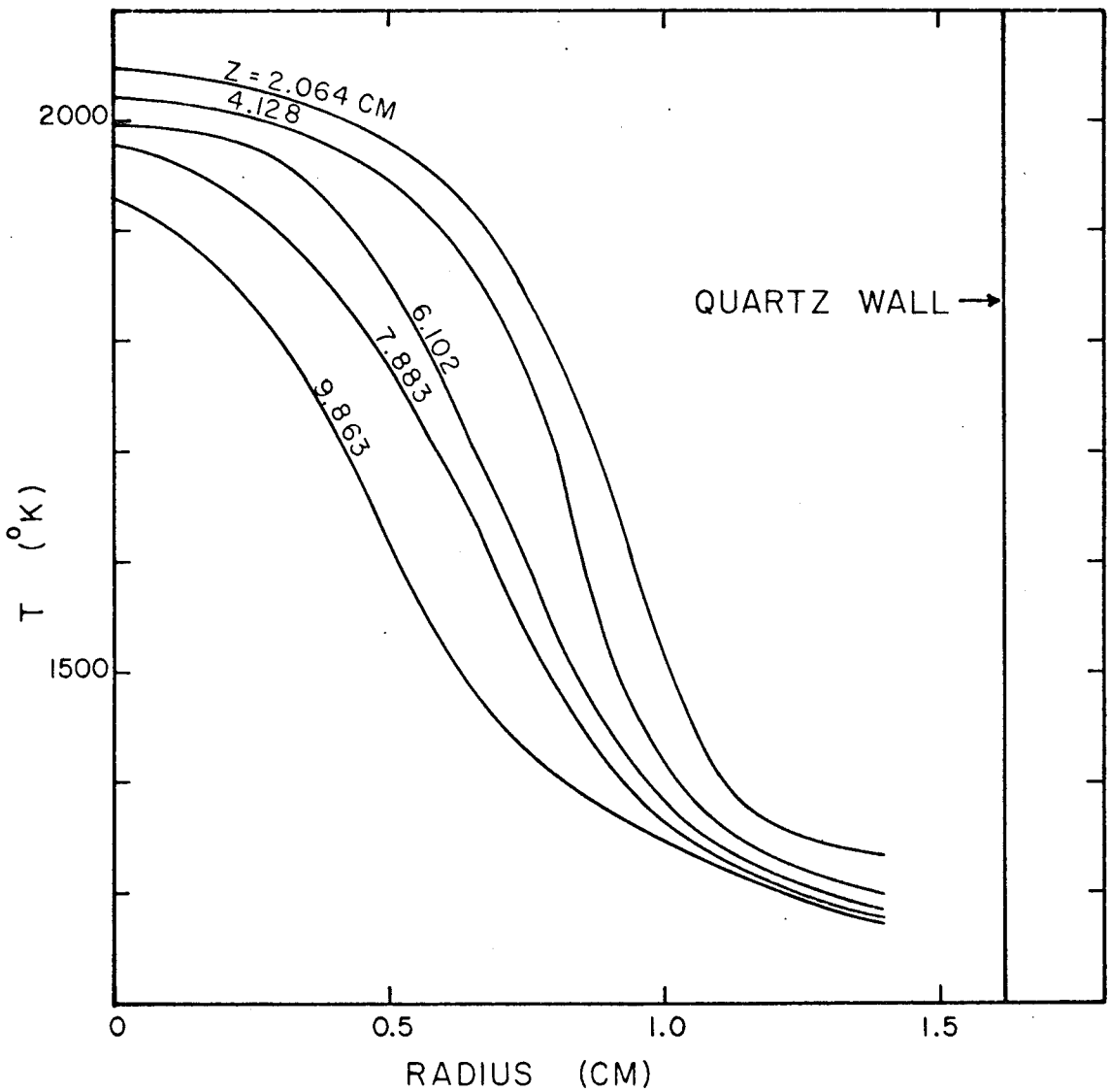

Figure II-11

Temperature distribution in the reactor when no gas was injected from the jacket. Temperatures shown are absolute temperatures. Scattering of the experimental data points was within ±5°K. z denotes axial distance measured below the plane of injection.

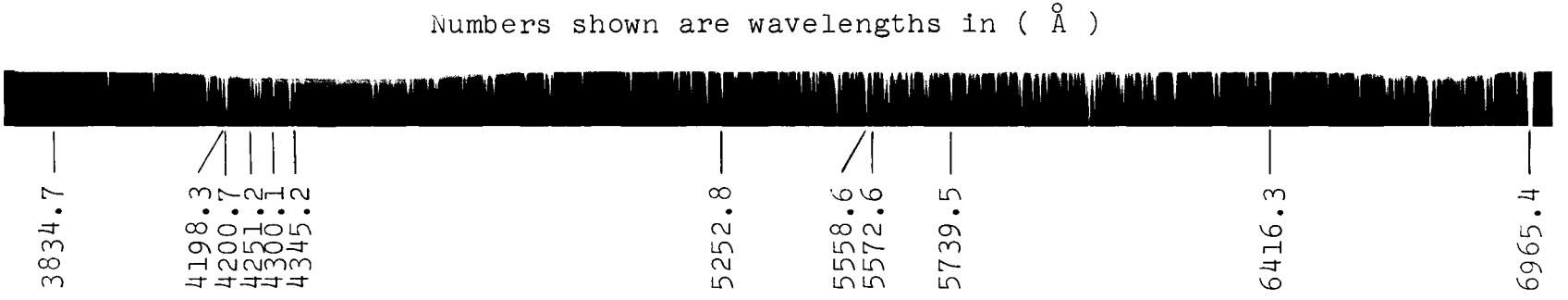

Figure II-12A Spectrogram for pure argon

Figure II-12B Spectrogram for argon + nitric oxide

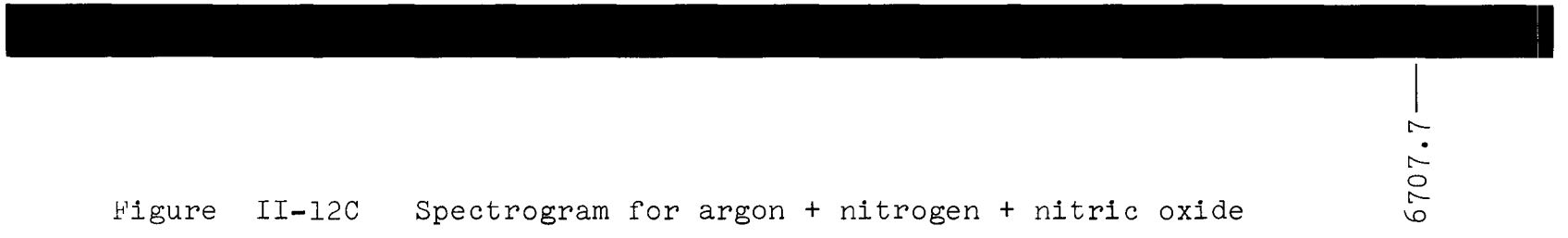

Figure II-12C Spectrogram for argon + nitrogen + nitric oxide

SUMMARY AND CONCLUSIONS

The plasma studied here was an RF-coupled, atmospheric-pressure, argon-plasma jet. An electric field was absent in the region of interest. It was assumed that the same kinetic temperature prevailed for all the particles at a given point in the plasma jet. The excitation temperatures were determined spectroscopically from the relative population densities of the higher excited states and varied between 3000 - 11000°K in the region where the plasma was studied. The electron densities in the same region were determined from the Saha-Boltzmann relationship for the first stage of ionization, and varied between 10^{12} - 10^{15} particles/cm^3. The axial velocities were determined by a flow-visualization technique using particles of boron nitride as tracers, and varied between 300 - 1200 cm/sec.

Some improved values of transition probabilities of argon I were developed for their usefulness in the spectroscopic studies. The values of transition probability for 18 lines of argon I in the spectral range of 5000 - 6500 Å are reported in Table I-1. It was found that the inhomogeneity of the source introduced an error of 4 - 5 per cent in the values of the transition probabilities.

Various spectroscopic methods of the measurement of temperatures in a plasma were evaluated. A comparison between the various methods is shown in Figure I-7. The temperatures

calculated from the absolute line intensities were always greater than the corresponding temperatures obtained from the relative population densities of 7 excited levels, which indicated an absence of complete thermodynamic equilibrium in the plasma jet.

The validity of the excitation equilibrium in the plasma jet was questioned. The higher-excitation population remained in equilibrium, while the lower-excitation population including the ground state showed a marked departure from equilibrium. The departure from equilibrium of the lower-excitation population was a strong function of the energy level, a weak function of the electron density and a very weak function of the temperature. The critical-energy level below which a substantial departure from equilibrium occurred was mainly a function of the temperature. The fractional departure from equilibrium of the excited states, expressed as the ratio of the actual population to the corresponding Saha-Boltzmann population was correlated to the temperature and the electron density by means of an empirical equation of the form:

$$\rho(p) = - AT^{B}n_e^{C}$$

The values of the constants A, B, C are given in Table I-2. The departure from equilibrium of the ground state is shown as a function of the parameter $\frac{1}{2.303kT}$ in Figure I-9. The ground state showed a great tendency to be underpopulated with a decreasing temperature in the decaying plasma studied.

For a complete thermodynamic equilibrium to exist in a plasma, the ground state should be in equilibrium with the excitation population, and the critical-energy level should be extended down to the ground level.

A flow-visualization technique was developed to obtain the velocity distribution in the plasma jet. Particles of boron nitride were used as tracers. A photographic method using two-plane pictures of the plasma jet enabled the velocities and the positions of the particles to be determined. The experimental velocity distribution was expressed as a third-order-least-squares fit. The experimental velocity distribution was improved by subjecting it to a material balance in the plasma jet. The improved velocity distribution is shown in Figure I-12. An energy balance in the plasma jet gave the radiated power of argon, which could be approximately expressed by means of equation (I-18).

A study of the recombination of electrons with ions indicated that the dissociative-molecular-ion mechanism could satisfactorily explain the observed rates of recombination, which were obtained by solving the equation of continuity for the electrons. A summary of the dissociative-molecular-ion mechanism including the values of the pertinent rate constants is given in Table 2 of Appendix A-7. The collisive-radiative model of plasmas was found to be inadequate to explain the excitation population and the recombination rates in the

argon plasma under atmospheric pressure, mainly because of the following reasons:

1. The collisive-radiative model does not take into account the effect of the metastable level in argon, which may have a long life-time comparable to that of the ground state.
2. The collisive-radiative model neglects the atom-atom collisions which can become as effective as the electron-atom collisions, and may result in the inelastic processes when the gas densities are high compared with the electron densities. Especially important are the three-body-collision processes involving atoms.

An important implication of the dissociative-molecular-ion mechanism of recombination involving bimolecular gases, from the point of view of chemical reactions is the formation of a large amount of atomic species which are reactive.

The decomposition of nitric oxide was studied in the argon plasma in the range of temperatures between 1300 - 1750 $^{\circ}$K. The region of the reactor chosen for this study was below the region investigated spectroscopically. The temperatures were determined with help of an optical pyrometer and a ceramic probe which was inserted into the plasma. The concentrations of NO and N_2 were determined by a gas-chromatographic technique. The rates of decomposition of NO were obtained by solving the equation of continuity for NO. The observed rates of decomposition were about 4 orders of

magnitude greater than those observed by other workers in the absence of the plasma. The apparent order of the reaction with respect to NO increased from 1.33 to 1.85 with the addition of excess N_2. The presence of excess N_2 also decreased the rate of decomposition of NO. The apparent activation energy of the reaction was about 9 kcal/g mol which was significantly lower than the values obtained by other workers in the absence of the plasma. These observations were consistent with a chain mechanism involving atoms of oxygen and nitrogen. The proposed chain mechanism is given by:

$$NO + N \underset{k_{-1}}{\overset{k_1}{\rightleftharpoons}} O + N_2$$

$$NO + O \underset{k_{-2}}{\overset{k_2}{\rightleftharpoons}} N + O_2$$

and the corresponding rate expression is given by:

$$-\frac{d(NO)}{dt} = \frac{2k_1(N)(NO)^2}{(k_{-1}/k_2)(N_2) + (NO)}$$

A steady state for the atomic species which act as the chain carriers was assumed. The increased rates of decomposition of NO can be attributed to the large concentration of the atomic nitrogen which was formed as the result of the reactions between the molecular nitrogen and the excited atoms and ions of argon present in the plasma. The values of the

rate parameters in the above rate expression were obtained from the observed rates as:

$$(N)k_1 = 1.73(\pm 0.2) \times 10^3 \, e^{-\frac{13900(\pm 700)}{RT}}$$

$$\frac{k_{-1}}{k_2} = 2.26(\pm 0.17) \, e^{-\frac{4325(\pm 300)}{RT}}$$

The experimental data covered the following conditions:

$$1.2 \times 10^{-3} < x_{NO} < 5.5 \times 10^{-3}$$

$$6.0 \times 10^{-4} < x_{N_2} < 2.7 \times 10^{-2}$$

$$1300^\circ K < T < 1750^\circ K$$

General Implications

It can be concluded from the study of decomposition of NO in the argon plasma that the role of the electrons in the reaction was to maintain the concentration of the excited atoms of argon by means of inelastic collisions. The excited atoms and ions in turn, led to the formation of atomic species of nitrogen which played the important role of chain carriers in the reaction. In principle, the concentration of the atomic nitrogen in the above rate expression could be obtained as a function of the independent variables defining the state of the plasma, namely, the temperature and the electron density. In practice however, all the excitation cross-sections and the reaction cross-sections required for the calculation of the steady-state concentration of the atomic

nitrogen were hardly known. Therefore, it will suffice to say that the reaction rate constant for a plasma reaction may be expressed as a function of two independent parameters:

$$k = f(T, n_e)$$

in contrast with:

$$k = f(T)$$

for a thermal reaction. A general reaction rate theory set to explain reactions in plasmas at sufficiently high gas densities would include electronic collisions and radiative transitions, in addition to the atomic collisions which are usually considered in evaluating the rates of chemical reactions.

REFERENCES

1. T. B. Reed, J. Appl. Phys., 32, 821, (1961).
2. T. B. Reed in "The Application of plasmas to Chemical Processing", edited by R. F. Baddour and R. S. Timmins, M. I. T. Press, Cambridge, Massachusetts, (1967).
3. "Fixed Nitrogen" edited by H. A. Curtis, Chap. 4, The Chemical Catalog Co., New York, (1932).
4. R. S. Timmins and P. R. Amman in "The Application of Plasmas to Chemical Processing", edited by R. F. Baddour and R. S. Timmins, M. I. T. Press, Cambridge, Massachusetts, (1967).
5. D. R. Bates and A. Dalgarno in "Atomic and Molecular Processes", edited by D. R. Bates, Academic Press, New York, (1962).
6. L. B. Loeb, "Basic Processes of Gaseous Electronics", University of California Press, (1955).
7. E. J. Hellund, "The Plasma State", the Reinhold Publishing Co., New York, (1961).
8. "Plasma Diagnostic Techniques", edited by R. H. Huddlestone and S. L. Leonard, Academic Press, New York, (1965).
9. H. R. Griem, "Plasma Spectroscopy", McGraw-Hill Book Co., New York, (1964).
10. "Instruction Manual for Model RJB Lock-In Amplifier" by Electronics, Missiles and Communications, Inc., New York.

11. "Temperature, Its Measurement and Control in Science and Industry", part 1, vol. III, edited by C. M. Herzfeld, Reinhold Publishing Co., New York (1962).

12. E. R. F. Winter and C. J. Cremers, University of Minnesota Report ARL 62-388, (July 1962).

13. W. K. McGregor and L. E. Brewer in "Proceedings of VIth International Conference on Ionization Phenomena in Gases", vol. I, Paper II-28, Paris, (1963).

14. D. R. Bates and A. E. Kingston, Planetary and Space Science, 11, 1, (1963).

15. R. W. P. McWhirter and A. G. Hearn, Proc. Phys. Soc., 82, 641, (1963).

16. E. Hinnov and J. G. Hirschberg, Phys. Rev., 125, 795, (1962).

17. A. T. Hattenburg and H. J. Kostkowski in "Temperature, Its Measurement and Control in Science and Industry", edited by C. M. Herzfeld, vol. III, Part I, p. 587, Reinhold Publishing Co., New York, (1962).

18. D. R. Simon and K. C. Rogers, J. Appl. Phys., 37, 2255 (1966).

19. J. F. Bott, "A Spectroscopic Investigation of a Helium Plasma Arc", Harvard University Publication, Technical Report No. 25, (January 1966).

20. J. F. Bott, Phys. Fluids, 9, 1540, (1966).

21. M. P. Freeman, J. Q. S. R. T., 8, 435, (1968).

22. P. D. Schloz and T. P. Anderson, J. Q. S. R. T., 8, 1411, (1968).

23. L. E. Brewer and W. K. McGregor in "Proceedings of VIth International Conference on Ionization Phenomena in Gases", vol. I, Paper II-27, Paris, (1963).

24. T. K. Chu and C. F. Gottschlich, A. I. A. A. Journal, 6, 114, (1968).

25. R. W. P. McWhirter in "Plasma Diagnostic Techniques", edited by R. H. Huddlestone and S. L. Leonard, Academic Press, New York, (1965).

26. E. I. Asinovskii and A. V. Kirillin, Int. Chem. Eng., 7, 281, (1967).

27. D. J. Collins and W. A. Menard, Trans. A. S. M. E., J. Heat Transfer, Series C, 89, 52, (1966).

28. C. F. Knopp and A. B. Cambel, Phys. Fluids, 9, 989, (1966).

29. R. A. Matula, Trans. A. S. M. E., J. Heat Transfer, Paper 67-WA/HT-3, (1967).

30. E. C. Beaty in "Proceedings of Vth International Conference on Ionization Phenomena in Gases", vol. I, Paper DO, Paris, (1963).

31. M. A. Biondi and S. C. Brown, Phys. Rev., 75, 1700, (1949).

32. D. R. Bates and H. S. W. Massey, Proc. Royal Soc., A-192, 1, (1947).

33. F. Haber and J. E. Coates, Z. Physik. Chemie, 69, 338 (1909).

34. Y. B. Zeldovich, Acta Physiochim. U. R. S. S., 21, 577 (1946).

35. K. Vetter, Z. Electro. Chem., 53, 369, (1949).

36. F. Kaufman and L. J. Decker in "VIIth Symposium (International) on Combustion",pp. 57 - 60, Butterworths Publication Ltd., London, (1959).

37. H. Wise and M. French, J. Chem. Phys., 20, 22, (1952).

38. F. Kaufman and J. R. Kelso, J. Chem. Phys., 23, 1702, (1955).

39. E. Freedman and J. W. Daiber, J. Chem. Phys., 34, 1271, (1961).

40. K. L. Wray and J. D. Teare, Avco-Everett Research Laboratory, Research Report 95, (June,1961).

41. K. L. Wray, Avco-Everett Research Laboratory, Research Report 104, (June,1961).

42. R. R. Sakaida, R. G. Rinker, R. F. Cuffel and W. H. Corcoran, Ana. Chem., 33, 32, (1961).

43. J. M. Trowell, Ana. Chem., 37, 1152, (1965).

44. R. N. Dietz, Ana. Chem., 40, 1576, (1968).

45. O. L. Hollis, Ana. Chem., 38, 309, (1966).

46. W. F. Wilhite and O. L. Hollis, J. Gas Chromatography, 6, 84, (1968).

47. R. B. Bird, W. E. Stewart and E. N. Lightfoot,

"Transport Phenomena", p. 511, John Wiley & Sons Inc., New York, (1962).

48. P. R. Ammans and R. S. Timmins, Avco Corp. Research Report 65-4, (March,1965).

49. M. E. Morrison, R. G. Rinker and W. H. Corcoran, I. & E. C. Fundamentals, 5, 175, (1966).

50. F. Burhorn and R. Wienecke, Z. Physik. Chemie, 215, 269, (1960).

51. A. A. Frost and R. G. Pearson, "Kinetics and Mechanism", 2nd ed., Chapter X, John Wiley & Sons Inc., New York, (1961).

APPENDIX A-1

Determination of Absolute Spectral Response

The optical elements such as mirrors and lenses, the diffraction grating and the radiation detector used for making quantitative measurements of the incident light from the plasma do not have a uniform spectral response over the entire range of wavelengths. For quantitative interpretation of the recorded intensities, one must calibrate the experimental setup to determine its wavelength response. The following procedure makes use of a standard tungsten strip lamp placed in the position of the plasma, as the source of radiation for determining the absolute spectral response of the experimental setup.

The radiation from the tungsten lamp can be calculated by the use of modified Planck's equation:

$$I'_{\lambda} = \epsilon_{\lambda T} \tau_{\lambda} c_1 \lambda^{-5} (e^{\frac{c_2}{\lambda T}} - 1)^{-1} \qquad \text{(A1-1)}$$

The emissivity $\epsilon_{\lambda T}$ for tungsten is given by DeVos [1] as a function of wavelength and temperature. The lamp had a quartz envelope, for which the transmission factor τ_{λ} is close to unity. Further, the quartz tube used to confine the plasma has about the same transmission factor. Therefore τ_{λ} was ignored in the calculations. The values of Planck's constants are as follows[2]

$$C_1 = 3.7405 \times 10^{-12} \quad \text{(watt)(cm)}^2$$

$$C_2 = 1.43879 \quad \text{(cm)(°K)}$$

The lamp was operated at 5 volt d.c. and its surface temperature was measured with an optical pyrometer with an accuracy of ±3°K. The d.c. operation of the lamp was found to reduce the noise-level in the recorded signal. The intensity of radiation was recorded on the chart recorder under identical conditions as with the plasma.

A special correction for scattered intensity inside the spectrophotometer unit was necessary. The resolution of the incident light is not complete due to imperfect optics of the instrument. Thus, a part of the light emerging from the exit slit arises from the scattered light from other wavelengths. The amount of scattered intensity was determined at three different wavelengths, by the use of Kodak wavelength filters 34A, 74 and 29 which have peak responses at 4500 Å, 5200 Å and 6400 Å and have a bandwidth of about 900 Å. These filters were put in turn in the optical path of the incident light and the recorded output was compared with the output without any filter. Allowance was made for the transmission characteristics of the filters which were previously determined with the help of a mercury lamp, which has a well defined spectrum. Further analysis with Kodak filter 2C, which cuts off radiation below 3500 Å, but transmits most radiation between 4000 - 6000 A indicated that the

scattered intensity arose from wavelengths higher than the wavelength being scanned. On these considerations, it was possible to write down the contribution to the observed intensity from scattering as follows:

$$I_i^{ob} = I_i + \sum_{j=1}^{n} a_{ij} I_j^{ob} \qquad \text{(A1-2)}$$

$$a_{ij} = 0 \quad \text{for} \quad j < i$$

Here I_i^{ob} is the observed intensity at wavelength λ_i and I_i is the incident intensity. The coefficients a_{ij} are characteristic of the spectrophotometer, and their experimental values based on a wavelength interval of 250 Å are listed in Table A1-1. The table indicates that scattering becomes important below 3700 Å or so. It was found that use of Kodak 2C filter which cuts off radiation below 3500 Å adequately evaluates the net scattering below this wavelength and a detailed analysis using the a_{ij} coefficients is not necessary.

The spectral response was calculated as the ratio of divisions on the chart recorder obtained after the scattering correction to the actual radiation from the tungsten source. The response was evaluated at two positions along the axis of the plasma jet in order to detect any effect of slight change in the focal distance of the scanning mirrors, but no such effect could be detected except at wavelengths below 3400 Å. The results of the calibration are tabulated

in Table A1-2. Figure A1-1 shows the results in a graphical form. The response below 3400 Å shown in the results represents an average value for the two axial positions.

The reproducibility of calibration was within 1%. The total error in calibration is estimated to be less than 4% in the visible range and about 8% in the ultraviolet range. About 3% of the total error arises from the uncertainty of the temperature of the strip and the emissivity of its surface, and the rest of the error is mainly due to error in estimating the scattered intensity.

The intensity of radiation from the tungsten strip, I'_λ refers to the energy radiated per unit time by unit surface of the strip in unit wavelength interval and in unit solid angle. To obtain total radiation in a spherical volume, one must multiply by a factor of 4π. Further, to obtain the total radiation from a spectral line, one must integrate the area under the intensity curve traced by the recorder pen, which traces the intensity as a function of the wavelength, a typical curve being shown in Figure II-4. To obtain the radiation in unit frequency interval instead of unit wavelength interval, such as required in continuum radiation measurements, one must multiply by a factor of $\frac{\lambda^2}{c}$. The radiation calculated in the above manner always represents total radiation arising from the unit cross-section of the entire strip of the plasma observed by the instrument. One

must therefore interpret the results of intensity measurements judiciously.

REFERENCES

1. J. C. DeVos, Physica, 20, 690, (1954).

2. E. A. Mechtly, "International System of Units, Physical Constants and Conversion Factors", NASA Rept. SP-7012, (1964).

Table A1-1 a_{ij} coefficients for evaluating the scattered intensity. The two digit numbers following the coefficients are powers of 10 to be multiplied.

$\lambda_i \rightarrow$ / $\lambda_j \downarrow$	2500 Å	2750 5000	3000 5250	3250 5500	3500 5750	3750 6000	4000 6250	4250 6500	4500 6750	4750 7000
2500 Å	0.00 00	3.75-03 2.06-04	6.20-03 1.90-04	8.06-03 2.31-04	8.70-03 1.83-04	5.16-03 1.27-04	1.42-03 0.00 00	6.13-04 0.00 00	3.36-04 0.00 00	2.40-04 0.00 00
2750	0.00 00	0.00 00 3.39-04	5.17-03 3.06-04	9.68-03 3.53-04	7.14-03 3.15-04	3.68-03 3.47-04	1.81-03 3.29-04	8.82-04 0.00 00	4.52-04 0.00 00	4.25-04 0.00 00
3000	0.00 00	0.00 00 4.66-04	0.00 00 4.13-04	8.05-03 4.63-04	7.59-03 3.88-04	4.21-03 5.59-04	2.00-03 6.58-04	1.15-03 0.00 00	6.95-04 0.00 00	5.68-04 0.00 00
3250	0.00 00	0.00 00 5.69-04	0.00 00 5.06-04	0.00 00 5.48-04	8.70-03 4.58-04	4.04-03 7.46-04	2.07-03 8.58-04	1.45-03 0.00 00	9.23-04 0.00 00	7.65-04 0.00 00
3500	0.00 00	0.00 00 6.51-04	0.00 00 5.68-04	0.00 00 6.30-04	0.00 00 5.47-04	3.68-03 9.07-04	2.00-03 7.57-04	1.72-03 1.84-04	1.16-03 0.00 00	8.56-04 0.00 00
3750	0.00 00	0.00 00 7.84-04	0.00 00 6.76-04	0.00 00 7.12-04	0.00 00 6.50-04	0.00 00 1.06-03	1.61-03 8.22-04	1.79-03 1.84-04	1.46-03 0.00 00	9.93-04 0.00 00
4000	0.00 00	0.00 00 9.17-04	0.00 00 7.48-04	0.00 00 7.91-04	0.00 00 6.94-04	0.00 00 1.23-03	0.00 00 8.22-04	1.65-03 1.84-04	1.61-03 0.00 00	1.16-03 0.00 00
4250	0.00 00	0.00 00 9.72-04	0.00 00 8.05-04	0.00 00 8.73-04	0.00 00 8.05-04	0.00 00 1.39-03	0.00 00 8.88-04	0.00 00 1.84-04	7.19-04 0.00 00	1.05-03 0.00 00
4500	0.00 00	0.00 00 8.88-04	0.00 00 8.19-04	0.00 00 9.97-04	0.00 00 8.62-04	0.00 00 1.53-03	0.00 00 8.88-04	0.00 00 1.84-04	0.00 00 0.00 00	5.14-04 0.00 00
4750	0.00 00	0.00 00 3.67-04	0.00 00 5.83-04	0.00 00 9.06-04	0.00 00 8.66-04	0.00 00 1.05-03	0.00 00 9.87-04	0.00 00 2.76-04	0.00 00 0.00 00	0.00 00 0.00 00
5000	0.00 00	0.00 00 0.00 00	0.00 00 3.21-04	0.00 00 6.05-04	0.00 00 7.50-04	0.00 00 1.74-03	0.00 00 1.02-03	0.00 00 2.76-04	0.00 00 0.00 00	0.00 00 0.00 00
5250	0.00 00	0.00 00 0.00 00	0.00 00 0.00 00	0.00 00 3.38-04	0.00 00 6.13-04	0.00 00 1.67-03	0.00 00 9.87-04	0.00 00 2.76-04	0.00 00 0.00 00	0.00 00 0.00 00
5500	0.00 00	0.00 00 0.00 00	0.00 00 0.00 00	0.00 00 0.00 00	0.00 00 3.88-04	0.00 00 1.23-03	0.00 00 8.22-04	0.00 00 1.84-04	0.00 00 0.00 00	0.00 00 0.00 00
5750	0.00 00	0.00 00 0.00 00	0.00 00 0.00 00	0.00 00 0.00 00	0.00 00 0.00 00	0.00 00 6.78-04	0.00 00 7.57-04	0.00 00 1.38-04	0.00 00 0.00 00	0.00 00 0.00 00
6000	0.00 00	0.00 00 0.00 00	0.00 00 0.00 00	0.00 00 0.00 00	0.00 00 0.00 00	0.00 00 0.00 00	0.00 00 4.93-04	0.00 00 0.00 00	0.00 00 0.00 00	0.00 00 0.00 00
6250	0.00 00	0.00 00 0.00 00	0.00 00 0.00 00	0.00 00 0.00 00	0.00 00 0.00 00	0.00 00 0.00 00	0.00 00 0.00 00	0.00 00 0.00 00	0.00 00 0.00 00	0.00 00 0.00 00
6500	0.00 00	0.00 00 0.00 00	0.00 00 0.00 00	0.00 00 0.00 00	0.00 00 0.00 00	0.00 00 0.00 00	0.00 00 0.00 00	0.00 00 0.00 00	0.00 00 0.00 00	0.00 00 0.00 00
6750	0.00 00	0.00 00 0.00 00	0.00 00 0.00 00	0.00 00 0.00 00	0.00 00 0.00 00	0.00 00 0.00 00	0.00 00 0.00 00	0.00 00 0.00 00	0.00 00 0.00 00	0.00 00 0.00 00
7000	0.00 00	0.00 00 0.00 00	0.00 00 0.00 00	0.00 00 0.00 00	0.00 00 0.00 00	0.00 00 0.00 00	0.00 00 0.00 00	0.00 00 0.00 00	0.00 00 0.00 00	0.00 00 0.00 00

Table A1-2

Spectral response of the setup. The corrected intensity is obtained after subtracting scattered intensity from the measured intensity. Response is expressed as:

$$G_\lambda = \frac{\text{corrected intensity}}{\epsilon_{\lambda T} \times \text{Black-body intensity}}$$

The brightness temperature was 1792°C. The two-digit number following the four-digit number is the power of 10 to be multiplied.

z = 11.89 cm

WAVELENGTH (Angstrom)	MEASURED INTENSITY	CORRECTED INTENSITY	BLACK-BODY INTENSITY	EMISSIVITY $\epsilon_{\lambda T}$	RESPONSE G_λ
2500	1.600 02	1.565 01	2.595 00	.427	1.777 01
2750	1.972 02	1.742 01	1.669 01	.459	2.274 00
3000	2.420 02	3.070 01	7.581 01	.468	8.671-01
3250	3.028 02	5.561 01	2.642 02	.467	4.508-01
3500	5.100 02	2.179 02	7.493 02	.469	6.200-01
3750	1.350 03	1.004 03	1.806 03	.472	1.178 00
4000	3.680 03	3.356 03	3.819 03	.476	1.671 00
4250	9.800 03	9.485 03	7.259 03	.466	2.803 00
4500	2.008 04	1.979 04	1.264 04	.463	3.502 00
4750	3.544 04	3.521 04	2.046 04	.459	3.748 00
5000	5.300 04	5.283 04	3.115 04	.457	3.711 00
5250	6.700 04	6.688 04	4.503 04	.455	3.264 00
5500	6.830 04	6.823 04	6.226 04	.452	2.424 00
5750	6.080 04	6.077 04	8.288 04	.448	1.637 00
6000	3.310 04	3.110 04	1.068 05	.445	6.575-01
6250	7.900 03	7.900 03	1.336 05	.440	1.344-01
6500	2.860 03	2.860 03	1.631 05	.437	4.012-02
6750	1.260 03	1.260 03	1.949 05	.434	1.490-02
7000	7.550 02	7.550 02	2.283 05	.430	7.691-03

z = 4.267 cm

WAVELENGTH (Angstrom)	MEASURED INTENSITY	CORRECTED INTENSITY	BLACK-BODY INTENSITY	EMISSIVITY	RESPONSE
2500	1.600 02	7.191 00	2.595 00	.427	6.490 00
2750	1.960 02	1.622 01	1.669 01	.459	2.118 00
3000	2.360 02	2.297 01	7.581 01	.468	6.473-01
3250	3.000 02	5.281 01	2.642 02	.467	4.281-01
3500	5.300 02	2.663 02	7.493 02	.469	7.468-01
3750	1.380 03	1.068 03	1.806 03	.472	1.253 00
4000	3.780 03	3.454 03	3.819 03	.476	1.924 00
4250	9.850 03	9.529 03	7.259 03	.466	2.817 00
4500	2.040 04	2.011 04	1.264 04	.463	3.436 00
4750	3.540 04	3.516 04	2.046 04	.459	3.744 00
5000	5.300 04	5.282 04	3.315 04	.457	3.710 00
5250	6.910 04	6.898 04	4.503 04	.455	3.367 00
5500	6.960 04	6.953 04	6.226 04	.452	2.471 00
5750	6.150 04	6.147 04	8.288 04	.448	1.656 00
6000	3.370 04	3.370 04	1.068 05	.445	6.702-01
6250	8.200 03	8.200 03	1.336 05	.440	1.395-01
6500	2.900 03	2.900 03	1.631 05	.437	4.152-02
6750	1.300 03	1.300 03	1.949 05	.434	1.537-02
7000	7.600 02	7.600 02	2.283 05	.430	7.742-03

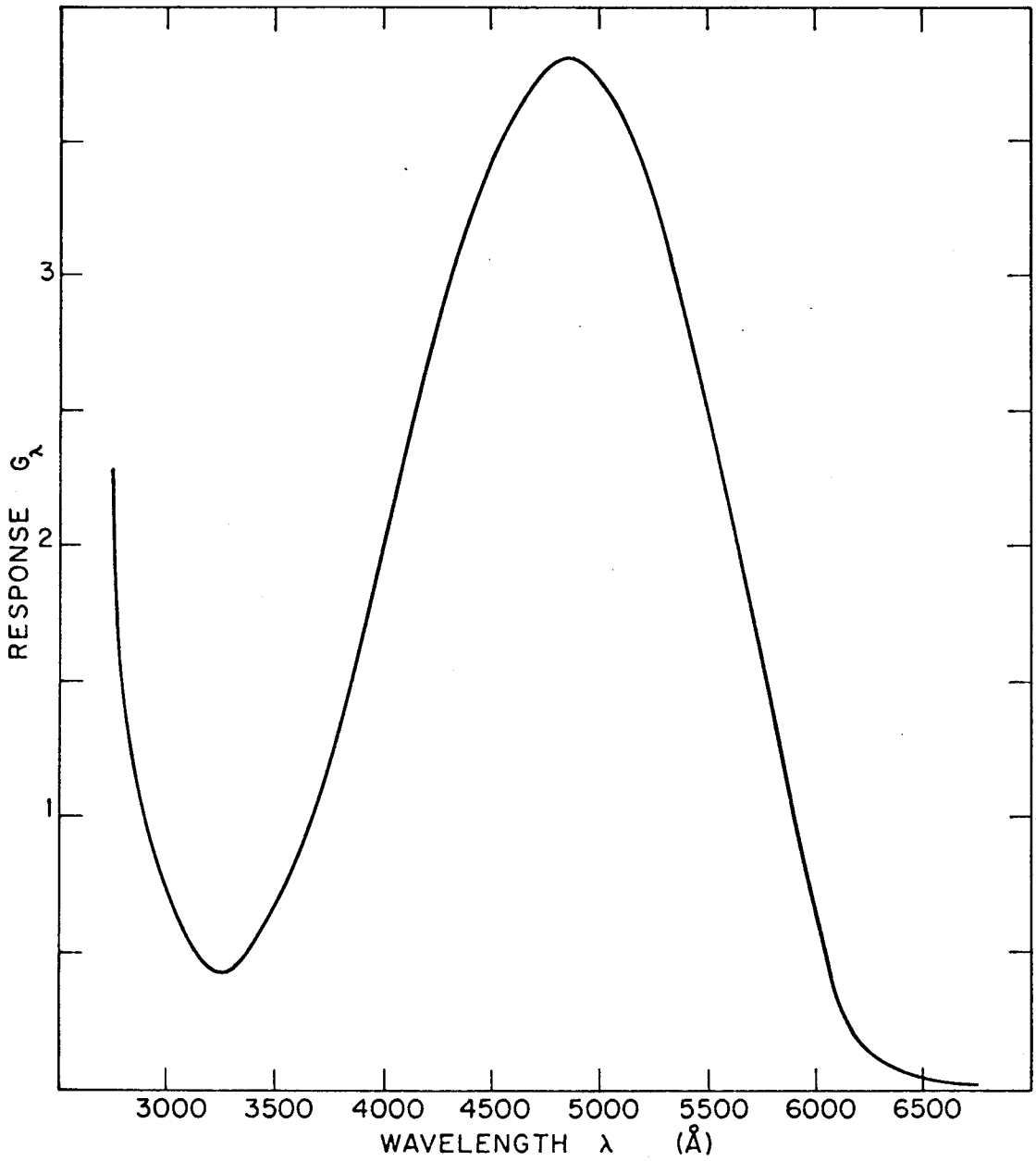

Figure A1-1

Spectral response of the setup. G is the ratio of measured chart divisions to the actual intensity of the standard source. Curve shown is an average value for two axial positions at 4.267 cm and 11.89 cm below the leading edge of the RF coil.

APPENDIX A-2

Purification of Argon

The argon gas used in this study was obtained from Linde division of the Union Carbide Corporation and had stated maximum impurities of 40 ppm; mostly H_2, N_2, H_2O, CO_2 and some hydrocarbons. Preliminary observations in the plasma indicated that small amount of impurities in the feed gas could affect the operation of the plasma generator and also the radiation characteristics of the plasma. To illustrate the effect of impurities on operation of the plasma generator, photographs of the plasma jet taken with different concentrations of nitrogen as an impurity in argon are shown in Figure A2-1. The scheme for mixing the impurity gas was the same as that shown in Figure II-2. It can be seen that the radiation from the plasma jet changes considerably with increasing amount of impurities in the feed gas, and the flame broadens in diameter and shrinks in length. The observations clearly pointed out the necessity for using highly pure feed gas, and therefore a scheme for further removal of the trace impurities was undertaken.

Chapala et al[1] found that most of the hydrogen can be removed from helium gas when it is passed over cupric oxide at 490 - 500°C. Gibbs et al[2] found that granules of copper heated to 600°C remove oxygen from argon almost quantitatively even at very high space velocities. A packing of

type 4A molecular sieve is known to hold back moisture, hydrocarbons, carbon dioxide, oxygen and most of nitrogen if the temperature is held very low[3].

The method for removal of traces of impurities from argon was based on passing the gas over heated cupric oxide followed by heated copper metal and finally through a column containing type-4A-molecular sieve held at very low temperature.

The purification train is shown pictorially in Figure A2-2 in which the essential constructional details of the apparatus are shown, disregarding dimensions. Argon from the storage cylinder bank was passed through a stainless steel tube, $\frac{7}{8}$ in I. D. and 36 in long, containing 350 g of CuO in section (A) followed by 60 gm of thin copper shavings in section (B). The CuO section was maintained at 530°C and the copper section at 625°C, as measured by calibrated thermocouples in contact with the outer wall of the stainless-steel tube. No attempt was made for accurate temperature measurement and control because it does not affect the results to any measurable degree. The two sections were heated by means of two electrical furnaces rated at 500 watts each, and controlled separately. The hot gas issuing out of the furnace was cooled down to room temperature in a forced circulation type cooler (C), of the variety used in household refrigeration. The gas was further cooled to -30°C in a double-pipe heat exchanger (D)

and then to -140°C in the scrubbing column (E). The packed portion of the scrubbing column was $1\frac{3}{8}$ in in diameter and 16 in long. The packing was Linde type 4A molecular sieve, in the form of $\frac{1}{16}$ in pellets. Liquid nitrogen evaporating in an outer jacket was used as the cooling medium. A thin wall of asbestos separated the packed column from the cooling jacket, the purpose of the insulation being to maintain the temperature of the argon above its freezing point. A finer temperature control could be achieved by means of an electrical heating element incorporated in the asbestos partition, but due to self-regulatory nature of the evaporative cooling system, the finer heating control was never necessary while the system was in operation. However, if the flow of argon was cut off for a long period, having liquid nitrogen in the cooling jacket, then the asbestos partition would not maintain the required temperature difference between the cooling jacket and the column, and the argon trapped in the column would freeze, blocking the passage of the gas, and calling for operation of the heater. The purified gas leaving the column was brought to near room temperature in heat exchanger (D) where it cooled the incoming gas.

Nitrogen being the most difficult impurity to remove, the following test was designed to estimate the amount of nitrogen in the purified argon. In the first part of the experiment, known amounts of nitrogen, namely 300 ppm and

700 ppm were premixed with argon and the intensity of $N_2^+(1-)$ band radiation at 3881Å band head was recorded, at the same fixed point in the plasma. In the second part of the test the purified gas was used and the intensity was again recorded. Comparison of the intensity with the case of known amounts of nitrogen indicated that the nitrogen in the purified gas was present in amount less than 3 ppm.

REFERENCES

1. I. D. Chapala, N. M. Ovchenkov and A. M. Kudryavtsev, Gazovaya Prom., 5, 48, (1960).
Chem. Abstracts, 54, 18903h, (1960).

2. D. S. Gibbs, M. J. Svec and R. E. Harrington, I. & E. Chemistry, 48, 289, (1956).

3. "Argon, Helium and the Rare Gases", edited by G. A. Coak, vol. II, Chap. XII, Interscience, New York, (1961).

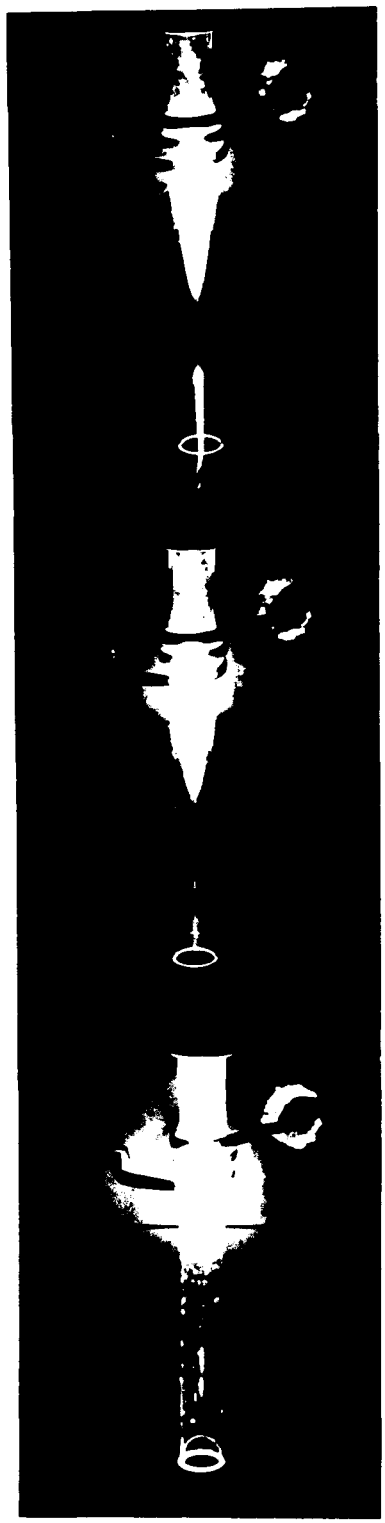

Pure Argon. The flame extended well below the open end of the tube. The white tail was mainly due to N_2(2 +ve) and N_2^+(1 -ve) radiation originating from the ambient air coming in contact with the highly excited argon.

Argon + 0.13% N_2. The flame shrank in length and expanded in diameter. The tail nearly disappeared. The visible radiation increased in strength in the upstream section.

Argon + 0.31% N_2. The flame shrank in length and expanded in diameter further. The tail vanished. The visible radiation was intense near the RF coil, but it was weak in the downstream section.

Figure A2-1 Effect of impurity in argon on the radiation characteristics of the plasma jet.

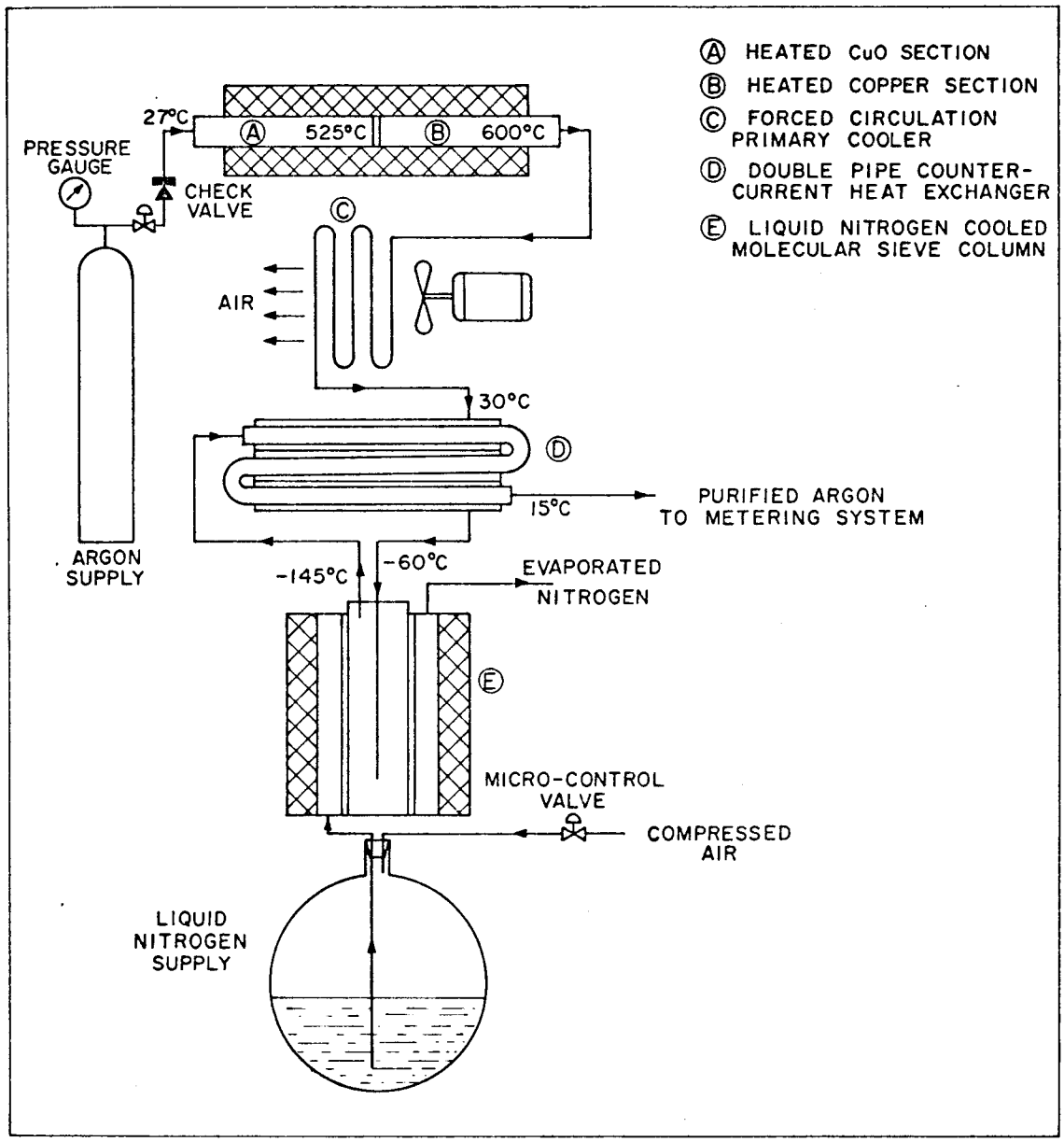

Figure A2-2

Apparatus for purification of argon. Indicated temperatures are normal steady-state values.

APPENDIX A-3

On Abel-Inversion

The Integral transform

$$I(r) = -\frac{1}{\pi} \int_{x=r}^{r_o} \frac{d\, I(x)}{\sqrt{x^2 - r^2}} \qquad (A3\text{-}1)$$

solves the Abel type integral equation

$$I(x) = 2 \int_{r=x}^{r_o} \frac{I(r)\, rdr}{\sqrt{r^2 - x^2}} \qquad (A3\text{-}2)$$

which often arises when a laterally integrated value I(x) of some observable is measured from which the radial distribution function I(r) must be obtained. Figure A3-1 illustrates the geometry of spectroscopic intensity measurements in which a cylindrically confined plasma is being scanned laterally.

Since the shape of the intensity curve is arbitrary, one must have recourse to numerical methods to solve equation (A3-1). Various numerical approaches have been proposed, from the simplest curve fitting technique of Pearce[1] to a sophisticated method of fitting Gegenüber polynomials to the measured intensity curve[2]. As pointed out by Gorenflo and Kovetz[2], noise superimposed on function I(x) appears as amplified fluctuations in the computed function I(r) because of the half order differentiation process involved in the transform of equation (A3-1), making the problem of

inversion very susceptible to the errors of measurement.

Nagler[3] proposed a simple method in which the circular cross-section of the source was divided into finite zones and an average value of radial intensity was assumed for each zone. Olsen[4] used a direct numerical approach in which he set:

$$\underline{I(r)} = B\underline{I(x)}$$

where $B_{ij} = \frac{2}{\pi\Delta x} \epsilon_{i-1,\, j-1}$ for $i=j$

$$B_{ij} = \frac{2}{\pi\Delta x}(\epsilon_{i-1,\, j-1} - \epsilon_{i-1,\, j-2}) \quad \text{for } i<j$$

$$B_{ij} = 0 \quad \text{for } i>j$$

and $$\epsilon_{ij} = \left((j+1)^2 - i^2\right)^{\frac{1}{2}} - (j^2 - i^2)^{\frac{1}{2}}$$

(A3-3)

Pearce[1] has also given a similar numerical technique.

Bockasten[5] fitted a third order polynomial curve to seccessive four values of I(x) and used the four constants to evaluate the coefficients similar to Olsen's B_{ij}.

Bockasten's calculations[5] show that the error in the radial intensity due to taking finite increments decreases with increasing number of intervals, but on the other hand, the uncertainty due to some fixed error in each of the independent observations becomes larger with increasing number of observations. His calculations substantiate the noise-amplifying character of the Abel-inversion process.

Gorenflo has pointed out[2] that location of the center (r=0) of the source having cylindrical symmetry may introduce a large error. Woodward[6] carried out numerical calculations using typical laboratory data on the plasma jet and compared the standard deviations in I(r) for a fixed standard deviation in I(x) expressed as a fraction of intensity at the center, for the methods of Pearce, Nagler, Olsen and Bockasten. Table A3-1 gives the comparison in a tabular form. He concluded that Nagler's method is the least accurate of the four methods studied and both Pearce's and Bockasten's methods give about the same degree of accuracy. Gorenflo's Gegenüber polynomial method is more complex than the above methods and does not yield improvement in the results. The table shows that the error becomes large at the center and the boundary of the plasma jet for all the methods studied. Bockasten[5] has noted that in most practical cases, the errors due to experimental measurements will mask the error involved in the numerical approximation.

As the conclusion of the above studies, one should observe the following precautions when interpreting the experimental intensity data taken by side-on measurements.

1. The measured intensities I(x) should be plotted on a large graph paper, and the dips and wiggles in the curve which have no physical significance, should be carefully smoothed out. Bockasten's third order

polynomial method for smoothing out the data is quite effective in the central part of the intensity curve, but does not yield good results near the boundary, where the change in intensity may be abrupt.

2. The center of the curve should be determind accurately. When possible, the side-to-side curve can be folded to determine the center. Cylindrical symmetry of the source is an essential condition in using the Abel transformation.

3. The Abel transformation assumes that the intensity at the boundary is zero. Residual intensity at the boundary if any, should be subtracted from all other intensities, or otherwise, forced to a zero value.

4. Least, but sufficient number of intervals should be chosen in the numerical integration of Abel's equation. The criterion for sufficiency is that the points should adequately represent the curvature in the plot of I(x).

5. Values of I(r) near the center should be given limited significance and the values near the boundary have almost no significance. Most accurate values of I(r) are obtained at approximately $r = 0.5r_o$.

An assumption implicit in equations (A3-1) and (A3-2) is that the self absorption of the spectral line is negligible. While this assumption holds good for argon plasma in

the wavelength range of 3000 - 6000 Å[7], one should verify it in each case. Freeman and Katz[8] have developed a method of inversion which takes into account small amount of self-absorption.

Some attempts have been made to automate the Abel-inversion procedure by the use of computers. Shumaker and Yokley[9] have described the use of an in-line analog computer in conjunction with a rotating prism for rapid scanning of the plasma, to obtain the I(r) values immediately. Paquette and Wiese[10] made use of a digital computer and an analog-to-digital converter to improve the accuracy of measurements.

It should be pointed out in the light of the conclusions drawn previously, that the rapid scanning methods described above may leave a large amount of experimental noise unfiltered and give erraneous results.

In the present work, Pearce's method using A_{ij} coefficients was preferred because it is simple to use and gives sufficiently good results. Table A3-2 gives the coefficients used to determine the radial intensities from the observed intensities. The error involved in this method for an assumed standard deviation of 1% in measured intensities varies between 1% to 6% depending on the radial position. As mentioned previously, at the center and the boundary, the error is considerably large.

In preparing the computer program for Abel-inversion and for surveying the various methods, Dr. Joe Woodward's help is greatly appreciated.

REFERENCES

1. W. J. Pearce, "Plasma Jet Temperature Study", WADC Technical Rep. p. 59, General Electric Co., (1960).
2. R. Gorenflo and Y. Kovetz, Institute Fur Plasma Physic, Rept. IPP/6/29, Garching bei Munchen, (Nov. 1964).
3. R. G. Nagler "Application of Spectroscopic Temperature Measuring Methods to Definition of a Plasma Arc Flame", Jet Propulsion Laboratory, Technical Rept., pp. 32-66, Pasadena, California, (Jan. 1961).
4. H. N. Olsen in "Temperature, Its Measurement and Control in Science and Industry", edited by C. M. Herzfeld, vol. III, Part 1, p.593, Reinhold, New York, (1962).
5. K. Bockasten, J. Opt. Soc. Am., 51, 943, (1961).
6. J. Woodward, unpublished paper, Chem. Eng. Dept., California Institute of Technology, Pasadena, California, (1965).
7. B. S. Malone and W. H. Corcoran, J. Q. S. R. T., 6, 443, (1966).
8. M. P. Freeman and S. Katz, J. Opt. Soc. Am., 50, 826, (1960).
9. J. B. Shumaker and C. R. Yokley, App. Optics, 3, 83, (1964).
10. D. R. Paquette and W. L. Wiese, App. Optics, 3, 291, (1964).

Table A3-1

Comparison Between Different Numerical Solutions of Abel Transformation

Number of samples = 25
Number of intervals = 10
Standard deviation in I(x) = 0.01

r=	Exact Inverse	Pearce		Nagler		Olsen		Bockasten	
		Inverse	Standard Deviation	Inverse	Standard Deviation	Inverse	Standard Deviation	Inverse	Standard Deviation
0.00	1.000			0.973	0.062	0.987	0.082	0.980	0.102
0.05	0.998	0.973	0.062						
0.10	0.990			0.973	0.062	1.019	0.052	1.025	0.056
0.15	0.978	0.985	0.039						
0.20	0.960			0.997	0.112	0.937	0.034	0.941	0.034
0.25	0.938	0.911	0.026						
0.30	0.910			0.825	0.128	0.914	0.030	0.916	0.032
0.35	0.878	0.874	0.021						
0.40	0.840			0.923	0.138	0.828	0.033	0.834	0.032
0.45	0.798	0.787	0.025						
0.50	0.750			0.651	0.159	0.745	0.026	0.751	0.025
0.55	0.698	0.696	0.019						
0.60	0.640			0.741	0.163	0.631	0.021	0.640	0.020
0.65	0.578	0.578	0.016						
0.70	0.510			0.417	0.161	0.493	0.019	0.505	0.018
0.75	0.438	0.441	0.014						
0.80	0.360			0.466	0.168	0.346	0.021	0.363	0.021
0.85	0.278	0.294	0.016						
0.90	0.190			0.121	0.171	0.161	0.020	0.182	0.014
0.95	0.098	0.127	0.016						
1.00	0.000			0.133	0.173	-	-	-	-

Table A3-2

Numerical Values of A_{ij} in Pearce's Solution of Abel's Transformation.
(Numbers in superscript denote power of 10 to be multiplied)

i \ j	1	2	3	4	5	6	7	8	9	10
1	5.000^{0}	-2.887^{0}	-8.207^{-1}	-3.692^{-1}	-2.068^{-1}	-1.315^{-1}	-9.086^{-2}	-6.647^{-2}	-5.073^{-2}	-3.997^{-2}
2	0	-2.887^{0}	-1.415^{0}	-4.827^{-1}	-2.416^{-1}	-1.454^{-1}	-9.743^{-2}	-6.996^{-2}	-5.274^{-2}	-4.122^{-2}
3	0	0	-2.236^{0}	-1.038^{0}	-3.651^{-1}	-1.879^{-1}	-1.159^{-1}	-7.928^{-2}	-5.796^{-2}	-4.437^{-2}
4	0	0	0	-1.890^{0}	-8.531^{-1}	-3.029^{-1}	-1.574^{-1}	-9.814^{-2}	-6.784^{-2}	-5.008^{-2}
5	0	0	0	0	-1.667^{0}	-7.398^{-1}	-2.635^{-1}	-1.375^{-1}	-8.618^{-2}	-5.990^{-2}
6	0	0	0	0	0	-1.508^{0}	-6.616^{-1}	-2.359^{-1}	-1.234^{-1}	-7.750^{-2}
7	0	0	0	0	0	0	-1.387^{0}	-6.037^{-1}	-2.153^{-1}	-1.127^{-1}
8	0	0	0	0	0	0	0	-1.291^{0}	-5.586^{-1}	-1.992^{-1}
9	0	0	0	0	0	0	0	0	-1.213^{0}	-5.222^{-1}
10	0	0	0	0	0	0	0	0	0	-1.147^{0}

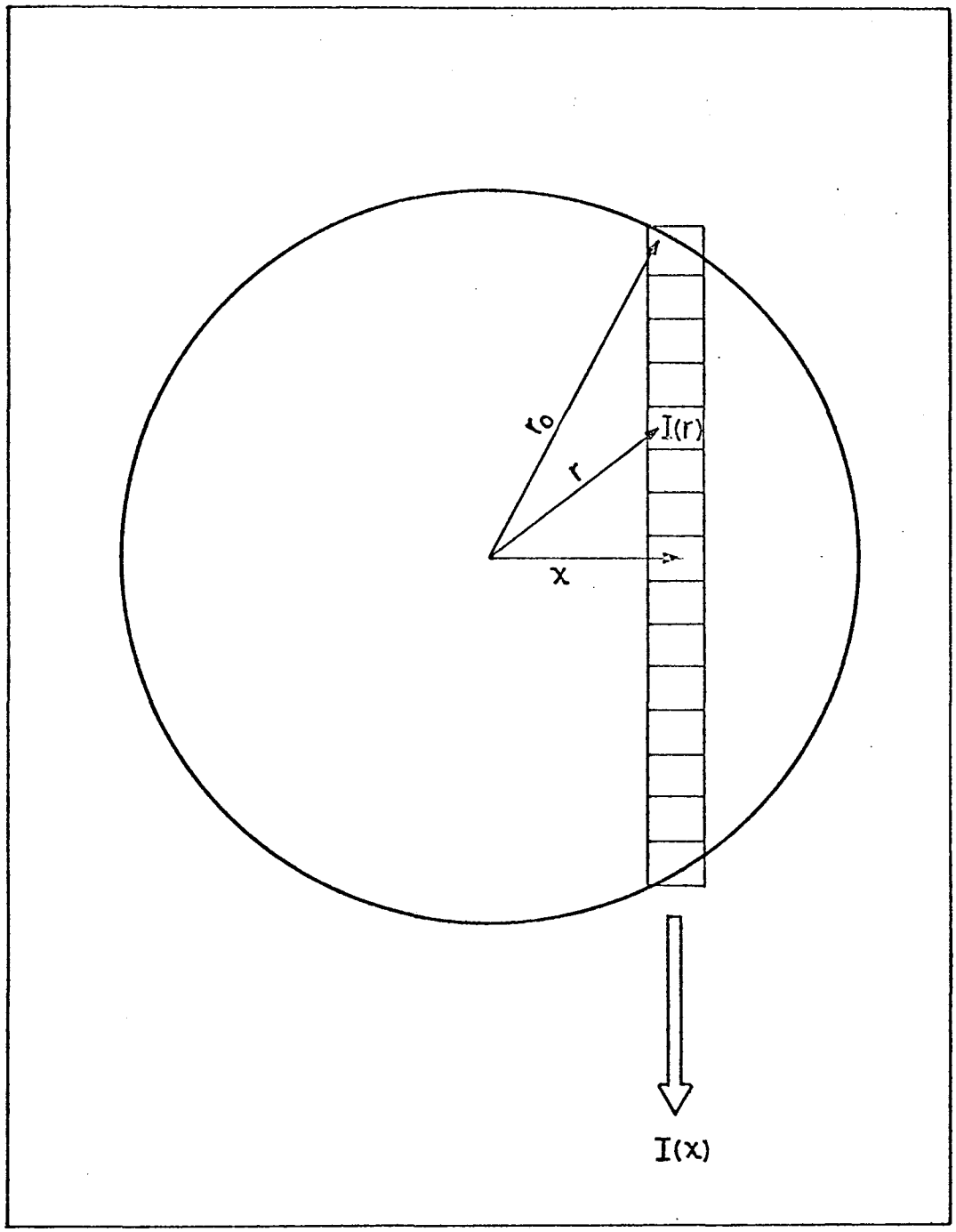

Figure A3-1

Spectroscopic measurement of intensity in a cylindrical source. The measured intensity I(x) is a sum of radial intensities I(r) arising from different zones of the plasma. Abel's transformation gives I(r) from the measured values of I(x).

APPENDIX A-4

J. Quant. Spectrosc. Radiat. Transfer. Vol. 8. pp. 1721–1730. Pergamon Press 1968. Printed in Great Britain

SOME NEW TRANSITION PROBABILITIES OF ARGON I IN THE RANGE OF 5000–6500 Å AND THE ROLE OF A NONUNIFORM SOURCE TEMPERATURE

S. V. DESAI and W. H. CORCORAN

California Institute of Technology, Pasadena, California 91109

(*Received* 17 *April* 1968)

Abstract—New or improved experimental values for certain transition probabilities of argon I were obtained using a radiofrequency, induction-coupled argon plasma as the source of excitation. Intensities of twenty-six lines of the argon I spectrum in the wavelength range of 3000–6500 Å were measured with a photomultiplier tube. The transition probabilities of eighteen new lines were determined from the known values for eight lines, assuming local thermodynamic equilibrium. The radial temperature gradient introduced a slight deviation from linearity in the plot of $\log(I_{nm}\lambda_{nm}/g_nA_{nm})$ vs. E_n, but because the effect was very small it was practically obscured by the larger errors in experimental measurements. For the gas under observation the measured temperature is the space-average temperature $\bar{T}_n$, defined by the relationship

$$\frac{1}{\bar{T}_n} = \frac{\sum_{r=1}^{s} (n_r/T_r)}{n_t}$$

where n_r is the number of atoms per unit volume at radial position r in the nth excited state, and n_t is the average number of atoms per unit volume at the nth excited state in the zone viewed by the spectrometer. The value of $\bar{T}_n$ is approximately 7 per cent lower than the true radial temperature at the axis of the jet, with the difference becoming less toward the periphery, and is weakly dependent on the level of excitation.

INTRODUCTION

THE INTENSITY of atomic line radiation from a homogeneous gas is given by:

$$I_{nm} = \frac{hcg_n n_o A_{nm}}{\lambda_{nm} Q_0} e^{-E_n/kT} \tag{1}$$

Here, A_{nm} is the Einstein transition probability for a transition from the upper energy level designated by the subscript n to the lower energy level m. For simple spectra such as hydrogen and helium, values of A_{nm} can be obtained from quantum-mechanical calculations with a fair degree of accuracy.[1] For complex spectra such as argon, attempts have been made to calculate the transition probabilities,[2] but the results do not agree well with the experiments except for a few lines. Experimental values of A_{nm} for argon I have been reported,[3,4] and a previous publication from this laboratory[5] gave dependable values of A_{nm} for twenty-eight lines of argon I.

The method of evaluation of A_{nm} is based on equation (1) rearranged in the following form:

$$\log \frac{I_{nm}\lambda_{nm}}{g_n A_{nm}} = \log C - \frac{E_n}{2{\cdot}303kT}. \tag{2}$$

Equation (2) is really valid only when all the emitters are at the same temperature, a condition which in practice is hard to establish at higher temperatures. The aim of the present investigation was to evaluate the effect of the non-uniformity of the temperature of the source on the determination of transition probabilities and to establish new values of transition probabilities for argon I in the range from 5000 Å to 6500 Å.

EXPERIMENTAL APPARATUS

Figure 1 is a schematic diagram of the experimental apparatus. A plasma generated by induction heating with a radiofrequency unit similar to that described by REED[6] was the source of radiation. The feed rate of argon to the plasma generator was 2·5 l/min for the core and 12 l/min for the cooling stream concentric with the core. There was significant mixing between the two coaxial streams in the heating zone. Net power input to the gas was held constant at 1·6 kW, and a test zone which was 1·4-in. below the bottom turn of the RF coil was selected for measurements. Radiation from the plasma passed via an optical scanning system composed of front-surface mirrors and a quartz-lithium-fluoride, achromatic, condensing lens into the spectrophotometric slit. The 0·5-meter spectrophotometer, a

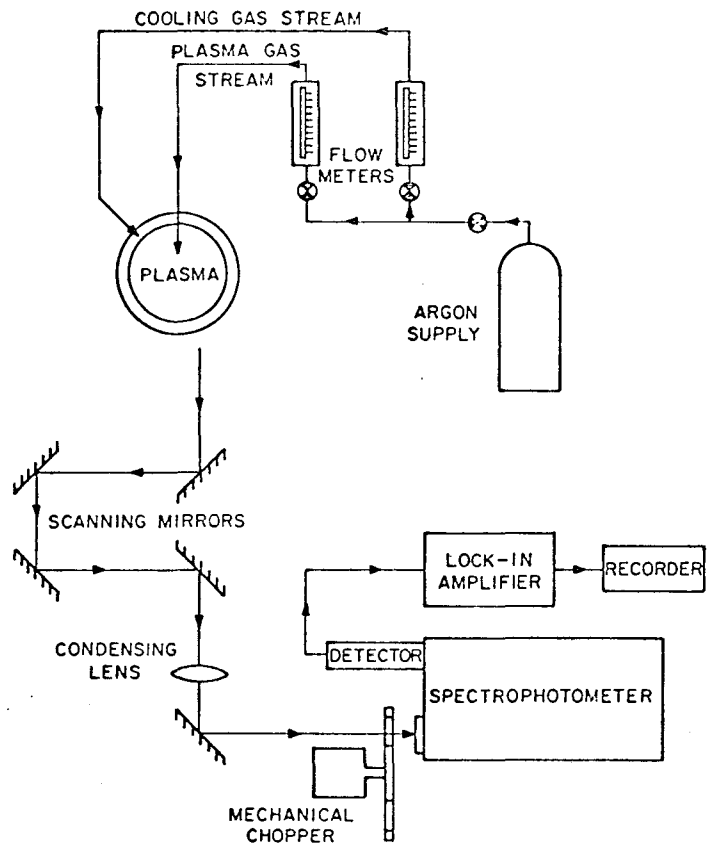

FIG. 1. Schematic diagram of the experimental apparatus showing the feed streams and the instrumentation for measurement of intensities.

wavelength scanning instrument of the Ebert type, had a grating with 1180 grooves/mm which gave a dispersion of 16 Å/mm in the first order. An RCA type 1P28 photomultiplier tube was used as the detector, and a lock-in amplifier in conjunction with a mechanical chopper in front of the entrance slit of the spectrophotometer was used to amplify the signal from the detector to a level of approximately 1 mV. A record of the signal was traced on a chart recorder fitted with an electronic integrator which allowed a measure of line intensity to be obtained immediately. The entrance slit was 1·5 mm in height and 60 μ in width, and the corresponding dimensions of the exit slit were 3 mm and 60 μ.

Overall spectral response of the system was obtained by the use of a standard, tungsten-strip lamp, and an optical pyrometer was used to measure the temperature of the tungsten strip. A comparison of the observed intensity with the actual intensity of radiation of the tungsten strip made it possible to determine the absolute spectral response of the system. The radiation of the tungsten strip at different wavelengths was calculated by multiplying the Planck function by the emissivity for tungsten as reported by DEVOS.[7]

EXPERIMENTAL PROCEDURE

In the first part of the experiment, eight different lines of the spectrum of argon I for which the values of the transition probabilities were known were scanned at the rate of 2 Å/min for six different positions along a line perpendicular to the axis of the plasma jet, starting from the center. A preliminary scan indicated that the plasma jet was quite symmetrical about the axis; hence only one side of the jet was scanned. Intensities at ten equal intervals in the direction of scanning were interpolated from the measured intensities. The value of intensity at the wall of the quartz tube, which was used to confine the plasma jet, was subtracted from other intensities.

In the second part of the experiment, twenty-six lines of the spectrum of argon I, including the eight lines for which the transition probabilities were previously determined in this laboratory, were scanned at the central position. The same experimental conditions were maintained for the two parts of the experiments, but the test zone for the second part was slightly downstream from that in the first part.

Stability of the plasma was checked from time to time during the experiment, and each line was scanned at least three times. Agreement of the intensities was within ± 5 per cent for a given line at a given position. The intensities could be reproduced within ± 5 per cent after shutting off the plasma and re-lighting it.

RESULTS AND DISCUSSION

For the determination of the nineteen new or improved transition probabilities of the argon I spectrum reported in Table 2, a straight-line plot of $\log(I_{nm}(x)\lambda_{nm}/g_nA_{nm})$ vs. E_n was prepared in accordance with equation (2) using the measured intensities of the eight lines with fairly accurately known transition probabilities cited in Table 1. Figure 2 is the resulting plot. $I_{nm}(x)$ represents the measured intensity of line radiation and is to be distinguished from $I_{nm}(r)$ which is subsequently used to denote the calculated intensity at a given radius. The values of $\log I_{nm}(x)\lambda_{nm}/g_nA_{nm}$ and hence the transition probabilities for the eighteen lines reported in Table 2 were obtained from this plot. The spectral line at 6043·2 Å arises from two different upper energy levels, and so two transition probabilities were

obtained for the single line. Table 2 also gives a comparison between the newly developed values of transition probabilities and some previously reported values.[4]

TABLE 1. TRANSITION PROBABILITIES OF ARGON I USED TO ESTABLISH STRAIGHT LINE IN FIG. 2

Wavelength (Å)	E_n (cm^{-1})	g_n	$A_{nm} \times 10^{-5}$ (sec^{-1})	Reference
3406·17	124 749·89	1	3·53	(5)
3834·68	121 470·30	1	6·91	(5)
4198·32	117 563·02	1	24·22	(5)
4200·67	116 942·81	7	8·01	(5)
4251·18	116 660·05	3	0·89	(5)
4345·17	118 407·49	3	2·73	(5)
5558·6	122 086·97	5	21·7	*
5572·6	123 557·46	7	11·3	*

* Unpublished work from this laboratory.

TABLE 2. EXPERIMENTAL TRANSITION PROBABILITIES OF ARGON I

Wavelength (Å)	E_n (cm^{-1})	g_n	$A_{nm} \times 10^{-5}$ sec^{-1} (present work)	$A_{nm} \times 10^{-5}$ sec^{-1} (Ref. 4)
5118	125 113·48	5	11·45	
5162·4	123 468·03	3	26·2	
5177·6	124 771·67	5	6·7	
5187·3	123 372·98	5	20·9	
5373·6	124 692·02	5	5·75	
5424	123 903·30	5	12·5	
5495·9	123 653·24	9	28·5	
5506·4	119 212·93	7	2·55	
5606	121 932·91	3	28·65	15·0 (±25%)
5739·7	123 505·54	5	15·68	
5888·7	122 440·11	5	21·3	
5912·1	121 011·98	3	15·24	
6032·1	122 036·13	9	33·2	21·0 (±25%)
6043·2*	122 160·22	7	19·6	
	123 832·50	7	30·6	
6052·7	120 619·08	5	2·19	2·5 (±25%)
6059·3	120 619·08	5	4·38	3·8 (±25%)
6145·4	120 619·08	5	6·85	
6416·3	119 683·11	5	19·5	

* Arises from two transitions having almost equal differences between the upper and the lower energy levels. The reported value of A_{nm} is based on the total measured intensity.

ADCOCK and PLUMTREE's[4] values for the transition probabilities related to the lines at 5558·6 Å and 5572 Å seem to be much lower than the present values. The values from the present work have been checked in this laboratory at least six times in the temperature range between 4500°K to 6500°K with a standard deviation of less than ±2 per cent.

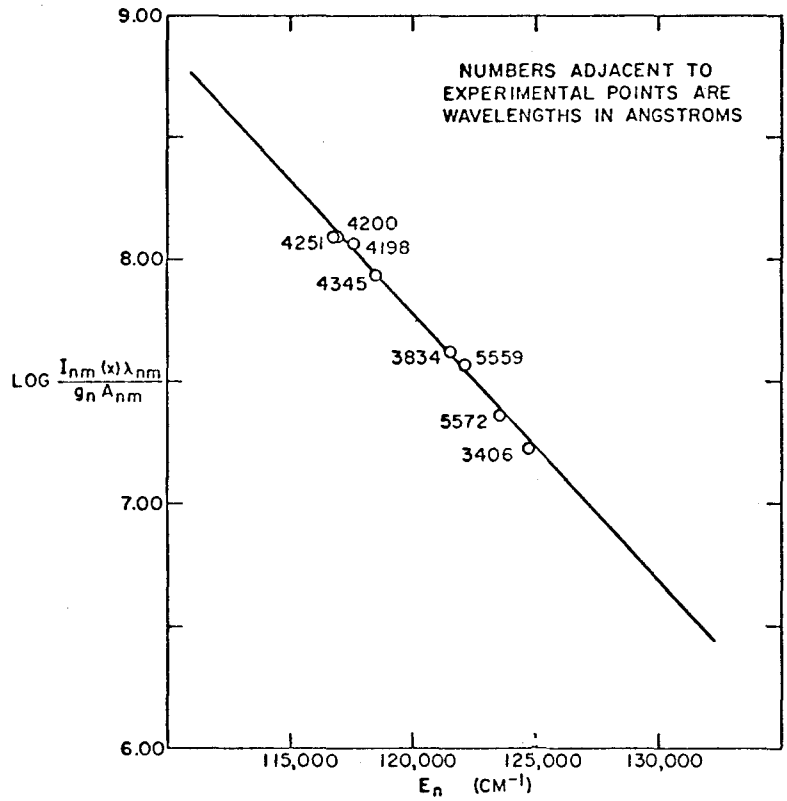

FIG. 2. Determination of transition probabilities. Plot of log $(I_{nm}(x)\lambda_{nm}/g_nA_{nm})$ vs . E_n for determination of transition probabilities. The value of the temperature corresponding to the slope of the line is 5700°K.

Examination of Gericke's paper[8] which is referred to by ADCOCK and PLUMTREE[4] revealed that Gericke used photographic techniques to measure intensities of lines with wavelengths higher than 4500 Å. The photoelectric method used in the present work is inherently more reliable because of better reproducibility and a better signal–noise ratio.

A possible source of error in transition probability measurements is deviation from local thermodynamic equilibrium in the plasma. Great caution must be exercised in the use of equation (1) since it is based on equilibrium between all energy levels including the ground state. On the other hand, use of equation (2) requires equilibrium only among the excited states in question, which is a less severe condition to satisfy. In this laboratory[9] and also in BOTT's work[10] it has been shown that in an atmospheric argon plasma, local thermodynamic equilibrium among the higher excited states does exist for temperatures above 3000°K, but the ground state is underpopulated below about 8000°K.

In the present experiment, the error in measurement of intensity was within ± 5 per cent, and the error in the slope resulting from the inhomogeneity of the plasma was estimated to be ± 5 per cent. The maximum error in transition probabilities is then estimated to be about ± 10 per cent on a relative basis. Values presented in Table 2 have been normalized on the absolute scale with help of the values from Table 1. It is possible that gross systematic

errors were introduced in the process of improvement by various workers of the original values presented in Table 1. For example, Gericke used the absolute transition probability of the argon II line at 4348 Å as given by OLSEN[11] to normalize his values[8] which were further improved by ADCOCK and PLUMTREE[4] and MALONE and CORCORAN.[5] The systematic errors involved in the process of improvement are estimated to be less than 8 per cent. Thus the values presented in Table 2 can be in error by ± 18 per cent on the absolute scale.

The observed intensities $I_{nm}(x)$ represented the sum of the intensities arising from a non-isothermal strip in the direction of observation. A typical case of measurement of intensity is depicted in Fig. 3. Suppose that the non-isothermal strip is composed of s cells, each of

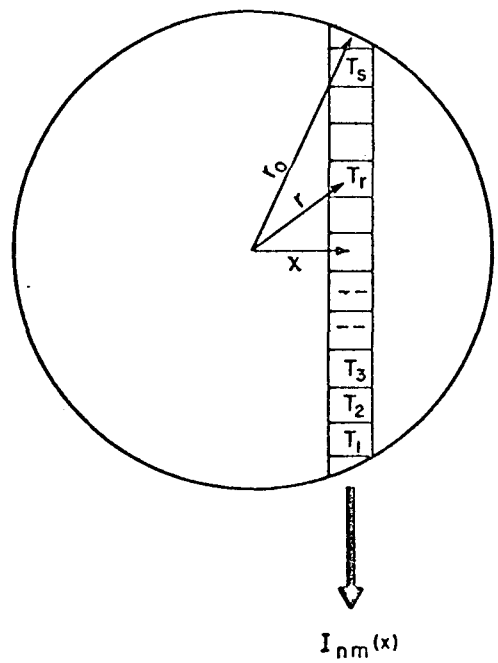

FIG. 3. Cross-section of a cylindrical plasma jet showing cells at different temperatures.

which may be assumed to be isothermal. Since the measured intensity is the sum of intensities arising from these cells, it can be expected that the measured temperature will be just an average of the temperature of these cells, and the idea of a space-average temperature can be elaborated as follows:

The measured intensity can be written as

$$I_{nm}(x) = [I_{nm}(1) + I_{nm}(2) + \cdots + I_{nm}(r) \cdots + I_{nm}(s)]\,\Delta x. \tag{3}$$

Here, Δx is the length of each cell. Equation (3) is valid for the lines for which there is no self-absorption. In accord with equation (1), the measured intensity can be presented as:

$$I_{nm}(x) = \frac{hcA_{nm}\Delta x}{\lambda_{nm}} \sum_{r=1}^{s} \frac{n_0 g_n}{Q_0} e^{-E_n/kT_r} \tag{4}$$

where the true radial intensity is given by

$$I_{nm}(r) = \frac{hcA_{nm}g_n n_0}{\lambda_{nm}Q_0} e^{-E_n/kT_r}. \tag{5}$$

The excitation temperature for the isothermal case is established from the slope of the straight line passing through the plot of $\log(I_{nm}\lambda_{nm}/g_nA_{nm})$ vs. E_n, the value of the slope being $-(1/2{\cdot}303kT)$. For the non-isothermal case, equation (4) can no longer be put in a linear form similar to equation (2). Instead, the slope of the plot is given by

$$\text{Slope} = \frac{\partial \log[I_{nm}(x)\lambda_{nm}/g_nA_{nm}]}{\partial E_n} = -\frac{\sum_{r=1}^{s}(n_0g_n/kT_rQ_0)e^{-E_n/kT_r}}{2{\cdot}303\sum_{r=1}^{s}(n_0g_n/Q_0)e^{-E_n/kT_r}} \tag{6}$$

Consideration of equation (5) gives the slope as:

$$\text{Slope} = -\frac{\sum_{r=1}^{s}[I_{nm}(r)/kT_r]}{2{\cdot}303\sum_{r=1}^{s}I(r)} \tag{7}$$

Because $(n_0g_n/Q_0)e^{-E_n/kT_r}$ represents the number-density of atoms in the given cell which are in the nth excited level, the above equation may be written as

$$\text{Slope} = -\frac{1}{2{\cdot}303k\bar{T}_n} = -\frac{\sum_{r=1}^{s}[I_{nm}(r)/kT_r]}{2{\cdot}303\sum_{r=1}^{s}I_{nm}(r)} = -\frac{\sum_{r=1}^{s}(n_r/kT_r)}{2{\cdot}303n_t} \tag{8}$$

where n_t is the average number-density of the nth excited state in the strip under observation, and the quantity $\bar{T}_n$ is the space-average temperature of the nth excitation level. The average temperature $\bar{T}_n$ can thus be established experimentally by measuring the slope of the line obtained by plotting $\log(I_{nm}(x)\lambda_{nm}/g_nA_{nm})$ vs. E_n. It has the property that the total gas under observation will emit line radiation in accordance with equation (1). The definition of average temperature according to equation (8) holds good when a Boltzmann distribution exists between the excited levels and when self-absorption is negligible. Further, the average temperature so defined depends on the excitation level under consideration inasmuch as the distribution of atoms in the excited levels is governed by the temperature.

For numerical evaluation of the radial intensities, Bockasten's a_{jk} coefficients[12] were applied to the measured intensities at different positions. The resulting true radial intensity distributions are shown in Fig. 4 for the eight lines considered in earlier work in this laboratory. True radial temperature distributions were obtained from the slopes of the straight lines passing through the plots of $\log(I_{nm}(r)\lambda_{nm}/g_nA_{nm})$ vs. E_n at ten different radial positions. The experimental space-average temperature distribution was obtained in a similar way by using the measured intensities $I_{nm}(x)$ instead of the radial intensities $I_{nm}(r)$, and the resulting

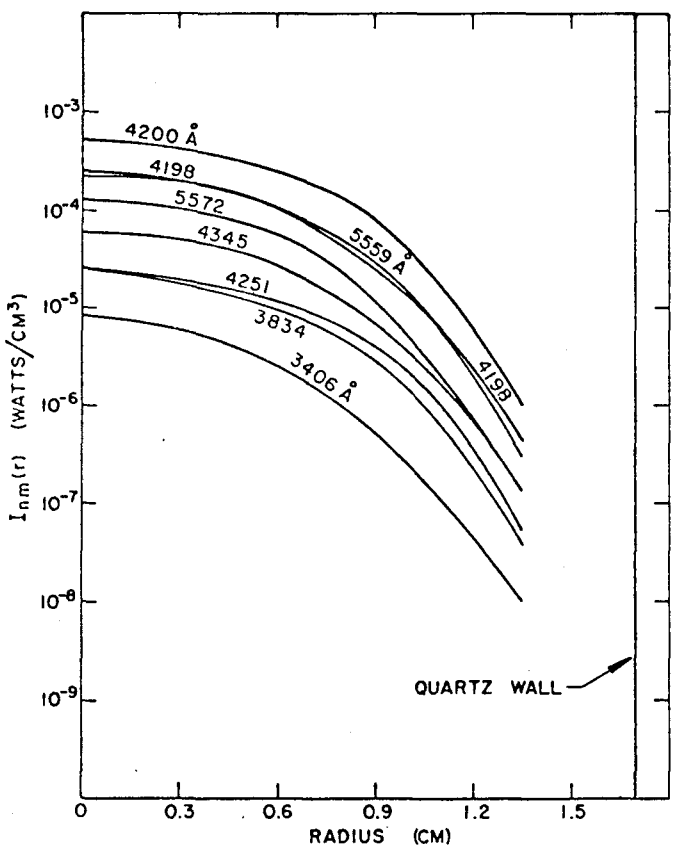

FIG. 4. Radial intensity distribution for eight lines of argon I.

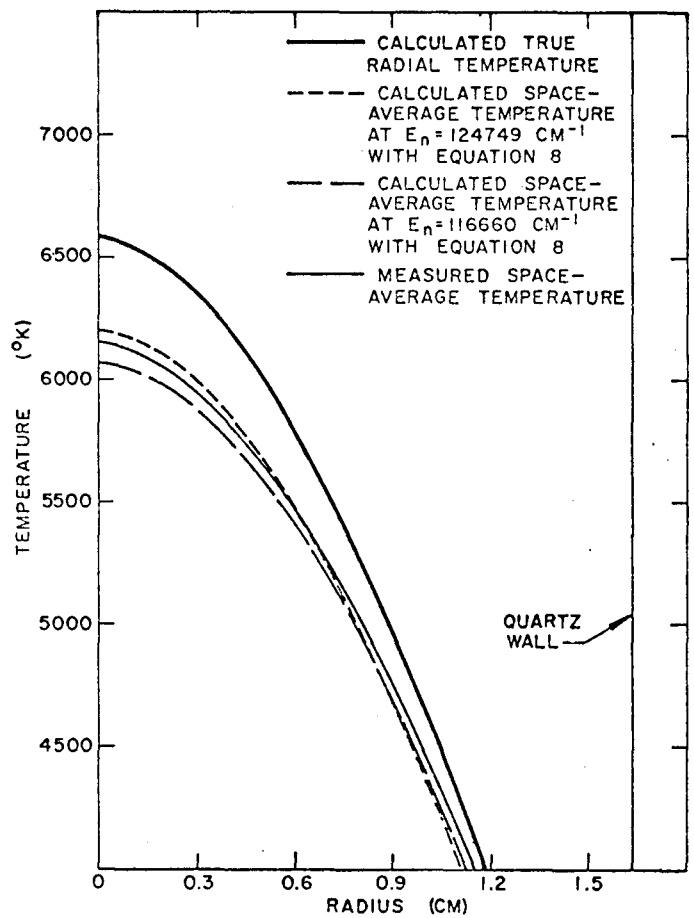

FIG. 5. True radial temperature distribution and the corresponding space-average temperature distribution.

temperature distribution is shown in Fig. 5. The true radial temperature at a given position is always higher than the corresponding space-average temperature because the latter represents a mean value between the radial temperature and the temperature at the boundary.

Numerical calculations for checking the validity of equation (8) were based on matrix inversion of Bockasten's a_{jk} coefficients in conjunction with equation (8). The space-average temperature distribution calculated from the inverted intensities of the lines at 4521 Å and 3406 Å having energy levels of 116 660·05 cm^{-1} and 124 749·89 cm^{-1}, respectively, is also included in Fig. 5 in order to illustrate the effect of the energy level on the space-average temperature. The space-average temperatures are approximately 7 per cent lower than the corresponding true radial temperatures at the axial position, and the amount of discrepancy is only weakly dependent on the energy level under consideration. It can be deduced from Fig. 5 that a plot of $\log(I_{nm}(x)\lambda_{nm}/g_nA_{nm})$ vs. E_n would tend to show a slight negative curvature in spite of local thermodynamic equilibrium, but in general the curvature will be obscured by the experimental errors and the uncertainty of the values of transition probabilities.

CONCLUSIONS

In the measurement of transition probabilities, equation (2) is preferred over equation (1) because equation (2) requires only local thermodynamic equilibrium between the excited states in question. The resulting transition probabilities can be viewed with confidence on a relative basis, but their absolute accuracies depend upon the absolute accuracy of the transition probability used for normalization.

If a temperature gradient exists in the plasma, then the measured temperature represents a space-average over the strip of the source in the line of sight. The space-average temperature is approximately 5–7 per cent lower than the true temperature at the axial position and will introduce an error of about 5–7 per cent in the transition probabilities. That discrepancy in temperature will give rise to a slight amount of curvature in the plot of $\log(I_{nm}(x)\lambda_{nm}/g_nA_{nm})$ vs . E_n, but the curvature will be probably obscured by other larger errors in measurements.

Acknowledgement—Work presented here was supported by the National Center for Air Pollution Control, Bureau of Disease Prevention and Environmental Control, of the Public Health Service. That support is gratefully acknowledged.

NOTATION

A_{nm}	transition probability for radiation from energy level n to m	$\frac{1}{sec}$
c	velocity of light in vacuum	cm/sec
C	spectroscopic constant	
E_n	upper energy level	$\frac{1}{cm}$
g_n	statistical weight of the upper energy level	
h	Planck's constant	sec/cm
I_{nm}	intensity of line radiation for transition from energy level n to level m	W/cm^3
$I_{nm}(x)$	measured intensity of line radiation for transition from energy level n to m per unit area	W/cm^2
$I_{nm}(r)$	calculated radial intensity per unit volume	W/cm^3

k	Boltzmann constant	$\frac{1}{(cm)(°K)}$
n_0	total number of atoms in unit volume	$\#/cm^3$
n_r	number of atoms per unit volume at radial position r, in the nth excited state	$\#/cm^3$
n_t	average number of atoms per unit volume in the entire strip in the nth excited state	$\#/cm^3$
Q_0	partition function of neutral atoms	
r	radial position	cm
s	total number of temperature cells present in the strip under observation	
T	absolute temperature	°K
$\bar{T}_n$	space-average temperature of the nth excitation level	°K
T_r	temperature of a cell	°K
x	transverse position	cm
λ_{nm}	wavelength of spectral line for radiation from energy level n to m	Å

REFERENCES

1. H. R. GRIEM, *Plasma Spectroscopy*, Chapt. 2, McGraw-Hill, New York (1964).
2. R. H. GARSTANG and J. V. BLEFKOM, *J. Opt. Soc. Am.* **55**, 1054 (1965).
3. H. N. OLSEN, *JQSRT* **3**, 59 (1963).
4. B. D. ADCOCK and W. E. G. PLUMTREE, *JQSRT* **4**, 29 (1964).
5. B. S. MALONE and W. H. CORCORAN, *JQSRT* **6**, 443 (1966).
6. T. B. REED, *J. Appl. Phys.* **32**, 821 (1961).
7. J. C. DEVOS, *Physica* **20**, 690 (1954).
8. W. E. GERICKE, *Z. Astrophys.* **53**, 68 (1961).
9. S. V. DESAI and W. H. CORCORAN, "Investigation of the thermodynamic state of an argon plasma," to be published.
10. J. F. BOTT, *Phys. Fluids* **9**, 1540 (1966).
11. H. N. OLSEN, *Bull. Amer. Phys. Soc.* **5**, 121 (1959).
12. K. BOCKASTEN, *J. Opt. Soc. Am.* **51**, 943 (1961).

APPENDIX A-5

IMPROVED AND CORRECTED TRANSITION PROBABILITIES OF ARGON I IN THE RANGE OF 5000-6000 Å

(Accepted for publication in J.Quant.Spectrosc.Radiat.Trans.)

S. V. DESAI AND W. H. CORCORAN

California Institute of Technology

Pasadena, California 91109

Ms. #5358 B

March, 1969

The National Bureau of Standards[1] recently made a critical compilation of the transition probabilities, A_{nm}, of various elements including argon I. Use of those values of A_{nm} showed that the temperatures reported in Fig. 2 of a previous publication[2] were too low. As a consequence, the values of A_{nm} for the lines arising from energy levels higher than 120,000 cm^{-1} and reported in Table 2 of that paper[2] tended to be too high.

A new plot of $\log \frac{I_{nm}\lambda_{nm}}{g_n A_{nm}}$ vs. E_n is shown in Fig. 1 using the improved values of A_{nm} suggested by NBS [1] and noted in Table 1. The lines at 3406 Å and 3834 Å were excluded from the new plotting because their transition probabilities as reported by Malone and Corcoran[3] seemed too high on the same basis noted above. Data from the earlier paper[2] are included for comparison.

Table 2 gives the improved values of A_{nm} obtained from the new plot of $\log \frac{I_{nm}\lambda_{nm}}{g_n A_{nm}}$ vs. E_n, and the earlier data are also shown. A few errors in the values of E_n in the original table were pointed out by Dr. N. M. Nerheim[4] for which the authors are grateful. Use of the improved values of transition probabilities gave a corrected temperature distribution to replace Fig. 5 of reference (2), and the new plot is shown here as Fig. 2.

REFERENCES

1. "Atomic Transition Probabilities," Vol. II (a critical compilation for the elements sodium through calcium), NSRDS-NBS 22, to be published in 1969

2. S. V. Desai and W. H. Corcoran, JQSRT, 8, 1721 (1968)

3. B. S. Malone and W. H. Corcoran, JQSRT, 6, 443 (1966)

4. N. M. Nerheim, private communication from JPL

NOTATION

A_{nm}	transition probability for radiation from energy level n to m	$\frac{1}{sec}$
E_n	upper energy level	$\frac{1}{cm}$
g_n	statistical weight of the upper level	
$I_{nm}(x)$	measured intensity of line radiation from energy level n to m per unit area	$\frac{w}{cm^2}$
λ_{nm}	wavelength of spectral line for radiation from energy level n to m	$\mathring{A}$

TABLE 1.

TRANSITION PROBABILITIES OF ARGON I USED TO ESTABLISH THE CORRECTED STRAIGHT LINE IN FIG. 1

Wavelength (Å)	E_n (cm^{-1})	g_n	$A_{nm} \times 10^{-5}$ (sec^{-1})	Reference
4198.32	117,563.02	1	27.6	(1)
4200.67	116,942.81	7	10.3	(1)
4251.18	116,660.05	3	1.13	(1)
4345.17	118.407.49	3	3.13	(1)
5558.6	122,086.97	5	14.8	(1)
5572.6	123,557.46	7	6.9	(1)

TABLE 2. CORRECTED EXPERIMENTAL TRANSITION PROBABILITIES OF ARGON I

Wavelength (Å)	E_n (cm^{-1})	g_n	$A_{nm} \times 10^{-5}$ (sec^{-1}) Ref.(2)	Corrected Values
5118	125,113.48	5	11.45	6.23
5162.4	123,468.03	3	26.2	16.6
5177.6	124,771.67	5	6.7	3.73
5187.3	123,372.98	5	20.9	13.4
5373.6	124,692.02	5	5.75	3.2
5421.4	123,903.30	5	12.5	7.53
5495.9	123,653.24	9	28.5	17.7
5506.4	123,773.92	7	2.55	4.96
5606.7	121,932.91	3	28.65	21.3
5739.7	123,505.54	5	15.68	10.0
5888.7	122,440.11	5	21.3	14.9
5912.1	121,011.98	3	15.24	12.4
6032.1	122,036.13	9	33.2	24.3
6043.2*	122,160.22	7	19.6	14.4
	123,832.50	7	30.6	18.6
6052.7	120,619.08	5	2.19	1.84
6059.3	120,600.94	5	4.38	3.70
6145.4	123,557.46	7	6.85	6.35
6416.3	119,683.11	5	19.5	18.0

*Arises from two transitions having almost equal differences between the upper and the lower energy levels. The reported value of A_{nm} is based on the total measured intensity.

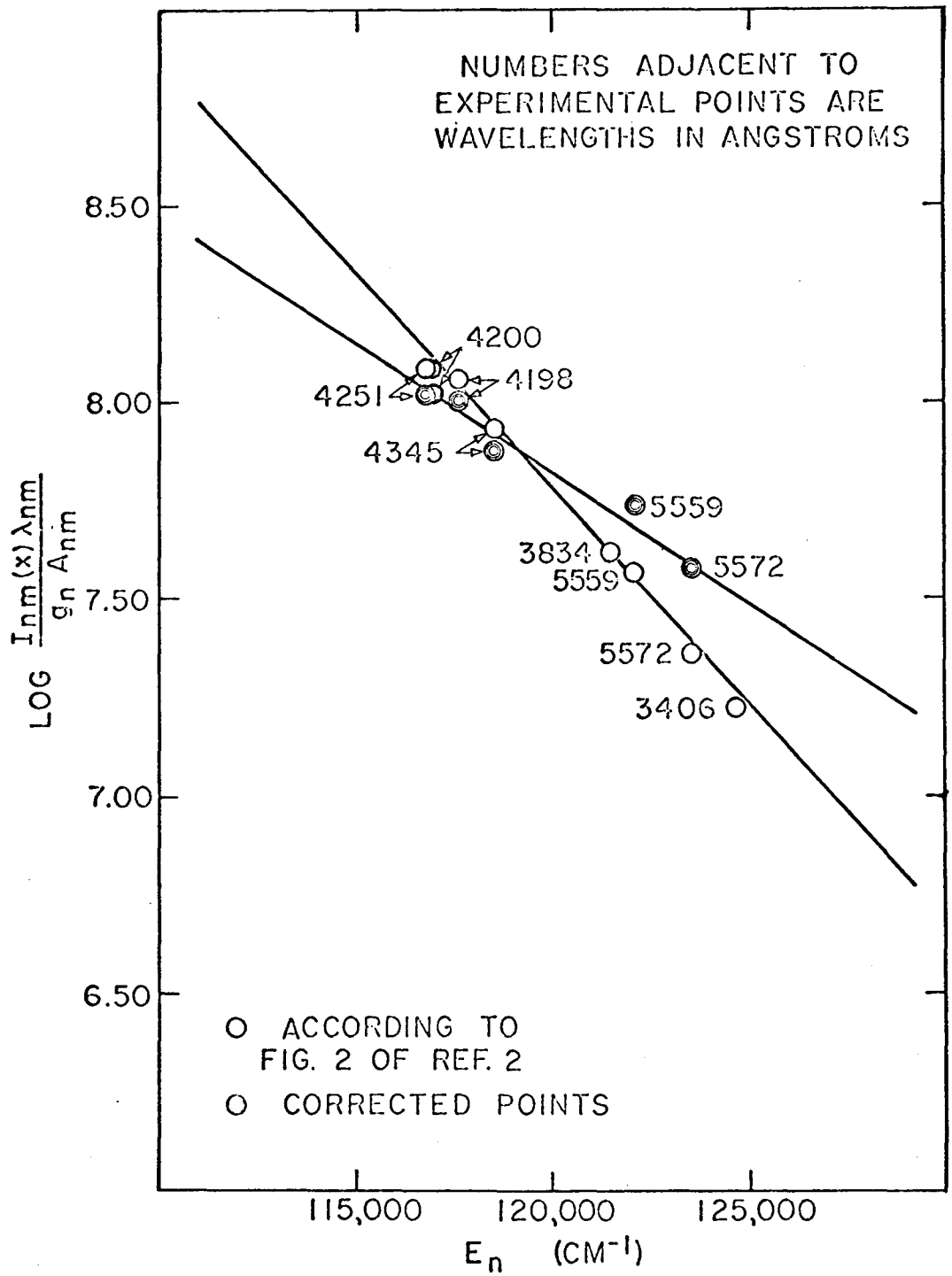

Figure 1 New values of the intensity function based on improved values of A_{nm} (1)

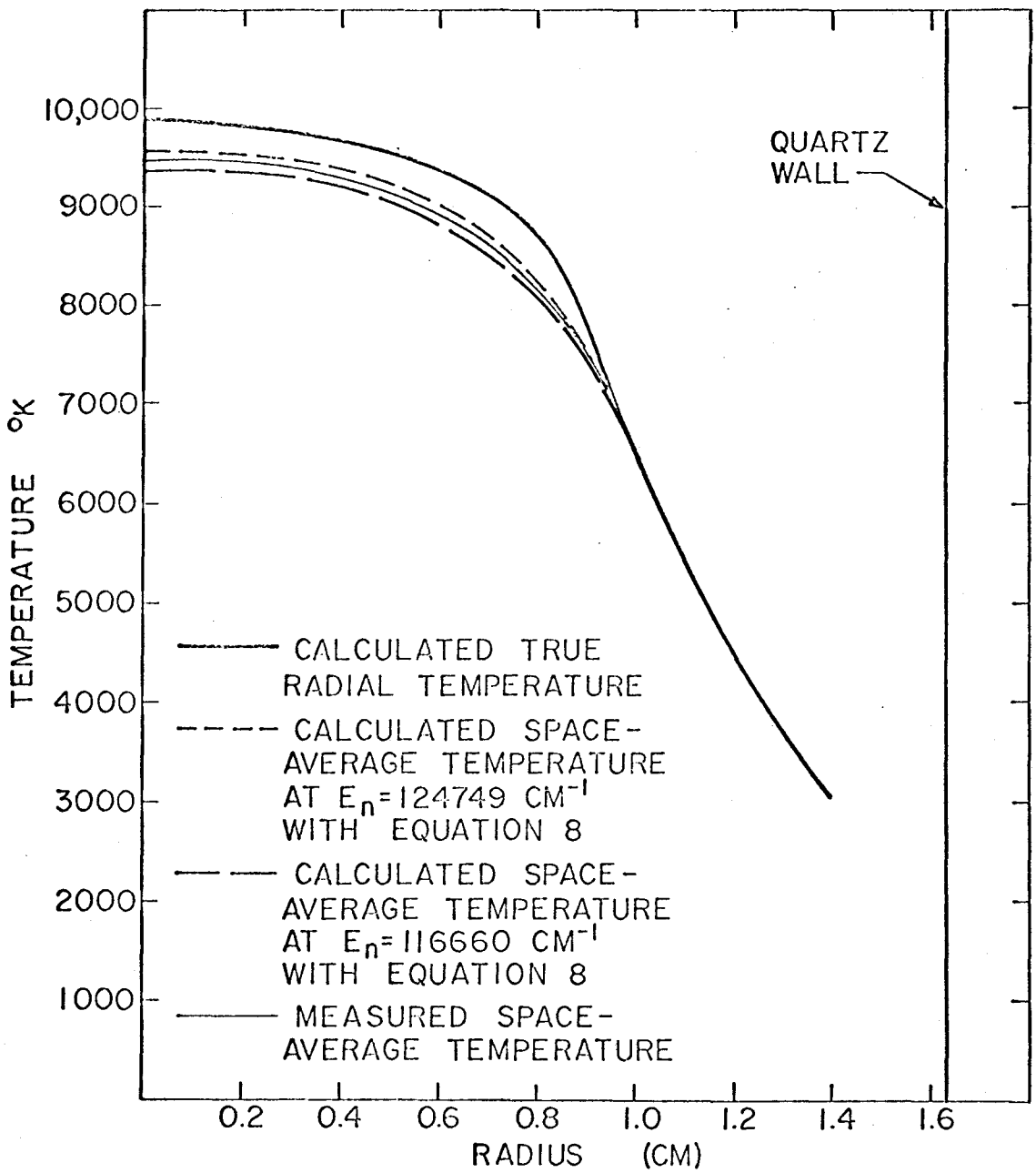

Figure 2 Corrected temperatures[2] based on improved values of A_{nm}[1] and appropriate use of Equation 8 of reference 2.

APPENDIX A-6

Reprinted from THE REVIEW OF SCIENTIFIC INSTRUMENTS, Vol. 39, No. 4, 612–614, April 1968
Printed in U. S. A.

Use of Particles of Boron Nitride in the Measurement of the Velocity Distribution in Laminar Flow in an Argon Plasma Jet

S. V. DESAI, E. S. DANIEL, AND W. H. CORCORAN
California Institute of Technology, Pasadena, California 91109
(Received 20 November 1967; and in final form, 2 January 1968)

MEASUREMENT of the velocity distribution in a plasma jet is usually difficult because of the high temperatures. For example, hot-wire or Pitot-tube measurements are hardly applicable at temperatures above the softening points of the materials involved. Grey *et al.*[1] have described a water-cooled probe to measure the impact pressure and other properties in a plasma jet. Such techniques are subject to errors from the flow disturbances created by the probe itself and from large temperature gradients present in the vicinity of the probe. Gottschlich *et al.*[2] have used a spectroscopic technique by which the velocity distribution in a plasma jet can be deduced from the known temperature distribution and use of an energy balance. Assumptions of thermodynamic equilibrium, a symmetrical configuration, optically-thin plasma, and negligible radiation were made by them, and those assumptions are not always valid. The feasibility of using a tracer produced by a laser beam has been explored by Chen.[3] As a tracer he used a plasma drop of high intensity produced by a laser pulse of a duration of 15 nsec. He followed the path of the tracer with a drum camera and deduced the velocity of the stream. Fristrom[4] has summarized the technique of using microscopic particles as tracers in combustion flames. He suggests intense background illumination to trace the path of the particles. The tracer method was extended to a plasma jet in the experiment described below, and a mirror system was used to determine the radial positions of the tracer particles.

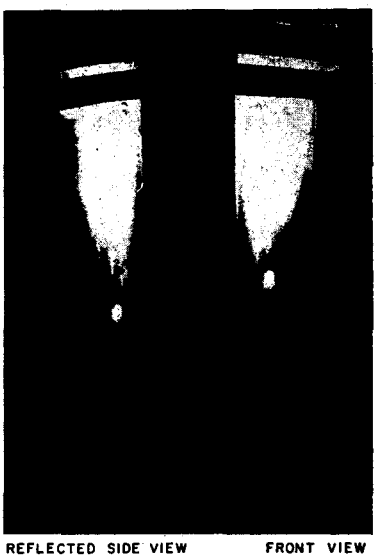

FIG 1. Typical two-plane picture of an argon plasma jet showing boron nitride streaks.

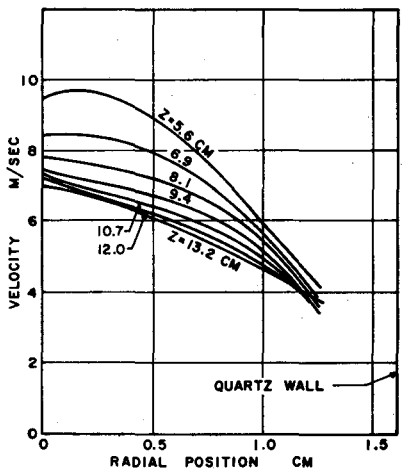

FIG. 2. Experimentally determined velocity distribution obtained by use of boron nitride particles in the core of an argon plasma jet. The curves represent a third-order, least-squares fit with a standard deviation of 0.69 m/sec. The axial position downstream from the leading edge of the bottom rf coil is indicated by Z.

NOTES

An argon plasma produced by a radio-frequency discharge was studied. It was cooled by a coaxial stream of argon confined in a cylindrical quartz tube. Particles of boron nitride having diameters in the region of 40–80 μ were used as tracers. Their low density of 2.2 g/cc, high melting point of 3000°K, and high emissivity make them ideally suited for the application. Selection of the particular size distribution was based on an analysis which showed that particle sizes of less than 200 μ would not be appreciably affected by the gravitational field.

A fluidized-bed device was used to introduce the particles into the stream of argon. They were injected into the cooling gas through peripheral holes above the rf coil. The mass rate of flow of the tracers was maintained as low as possible so that the solid particles did not influence the flow of plasma to any appreciable extent.

The paths of particles were traced by taking pictures of the plasma jet with a Honeywell Pentax model H3V camera equipped with a 110 mm lens. A nominal shutter speed of 1 msec was used. Calibration of the speed was carried out by means of an aluminum disk which had a diameter of 5.1 cm. Five holes were cut on the periphery of the disk which was driven by a synchronous motor. Pictures of the rotating disk were taken with the camera, and the background illumination was intense. Measurement on the negative of the lengths of the streaks produced by the holes allowed the average shutter speed to be calculated as 1.05 msec. Results of six pictures showed a reproducibility of $\pm 6\%$. A measuring magnifier was used to measure the lengths of the streaks produced by the particles. The scale factor for the image was determined by comparing the diameter of the plasma tube as it appeared on the negative with its actual diameter. Finally, the velocities were obtained by dividing the streak lengths of the tracer particles by the exposure time. A total of 205 particles was studied in 40 exposures.

The major difficulty encountered in use of the BN particles was in accurately locating the radial position of a particle in the plasma jet. To overcome this problem a three-dimensional mapping technique was used. The side view of the plasma jet was reflected with help of a mirror in such a way that the front view and the side view could be seen side-by-side in the picture area. Figure 1 shows a typical picture. Knowledge of the two coordinates of a streak as obtained from the two views allowed the radial position of a particle to be easily determined.

As noted, the velocities and positions of 205 particles were obtained from the pictures. The velocities were averages over the lengths of the streaks, and their coordinates were taken as the midpoints of the streaks. A third-order, least-squares fit was drawn through plots of the velocities which were presented as functions of radial and axial positions. The result is shown in Fig. 2. Analysis of the motion of a large number of particles makes the results less susceptible to random experimental errors. The standard deviation of the least-squares fit was 0.69 m/sec.

The method described is quite suitable for plasmas which are not too bright to obscure the glowing particles and which are at sufficiently high temperatures to make the BN particles glow intensely. Establishment of the radial position of a particle within 0.05 cm was not difficult with the mirror system. Errors in measurement were mainly from other sources such as variation of the shutter speed and variability in measurement of the length of a streak with a magnifier. The representation of velocity measurements by a polynomial fit may introduce some inaccuracies. Least-square fits of higher order were tried, but no significant improvement in the standard deviation was attained.

Work reported here was part of a program supported by the Public Health Service by way of the National Center for Air Pollution Control of the Bureau of Disease Prevention and Environmental Control. That support is gratefully acknowledged.

[1] J. Grey, M. P. Sherman, P. M. Williams, and D. B. Fradkin, A.I.A.A. J. 4, 98 (1966).
[2] F. Gottschlich, J. A. Enright, and F. C. Cadek, A.I.A.A. J. 4, 1085 (1966).
[3] C. J. Chen, J. Appl. Phys. 37, 3092 (1966).
[4] R. M. Fristrom and A. A. Westenberg, *Flame Structure* (McGraw-Hill Book Co., New York, 1965), pp. 113–131.

APPENDIX A-7

Recombination of Electrons and Ions in an Atmospheric Argon Plasma

(Accepted for publication in J.Quant.Spectrosc.Radiat.Trans.)

SATISH V. DESAI and WILLIAM H. CORCORAN

Chemical Engineering
California Institute of Technology
Pasadena, California 91109

November, 1968

Ms. 5387 - Rev. I

INTRODUCTION

Recombination of electrons with ions is a process of fundamental importance in the control of physical and chemical changes in plasmas and can be readily studied in a plasma jet. If the excitation by an external source ceases at some time or point in space, as in a plasma jet, the population densities of the various species present will tend to a new steady state. McWhirter and Hearn[1] showed that the time constants associated with excitation population are so small in comparison with the time constant of the ground-state population, that a steady-state approximation for the excited states can be nearly always made. As a consequence, recombination of ions and electrons must be accompanied by equal population of the ground state, which is a slow process. Recombination of electrons with ions is usually denoted by a second-order process corresponding to the equation

$$A^+ + e \xrightarrow{\alpha} A \tag{1}$$

so that the rate of recombination becomes

$$-\frac{dn_e}{dt} = \alpha\, n_e n_+ \tag{2}$$

where α is the recombination coefficient.

The inverse process of ionization can usually be neglected in decaying plasmas, at least in the initial stage, because of the low population in the ground state. The recombination coefficient α will

in general be a function of electron density and temperature, depending on the mechanism of recombination. A simple recombination of an atomic ion and an electron as indicated by equation (1) is highly improbable because of the large amount of energy which must be dissipated in the process.

Various mechanisms have been proposed to explain the observed rates of recombination in laboratory plasmas. The collisive-radiative model of Bates, Kingston and McWhirter[2] takes into account two processes, namely, a three-body recombination process in which the third electron absorbs the recombination energy and the radiative recombination process in which the excess energy is dissipated as radiation. The net rate of recombination is calculated as the rate of population of the ground state by collisive and radiative transitions from the excited states. Hinnov and Hirschberg have verified the collisive-radiative model in a helium afterglow at a pressure of a few microns of mercury[3]. Bates[4,5] observed that the rates of recombination in helium plasma at 10-30 mm Hg as measured by Biondi and Brown[6] were orders of magnitude larger than those predicted by the collisive-radiative mechanism or the electron-attachment mechanism[7] and suggested a dissociative mechanism involving diatomic helium ion:

$$He_2^+ + e \rightarrow He + He^*$$

Craggs suggested[8] that in a helium plasma at atmospheric pressure his evidence supports the mechanism of dissociation of a molecular ion. Biondi and Holstein[9] and Biondi[10] carried out experiments with a

helium plasma at a pressure of 50 mm of Hg. They observed substantial quenching of line radiation from the plasma by introducing 4 per cent of argon. They attributed the quenching effect to the prevention of formation of molecular ions. Later, Mulliken pointed out[11] that in molecular helium, only higher vibrational states can lead to dissociation. Therefore the dissociative-recombination mechanism is not likely to be important unless a high degree of vibrational excitation takes place. He also suggested that for noble gases other than helium, a large number of dissociative states of the molecule are available, hence the dissociative recombination is entirely likely to be important. Collins[12] proposed a dissociative-collisive recombination model which overcomes the difficulty raised by Mulliken by assuming a three-body collisional stabilization of the dissociating molecular ion.

In most of the experimental studies on rates of recombination, attempts have been made to propose a certain mechanism and support it with a narrow range of experimental conditions. The study of an argon plasma presented here was made in a flow system at atmospheric pressure in which the temperature and electron density varied from point to point. Recombination rates calculated as point functions encompassed a wide range of variables. Electron densities were in the region from 10^{12} to 10^{15} particles/cm^3 and temperatures from 3000 to 11000 °K. Analysis of the results showed that the dissociative-molecular-ion mechanism could satisfactorily explain the observed recombination rates for the given experimental conditions.

Experimental Apparatus

The source of radiation was an RF-heated plasma jet of argon confined in a quartz tube which was open to the atmosphere at one end. Intensities

were measured with a photomultiplier tube. A previous publication[13] described the experimental setup and the procedure for determination of wavelength response. The quartz tube extended 22 cm below the RF coil used to generate the plasma, and the test zone was between 4.267 cm and 11.89 cm below the coil. A white glow was present at the open end of the tube, and it was found to be mainly due to N_2^+ (1^-) band radiation arising from the hot argon coming in contact with atmospheric nitrogen.

Injection of less than 100 ppm of nitrogen into the argon plasma changed its radiation characteristics to the extent that the change was visually observable. The visible portion of the jet expanded in diameter and shrank in length with increasing amounts of nitrogen. Therefore in the interest of reproducibility, great precaution was taken to use pure argon in the plasma. RF heating has an advantage over the arc method in that contaminants from electrodes are avoided in the RF system. Although the manufacturer's specifications for the argon stated maximum impurities, mainly nitrogen and water, to be below 40 ppm., further purification was required. Purer argon was obtained by passing the gas over hot cupric oxide and then over hot copper metal to remove H_2 and O_2, respectively. That gas was then passed through a packing of 4-A molecular sieve held at -120 °C to remove water, hydrocarbons, carbon dioxide and most of the nitrogen. Spectroscopic observation of the plasma indicated that the purified gas had less than 3 ppm nitrogen, and other impurities were in undetectable amounts.

Experimental Procedure

By spectroscopic means, intensity measurements were made on seven different lines of the argon I spectrum for which spectroscopic data are

given in Table 1. Measurements were made from one side of the plasma jet and along a line of sight parallel to the diameter of the stream. Data were collected over 5 planes perpendicular to the axis of the jet and at positions 4.267, 6.172, 8.077, 9.982 and 11.890 cm from the bottom turn of the RF coil. At each plane, line intensities were measured at five transverse positions starting from the center. Only one side of the plasma was scanned because preliminary scans showed that the plasma was quite symmetrical about its axis. Each of the selected spectral lines was scanned three to four times, and an average value was taken.

Stability of the plasma was remarkable. After the warming-up period of about 2 hours, the intensities could be reproduced within ± 3 per cent during the experiment. Over a period of weeks, after shutting off the plasma and relighting it, the reproducibility was ± 5 per cent as compared to previous runs.

Analysis of Experimental Data

The measured line intensities were converted to true, radial intensities by the use of a numerical Abel transformation[14]. Population densities of the upper energy levels giving rise to the observed lines were calculated from the absolute intensities of the lines by means of the following equation

$$I_{nm} = \frac{hc}{\lambda_{nm}} A_{nm} n(n) \qquad (3)$$

Where the Boltzmann distribution prevails, there should be a straight-line relationship between $\log \frac{n(n)}{g_n}$ and E_n as follows:

$$\log \frac{n_E(n)}{g_n} = \log \frac{n_E(1)}{g_1} - \frac{E_n}{kT} \qquad (4)$$

The subscript E denotes that the levels in question are in equilibrium with each other. Figures 1(A) through 1(E) show plots of $\log \frac{n(n)}{g_n}$ as a function of E_n for the experimental data. Results are shown for 7 lines of argon I for 11 radial positions in each of five planes perpendicular to the axis of flow. The outermost radial position was 1.4 cm for the first and second planes and 1.2 cm for the third and fourth planes. Only the central position is shown in Figure 1(E) for the last plane because the intensities dropped sharply beyond a short radius.

Figure 1 shows that the lower excited states, in particular the $2p_2$ state which gives rise to the spectral line at 6965Å, show substantial departure from equilibrium. The states which are close to the ionization level are still in equilibrium with each other and with the free electrons. The excitation temperature, which is the same as the free-electron temperature under the above conditions, can be evaluated from the slopes of the straight lines passing through the higher excited states.

To establish the temperature profile below 3000 °K in the cooler part of the plasma, the temperatures near the quartz wall were obtained by inserting a ceramic tube through small apertures made through the quartz wall and reading the temperature of the glowing ceramic tube with an

optical pyrometer. Figure 2 shows the temperature distribution in the plasma up to a radius of 1.4 cm in the test zone. Temperatures between 3000 °K and 1500 °K are interpolated values, and the corresponding positions of the straight lines shown in Figures 1A through 1D are only approximate.

The Boltzmann line given by equation (3) was then used along with the Saha equilibrium relation to obtain electron densities in the plasma. An assumption was made that A^+ ions carry most of the charge and that they are equal in number to the free electrons. Then the Saha equation gives:

$$\frac{n_e^2}{n_E(n)} = 2\left(\frac{2\pi m_e kT}{h^2}\right)^{3/2} \frac{Z^+}{g_n} e^{\frac{-(E_+ - E_n)}{kT}} \qquad (5)$$

Figure 3 shows the electron-density profiles in the plasma.

In addition to the profiles for temperature and electron density, velocity profiles were required for time resolution of the data in order to obtain rates of recombination in the flow system. Velocity distributions had been previously obtained using particles of boron nitride as tracers[15]. The experimentally determined velocity profiles were further improved by use of the following simple relationship between temperature and axial velocity at a given point:

$$v_z = f(r)T \qquad (6)$$

The form of the equation results from the equation of continuity, and the function f(r) ideally is invariant with respect to axial position. Some variation due to experimental errors was noticed in actual calculations.

These minor variations were smoothed out, and the improved values of f(r) were used to calculate the velocity profiles from the spectroscopically determined temperature profiles. An assumption involved in calculating the velocity profiles in the manner described was that the radial component of the velocity was negligible. The velocity profiles are shown in Figure 4.

In the absence of a steady electric field, the steady-state equation of continuity for electrons in the test zone may be written as

$$\nabla \cdot \left(n_e \underline{v}\right) - \nabla \cdot \left(D_a \nabla n_e\right) + R_e = 0$$

where D_a is the ambipolar diffusion coefficient, and R_e is the rate of recombination of electrons in particles per cubic centimeter per second. A detailed solution of the continuity equation using a value for the ambipolar diffusion coefficient obtained from mobility data of argon[6, 16] ions showed that under the experimental conditions the effect of ambipolar diffusion on the recombination rate was negligible. The recombination coefficient α as defined in equation (2) was obtained as a point function from the measured recombination rates. An empirical equation relating the observed values of α to the temperature and the electron density was fitted to the data points and found to have the following form:

$$\alpha = 1.28 \cdot 10^5 \cdot T^{-1.8} \cdot 10^{-\frac{3410}{T}} \cdot n_e^{-0.64} \text{ cm}^3/(\text{particles})(\text{sec}) \qquad (7)$$

DISCUSSION

In the above analysis, the free-electron temperature was assumed to be equal to the kinetic temperature of the atoms and ions. Calculations indicated that the time constant for equilibration in the exchange of kinetic energy between electrons and atoms is of the order of 5 μsec. Because the test zone was sufficiently below the RF work coil, the above assumption is well justified. The temperature was treated as an independent variable although in principle the change of temperature was coupled with the microscopic rate processes within the plasma[17]. Treatment of the temperature as an independent variable in the present study was reasonable because attention was focused on rates of recombination only. The mechanism of energy transport was disregarded.

The total error in measurement of the absolute intensity of the plasma at a point, considering the fluctuations in the plasma, the calibration procedure, and the Abel transformation, was estimated at ±13 per cent. If to that error is added the maximum error of ±15 per cent for the transition probabilities, the total error in measurement of excitation population was nominally ±28 per cent. Errors in measurement of temperature and electron density are estimated at ±3 per cent and ±30 per cent, respectively, corresponding to the error in excitation population. The relative error in these quantities is expected to be much smaller. Velocities were known within about ±10 per cent.

In consideration of the wide range of temperatures (3000-11000°K) and electron densities (10^{12} - 10^{15} particles per cubic centimeter) covered by the experiments, one can view the variation of the recombination coefficient α with T and n_e as given by equation (7) with some confidence in spite of

errors in the absolute values of α by as much as a factor of 2. A significant fact is that α decreases with increasing electron density. According to the collisive-radiative model, α should have dependence on n_e of the form $n_e^{\,a}$, where $0 < a < 1$. For purely radiative recombination, $a \to 0$, and for purely collisive recombination, $a \to 1$. Thus the observed value of $a < 0$ cannot be explained on the basis of the collisive-radiative model.

The observed recombination rates are consistent with the dissociative mechanism involving molecular argon ion as postulated below:

(a) Formation of A_2^+ molecule by a three-body process

$$A^+ + A(1) + A(1) \underset{k_1'}{\overset{k_1}{\rightleftharpoons}} A_2^+ + A(1) \qquad (8)$$

(b) Non-radiative, two-body recombination of the molecular ion with a free electron to form an excited molecular intermediate

$$A_2^+ + e \underset{k_2'}{\overset{k_2}{\rightleftharpoons}} A_2^* \qquad (9)$$

(c) Decomposition of the molecular intermediate into two atoms, at least one of which is in the excited state

$$A_2^* \longrightarrow A(1) + A^* \qquad (10)$$

Recombination leading to a highly dissociative molecular state A_2^* is quite possible when the potential vs. atomic separation curve for A_2^* crosses the similar curve for the A_2^+ molecule[11, 18]. Because the intermediate state A_2^* is highly dissociative, it may be assumed that the formation of A_2^* is the rate-controlling step between equations (9) and

(10), so that one may write

$$A_2^+ + e \xrightarrow{k_2} A(1) + A^* \tag{11}$$

Now a steady-state approximation for the concentration of A_2^+ is introduced at this point and can be justified by the experimental results. If the molecular ion A_2^+ is highly reactive, then it will be depleted from the reacting mass by reaction (11) as fast as it is produced by reaction (8). Therefore the concentration of A_2^+ will be relatively small and stationary, and its rate of change will be negligible. In this situation, the overall rate of recombination may be written as:

$$-\frac{dn_e}{dt} = \frac{k_1 k_2 n_e^2 n_t^2}{k_1' n_t + k_2 n_e} \tag{12}$$

where the population density of the ground state is replaced by the total population density n_t without loss of precision, and it may be calculated from the ideal-gas law. The recombination coefficient becomes:

$$\alpha = \frac{k_1 n_t^2}{(k_1'/k_2) n_t + n_e} \tag{13}$$

It can be noted that equation (13) predicts decreasing values of α with increasing values of n_e in accordance with the experimental observations.

Expressions for k_1 were developed by Tolman[19], Loeb[20] and Kassel[21] wherein they applied kinetic theory to a ternary reaction. Kassel took into account the short-range repulsive forces between colliding atoms, and in his analysis, the three-body rate constant is given by

$$k_1 = \frac{8}{3}\pi^{\frac{3}{2}}\sigma^2\delta^3\phi\sqrt{\frac{kT}{m}}\, e^{-\frac{E}{kT}} \tag{14}$$

Equation (14) was used in the present analysis. E is the activation energy for the three-body interaction. The steric factor ϕ accounts for non-effective collisions. The quantity σ is the collision radius which can be obtained usually from the measurement of transport properties and has a value of 2.89 Å for argon. A collision is defined as the presence of the three particles within a certain distance δ of each other. Frost and Pearson[22] indicate that the available date for ternary rates of reaction suggest that δ is of the order of 1 Å. In the present analysis, δ was assumed equal to σ for the lack of better knowledge.

Table 2 gives a summary for the proposed reaction mechanism for the recombination of electrons. Experimental values of α were subjected to a least-squares analysis based on equations (13) and (14) to give the best values of ϕ and E which are shown in Table 2. Variation of k_1'/k_2 with temperature was obtained in the least-squares analysis, but this variation must be considered approximate. The standard deviation of 18 per cent for the values of α developed from the use of equations (13) and (14), which are based on mechanistic arguments, was considered encouraging when compared to the same standard deviation obtained for the best empirical fit given by equation (7).

In the above analysis, the assumption of steady-state made for the molecular ions in the derivation of equation (13) is supported by the consistency of the experimental data. This assumption should not be applied to all cases of recombination. For example, in microwave-discharge experiments at 300°K and at pressures of 10-20 mm Hg[10], and in shock-tube experiments at 3000°K and at pressures of 30-90 mm Hg[23], the values of α for argon were orders of magnitude greater than those predicted by equation (13). Also, they had no dependence on electron density. In those studies it is likely that

most of the A^+ ions were initially converted to A_2^+ ions, which explains the large observed rates of recombination and also the independence of α relative to n_e. Lower temperature would favor the formation of A_2^+ ions. In that case, the rate-limiting step in the recombination of electrons would indeed be the reaction shown by equation (11).

A comparison among the experimental values of α denoted by α_{exp}, the collisive-radiative values[2] denoted by α_{CR}, and the dissociative-molecular-ion values denoted by α_{DMI} is given in Table 3. An effective nuclear charge of unity was assumed in calculating α_{CR}. The negative values of α_{CR} at temperatures above 8000 °K indicate incipient ionization which should take place as the result of overpopulation of the ground state according to the collisive-radiative model. In the actual plasma, recombination rather than ionization was taking place under these conditions. It can be also seen that the collisive-radiative model predicts too low values of α at lower electron densities and temperatures. On the other hand, the values of α_{exp} are in good agreement with α_{DMI} over a wide range of experimental conditions. It must be remarked that a limitation of the experiments was that the range of variation of electron density for a given temperature was not great.

A study of the effect of introducing excess molecular ions in the system supported the dissociative-molecular-ion mechanism. About 760 ppm of nitrogen were premixed with argon to give formation of N_2^+ ions in amounts on the order of 10 ppm as estimated from the intensity of $N_2^+(1-)$ band radiation. Line radiation from argon was quenched rapidly in the upstream section, and the rate of quenching was slower in the downstream section. The quenching was also observed to a lesser extent with introduction of other diatomic gases, such as O_2 and NO, capable of forming molecular

ions, but it was completely absent with helium. The temperature profiles were not affected by the introduction of small amounts of these impurities. Since the electrons are in equilibrium with the higher-excitation population, one can deduce that the quenching of line radiation is accompanied by an enhanced rate of recombination of electrons. A molecular ion would be formed fairly easily from a nitrogen molecule by the following charge-exchange process:

$$A^+ + N_2(1) \longrightarrow N_2^+ + A(1) \qquad (15)$$

The following reaction, similar to the reaction shown in equation (11), would rapidly deplete the charges:

$$N_2^+ + e \longrightarrow N + N^* \qquad (16)$$

Recombination coefficients for N_2^+ and A_2^+ ions are known to be of the same order of magnitude[24]. The increased rate of recombination in the upstream section can be attributed to the higher concentration of molecular ions formed by the reaction shown in equation (15), bypassing the much slower three-body reaction shown in equation (8). As the concentration of either charge is depleted, reactions shown in equations (15) and (16) would be considerably slowed, explaining the reduced rate of recombination in the downstream section. In case of helium, the reaction shown in equation (15) is not likely because of the higher ionization potential of helium compared with argon, and a three-body mechanism such as that represented by equation (8) will be ineffective because of the low concentration of helium ions. Therefore, there would be no effect from the addition of helium on the recombination of electrons in argon. Thus the experimental observations are entirely consistent with the dissociative-molecular-ion model.

CONCLUSIONS

The analysis of the experimental results suggests that the collisive-radiative model for hydrogen-like plasmas is inadequate to explain the observed recombination rates in the argon plasma at atmospheric pressure. On the other hand, the dissociative-molecular-ion model with a steady-state approximation for the molecular ion does reasonably fit the experimental values for the recombination coefficients over a range of temperatures from 3000 to 11000 °K and for electron densities from 10^{12} to 10^{15} particles/cm^3. In partial support of the proposed mechanism it was observed that addition of bimolecular gases capable of forming molecular ions resulted in quenching of line radiation from the argon plasma as a result of increased rates of recombination of electrons.

ACKNOWLEDGMENT

Support for the work discussed here was provided by the Public Health Service by way of the National Center for Air Pollution Control. That support is gratefully acknowledged.

REFERENCES

1. R. W. P. McWhirter and A. G. Hearn, Proc. Phys. Soc., 82, 641 (1963).

2. D. R. Bates, A. E. Kingston and R. W. P. McWhirter, Proc. Roy. Soc., A267, 297 (1962).

3. E. Hinnov and G. Hirschberg, Phys. Rev., 125, 795 (1962).

4. D. R. Bates, Phys. Rev., 77, 718 (1950).

5. D. R. Bates, Phys. Rev., 78, 492 (1950).

6. M. A. Biondi and S. C. Brown, Phys. Rev., 75, 1700 (1949).

7. A. N. Prasad and J. D. Craggs, "Atomic and Molecular Processes," Ed. by D. R. Bates, Academic Press, New York, 1962.

8. J. C. Craggs, "Proc. of VIth Conference on Ionic Phenomena in Gases," paper III D O, Paris, 1963.

9. M. A. Biondi and T. Holstein, Phys. Rev., 82, 962 (1951).

10. M. A. Biondi, Phys. Rev., 83, 1078 (1951).

11. R. S. Mulliken, Phys. Rev., 136, A 962 (1964).

12. C. B. Collins, Phys. Rev., 140, A 1850 (1965).

13. S. V. Desai and W. H. Corcoran, J. Quant. Spectrosc. Radiat. Transfer, 8, 1721 (1968).

14. W. J. Pearce, "Plasma Jet Temperature Study," WADC Tech. Rep. 59-346, General Electric Co., 1960.

15. S. V. Desai, E. S. Daniel and W. H. Corcoran, Rev. Scientific Instruments, 39, 612 (1968).

16. E. C. Beaty, "Proc. of Vth International Conference on Ionization Phenomena in Gases," I, page 183, North-Holland, Amsterdam, 1962.

17. D. E. Oettinger and D. Berschader, AIAA Journal, 5, 1625 (1967).

18. D. R. Bates and A. Dalgarno, "Atomic and Molecular Processes," Ed. by D. R. Bates, Academic Press, New York, 1962.

19. R. C. Tolman, "Statistical Mechanics," Chemical Catalog Co., New York, 1927.

20. L. B. Loeb, "Basic Processes of Gaseous Electronics," pp. 586-89, University of California Press, Berkeley, California, 1955.

21. L. S. Kassel, "Kinetics of Homogeneous Gas Reactions," Chemical Catalog Co., New York, 1932.

22. A. A. Frost and R. G. Pearson, "Kinetics and Mechanism," p. 69, John Wiley and Sons, Inc., New York, 1961.

23. J. N. Fox and R. M. Hobson, Phys. Rev. Letters, 17, 161 (1966).

24. T. R. Connor and M. A. Biondi, Phys. Rev., 140, A 778 (1965).

25. "Atomic Transition Probabilities," Vol. II (a critical compilation for the elements sodium through calcium), NSRDS-NBS-22, to be published in 1969.

NOTATION

$A(1)$	argon atom in the ground state	
A^*	argon atom in the excited state	
A_2^*	excited intermediate molecule of argon	
A_{nm}	Einstein transition probability from state n to m	sec^{-1}
c	velocity of light	$(cm)(sec)^{-1}$
D_a	ambipolar diffusion coefficient	$(cm)^2(sec)^{-1}$
E	Activation energy for ternary reaction	cm^{-1} or eV
E_n	excitation energy of neutral argon at the n^{th} level referred to the ground state	eV
E_+	ionization energy of argon referred to the ground state	cm^{-1} or eV
g_n	statistical weight of the n^{th} excited level	
h	Planck constant	(erg)(sec)
I_{nm}	intensity of line radiation	$(watts)(cm)^{-3}$
k	Boltzmann constant	$(cm)^{-1}(°K)^{-1}$ $(eV)(°K)^{-1}$
k_1	specific rate constant for forward reaction in equation (8)	$(cm)^6(particles)^{-2}(sec)^{-1}$
k_1'	specific rate constant for reverse reaction in equation (8)	$(cm)^3(particles)^{-1}(sec)^{-1}$
k_2	specific rate constant for forward reaction in equation (9)	$(cm)^3(particles)^{-1}(sec)^{-1}$
k_2'	specific rate constant for reverse reaction in equation (9)	$(cm)^3(particles)^{-1}(sec)^{-1}$

k_3	specific rate constant for forward reaction in equation (10)	sec^{-1}
m	mass of argon atom	gm
m_e	mass of electron	gm
n(n)	population density of the n^{th} excited state; n(1) refers to population density of the ground state	$(particles)(cm)^{-3}$
$n_E(n)$	equilibrium population density of the n^{th} excited state; $n_E(1)$ refers to equilibrium population density of the ground state	$(particles)(cm)^{-3}$
n_e	density of electrons	$(particles)(cm)^{-3}$
n_+	density of neutral argon atoms	$(particles)(cm)^{-3}$
n_A^+	density of argon ions	$(particles)(cm)^{-3}$
n_t	total population density	$(particles)(cm)^{-3}$
N^*	nitrogen atom in the excited state	
r	radial position	cm
R_e	rate of recombination of electrons	$(particles)(sec)^{-1}(cm)^{-3}$
t	time	sec
T	temperature	°K
$\underline{v}$	vector velocity	$(cm)(sec)^{-1}$
v_z	velocity in the axial direction in the plasma jet	$(cm)(sec)^{-1}$
Z^+	partition function of the ions	
∇	vector operator, del	
α	recombination coefficient as defined	
δ	critical collision distance	cm
λ_{nm}	wavelength of radiation	Å
ν	frequency	$(cycles)(sec)^{-1}$
σ	collision radius	cm
ϕ	empirical coefficient or a steric factor	

Subscripts

m	energy state m
n	energy state n

TABLE 1. SPECTROSCOPIC DATA FOR THE OBSERVED LINES OF ARGON I.

Wavelength λ (Å)	Upper Level (Paschen)	Designation of Upper Level	Statistical Weight of Upper Level g_n	Energy of Upper Level E_n (cm^{-1})	Transition Probability for the Line $\times 10^{-5}$ (sec^{-1}) Ref. 13,25
3834.68	$4p_5$	6p(1/2)	1	121470.304	5.6*
4251.18	$3p_{10}$	5p(1/2)	3	116660.054	1.13
4300.10	$3p_8$	5p(2 1/2)	5	116999.389	3.94
4345.17	$3p_4$	5p'(1 1/2)	3	118407.494	3.13
5558.6	$5d_3$	5d(1 1/2)°	5	122086.974	14.8
5572.6	$5s_1''$	5d'(2 1/2)°	7	123557.459	6.9
6965.43	$2p_2$	4p'(1/2)	3	107496.463	67.0

* Improved value based on reference 25.

TABLE 2

Summary of data for a proposed reaction mechanism for recombination of electrons in an atmospheric argon plasma. Equation numbers correspond to the text.

Formation of molecular ion

$$A^+ + A(1) + A(1) \underset{k_1'}{\overset{k_1}{\rightleftharpoons}} A_2^+ + A(1) \qquad (8)$$

Dissociative recombination of molecular ion

$$A_2^+ + e \xrightarrow{k_2} A(1) + A^* \qquad (11)$$

Expression for recombination coefficient

$$\alpha = -\frac{dn_e}{dt}/n_e n_+ = \frac{k_1 n_t^2}{(k_1'/k_2)n_t + n_e} \qquad (2),(13)$$

Expression for k_1

$$k_1 = \frac{8}{3}\pi^{\frac{3}{2}}\sigma^2\delta^3\phi\sqrt{\frac{kT}{m}}\,e^{\frac{-E}{kT}} \qquad (15)$$

Experimental values

$\phi = 0.15\ (\pm\ .03)$

$E = 9900\ (\pm\ 800)\,cm^{-1}$ or $1.23\ (\pm\ 0.1)$eV

$$\frac{k_1'}{k_2} = 1.5 \times 10^{-3}\, e^{-\frac{18000}{kT}}$$

where k is the Boltzmann constant = 0.69502 $(cm)^{-1}\,(°K)^{-1}$

Error limits are standard errors obtained in the least-squares fit to the data points.

TABLE 3

Comparison of values of the experimental recombination coefficient for argon plasma with those predicted by the collisive-radiative[2] and the proposed dissociative-molecular-ion models. Values of α_{DMI} were obtained from a least-squares fit of experimental data. (see Table 2). Numbers following the letter E denote powers of 10 which are multipliers, e.g., E 15 ≡ 10^{15}

Axial Position (cm)	Radial Position (cm)	Temperature °K	Electron Density n_e (particles)/(cm)^3	Values of α in (cm)^3/(particles)(sec) Experimental α_{exp}	Collisive Radiative* α_{CR}	Dissociative Molecular Ion α_{DMI}
4.74	0	10530	0.77E 15	0.98E-12	-0.82E-09	0.94E-12
4.74	0.3	10370	0.72E 15	0.10E-11	-0.69E-09	0.10E-11
4.74	0.6	9896	0.58E 15	0.11E-11	-0.39E-09	0.12E-11
4.74	0.9	7972	0.24E 15	0.32E-11	-0.17E-11	0.27E-11
4.74	1.2	4718	0.28E 14	0.14E-10	0.22E-10	0.14E-10
5.70	0	9681	0.47E 15	0.13E-11	-0.30E-09	0.15E-11
5.70	0.3	9429	0.43E 15	0.16E-11	-0.20E-09	0.16E-11
5.70	0.6	8816	0.34E 15	0.23E-11	-0.69E-10	0.20E-11
5.70	0.9	6764	0.13E 15	0.54E-11	0.16E-10	0.46E-11
5.70	1.2	4270	0.16E 14	0.20E-10	0.21E-10	0.20E-10
6.65	0	8815	0.30E 15	0.17E-11	-0.72E-10	0.22E-11
6.65	0.3	8323	0.26E 15	0.23E-11	-0.21E-10	0.25E-11
6.65	0.6	7575	0.18E 15	0.40E-11	0.10E-10	0.34E-11
6.65	0.9	5851	0.63E 14	0.91E-11	0.17E-10	0.78E-11
6.65	1.2	3958	0.94E 13	0.28E-10	0.20E-10	0.28E-10
7.60	0	7995	0.20E 15	0.22E-11	-0.51E-11	0.31E-11
7.60	0.3	7231	0.16E 15	0.32E-11	0.14E-10	0.37E-11
7.60	0.6	6384	0.94E 14	0.69E-11	0.16E-10	0.58E-11
7.60	0.9	5136	0.32E 14	0.16E-10	0.18E-10	0.13E-10
7.60	1.2	3731	0.58E 13	0.39E-10	0.18E-10	0.38E-10
8.56	0	7407	0.14E 15	0.25E-11	0.11E-10	0.41E-11
8.56	0.3	6524	0.10E 15	0.39E-11	0.16E-10	0.54E-11
8.56	0.6	5629	0.51E 14	0.80E-11	0.17E-10	0.91E-11
8.56	0.9	4628	0.18E 14	0.17E-10	0.17E-10	0.19E-10
8.56	1.2	3518	0.39E 13	0.43E-10	0.17E-10	0.49E-10

* Including the effect of ionization

TABLE 3. (Cont.)

Axial Position (cm)	Radial Position (cm)	Temperature °K	Electron Density n_e (particles)/(cm)^3	Values of α in (cm)^3/(particles)(sec) Experimental α_{exp}	Collisive Radiative* α_{CR}	Dissociative Molecular Ion α_{DMI}
9.51	0	7097	0.10E 15	0.30E-11	0.11E-10	0.54E-11
9.51	0.3	6286	0.64E 14	0.56E-11	0.13E-10	0.76E-11
9.51	0.6	5379	0.31E 14	0.11E-10	0.15E-10	0.13E-10
9.51	0.9	4301	0.12E 14	0.19E-10	0.17E-10	0.25E-10
9.51	1.2	3291	0.29E 13	0.46E-10	0.17E-10	0.58E-10
10.46	0	6802	0.66E 14	0.69E-11	0.10E-10	0.73E-11
10.46	0.3	6095	0.40E 14	0.10E-10	0.11E-10	0.11E-10
10.46	0.6	5204	0.19E 14	0.16E-10	0.12E-10	0.18E-10
10.46	0.9	4079	0.78E 13	0.29E-10	0.16E-10	0.32E-10
10.46	1.2	3122	0.21E 13	0.67E-10	0.17E-10	0.69E-10
11.42	0	6442	0.38E 14	0.13E-10	0.90E-11	0.10E-10
11.42	0.3	5829	0.24E 14	0.17E-10	0.95E-11	0.15E-10
11.42	0.6	4983	0.12E 14	0.23E-10	0.11E-10	0.23E-10
11.42	0.9	3935	0.51E 13	0.41E-10	0.14E-10	0.42E-10
11.42	1.2	3028	0.15E 13	0.93E-10	0.15E-10	0.86E-10

* Including the effect of ionization

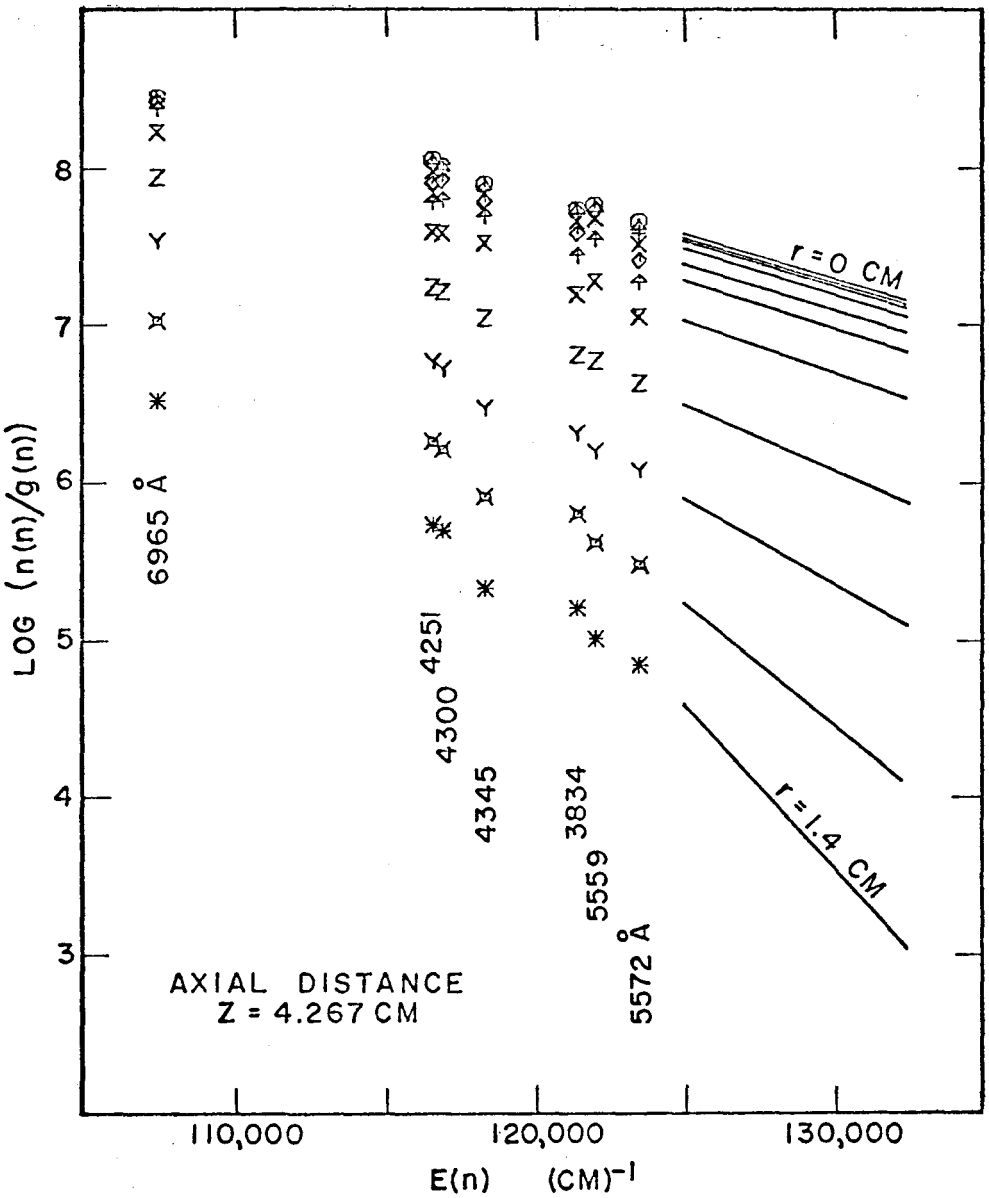

Fig. 1(A) Excitation Population in an Argon Plasma at Z= 4.267 cm.

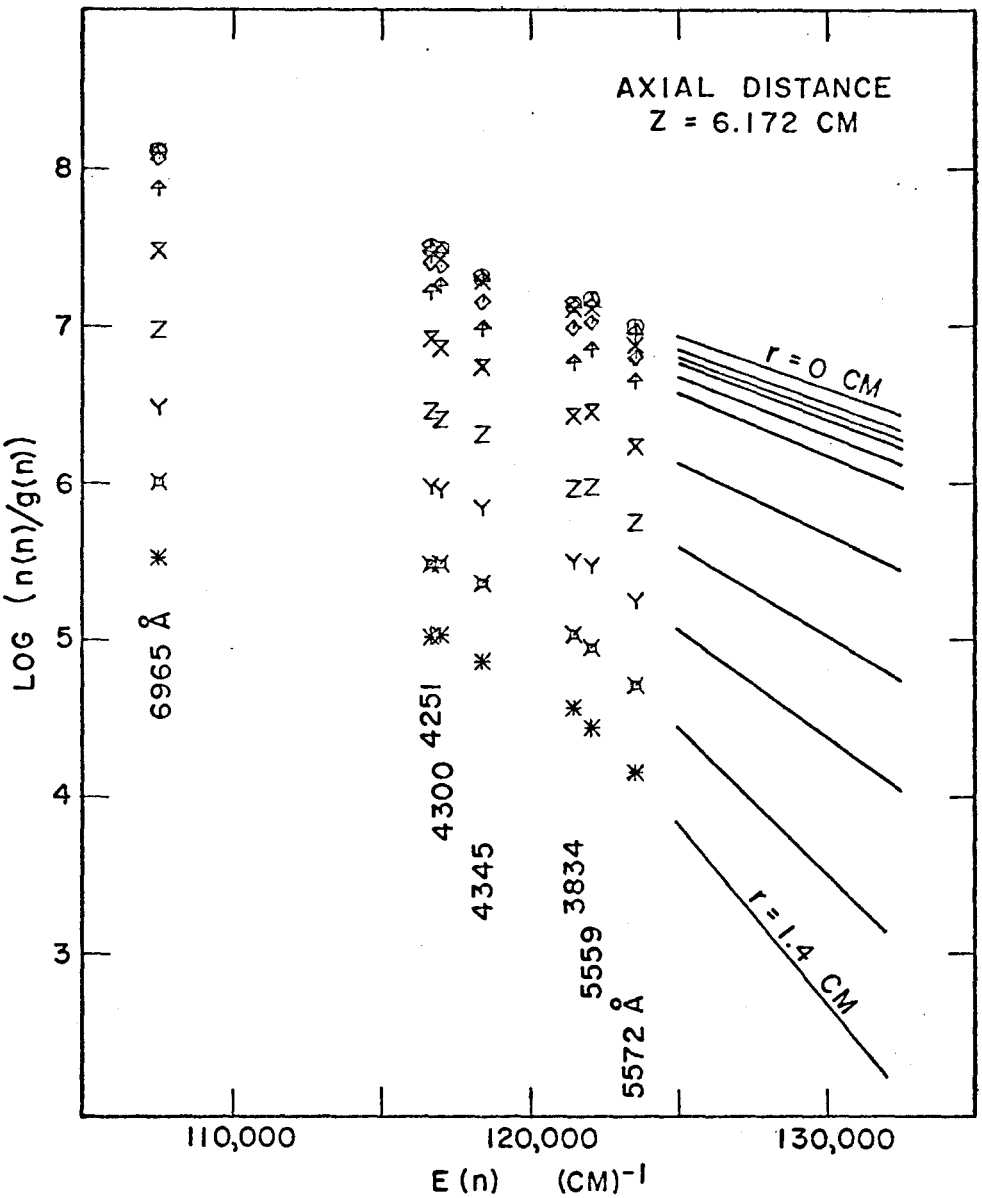

Fig. 1(B) Excitation Population in an Argon Plasma at Z = 6.172 cm.

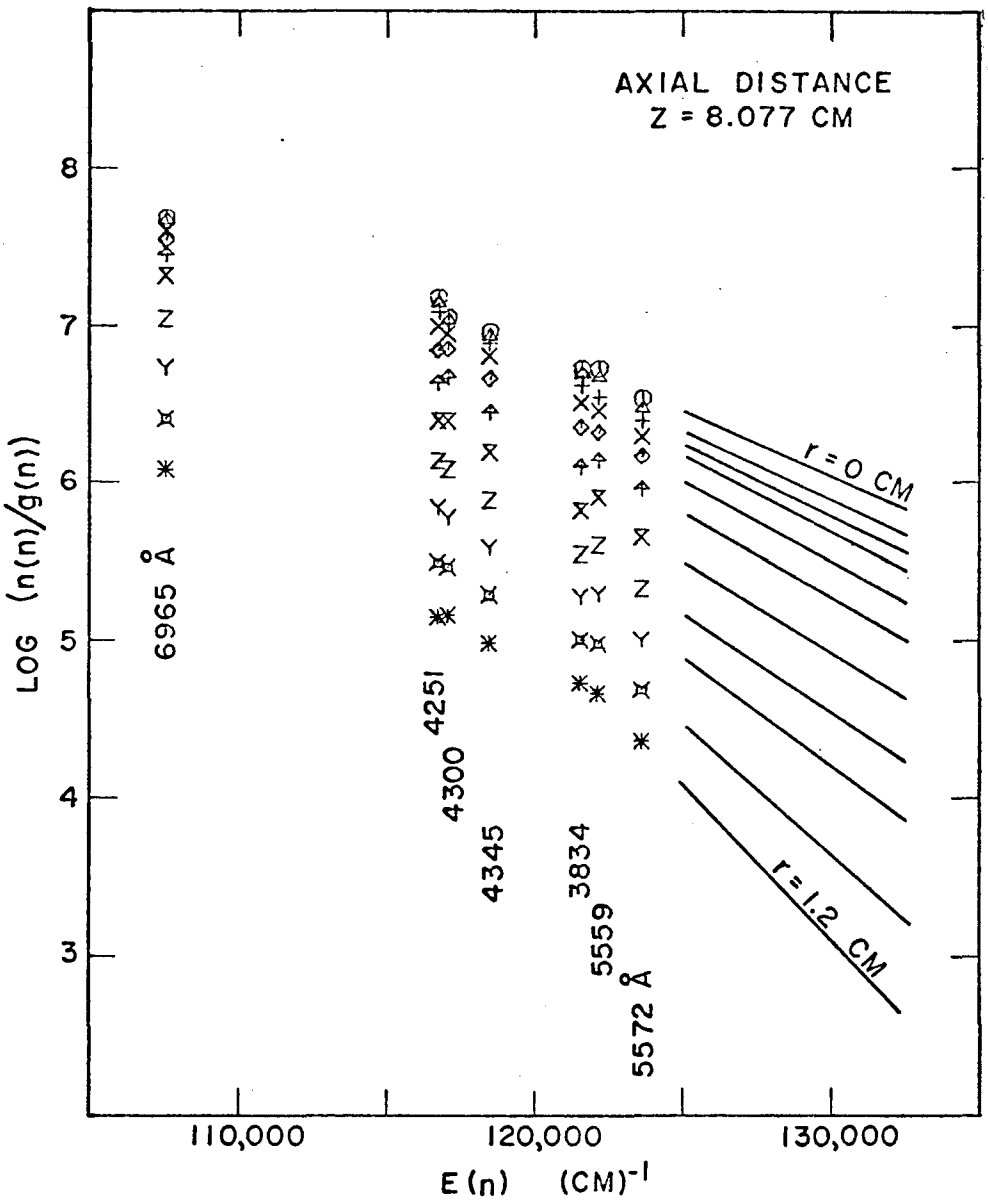

Fig. 1(C) Excitation Population in an Argon Plasma at Z = 8.077 cm.

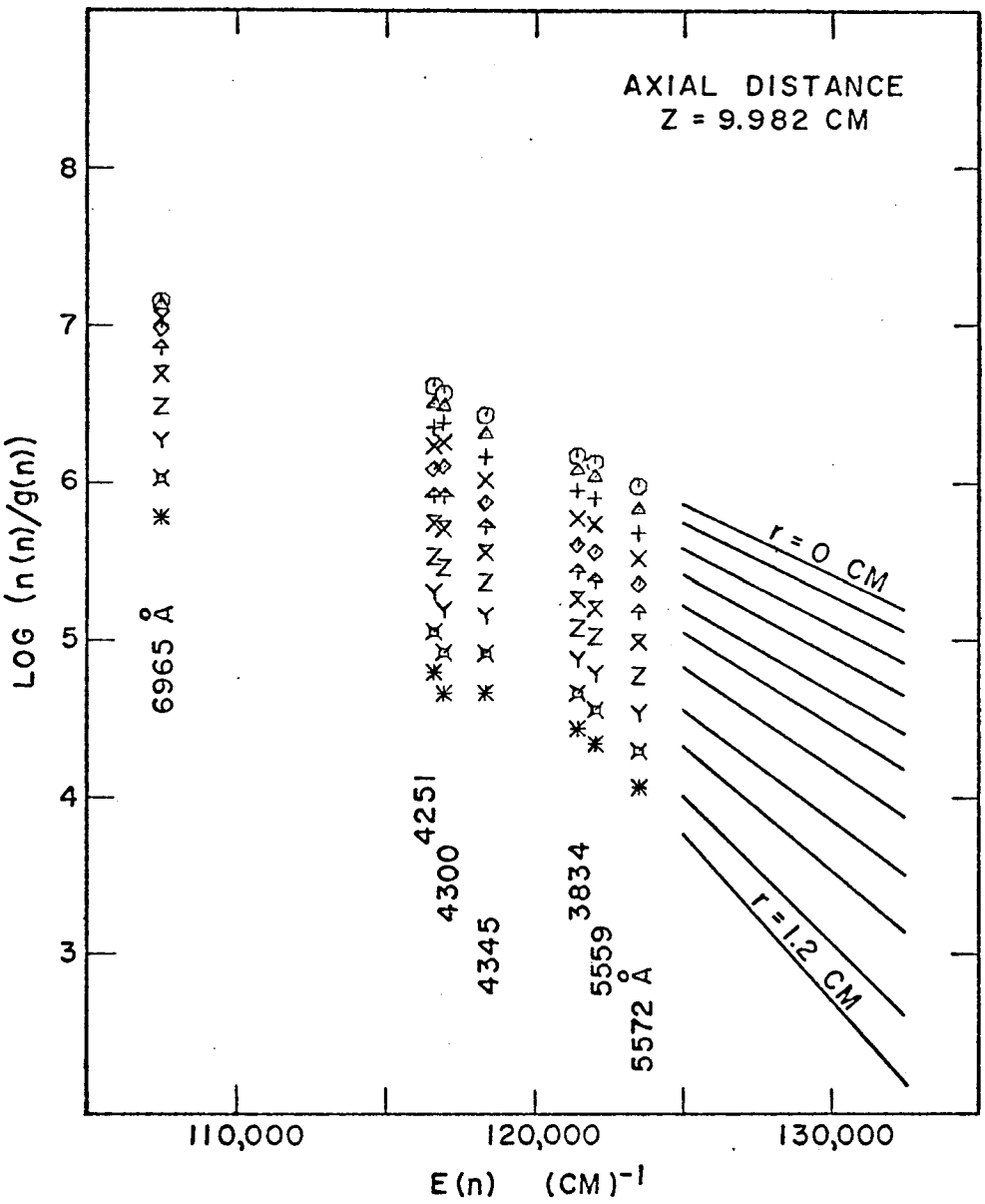

Fig. 1(D) Excitation Population in an Argon Plasma at Z = 9.98 cm.

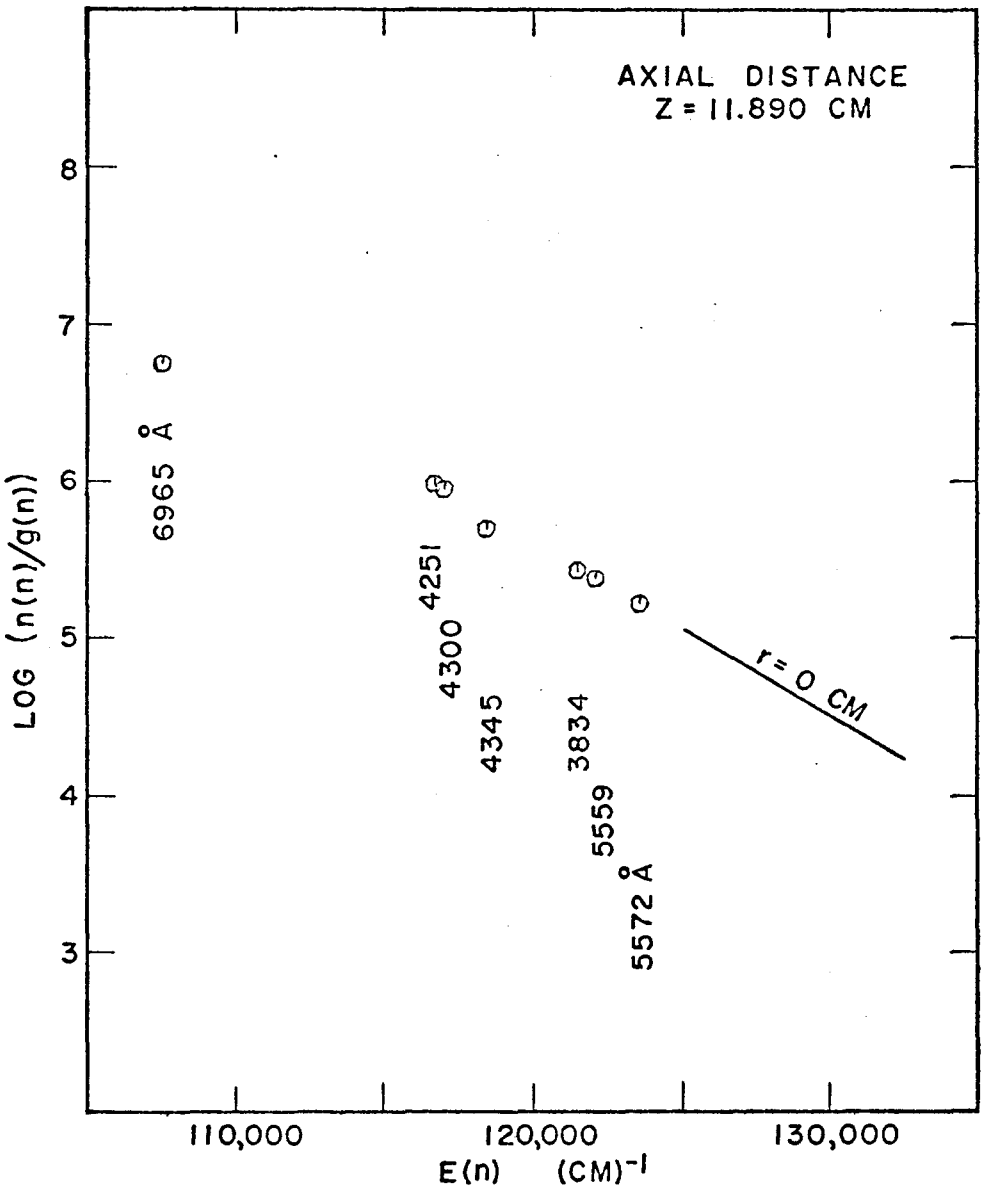

Fig. 1(E) Excitation Population in an Argon Plasma at Z = 11.89 cm.

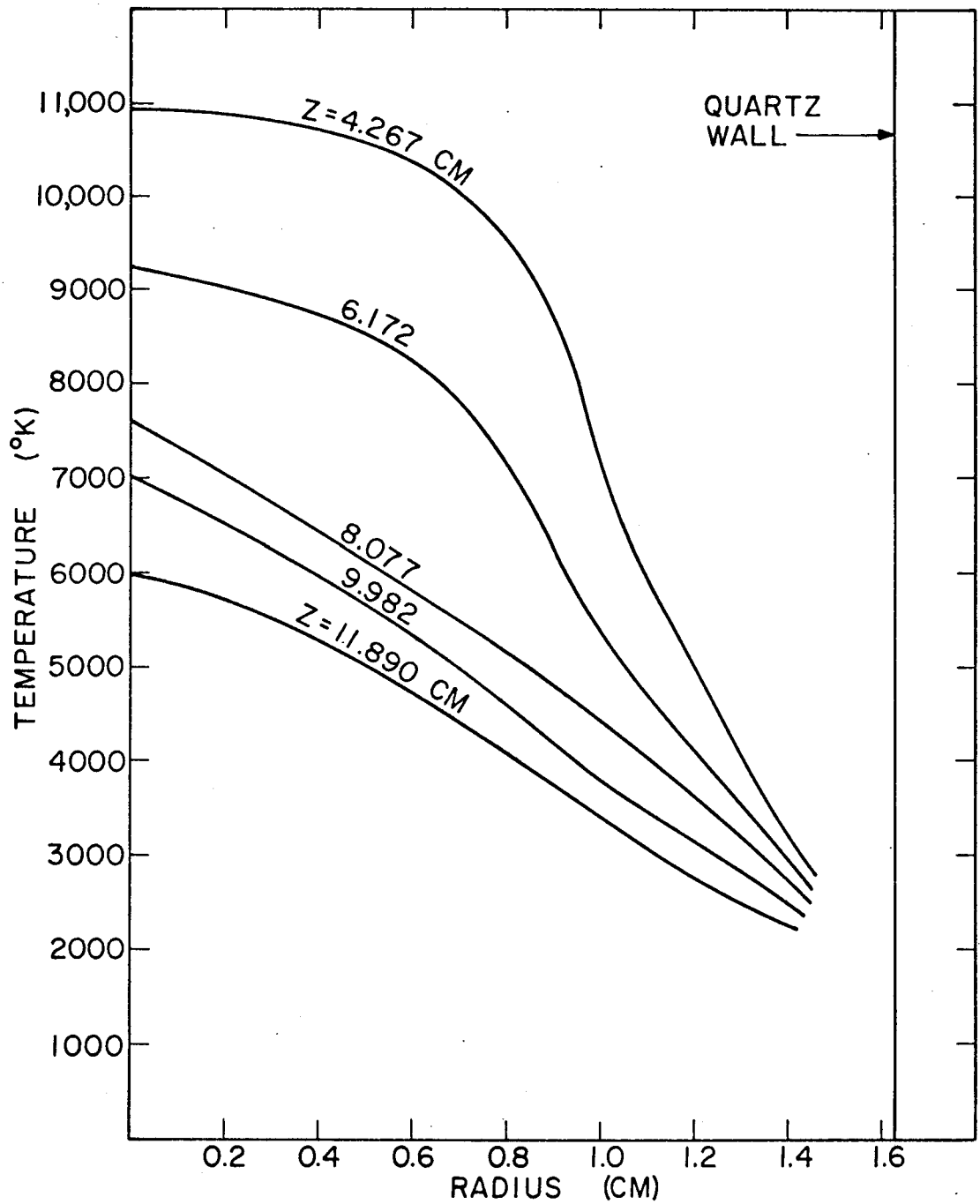

Fig. 2 Temperature Profiles in the Plasma Jet

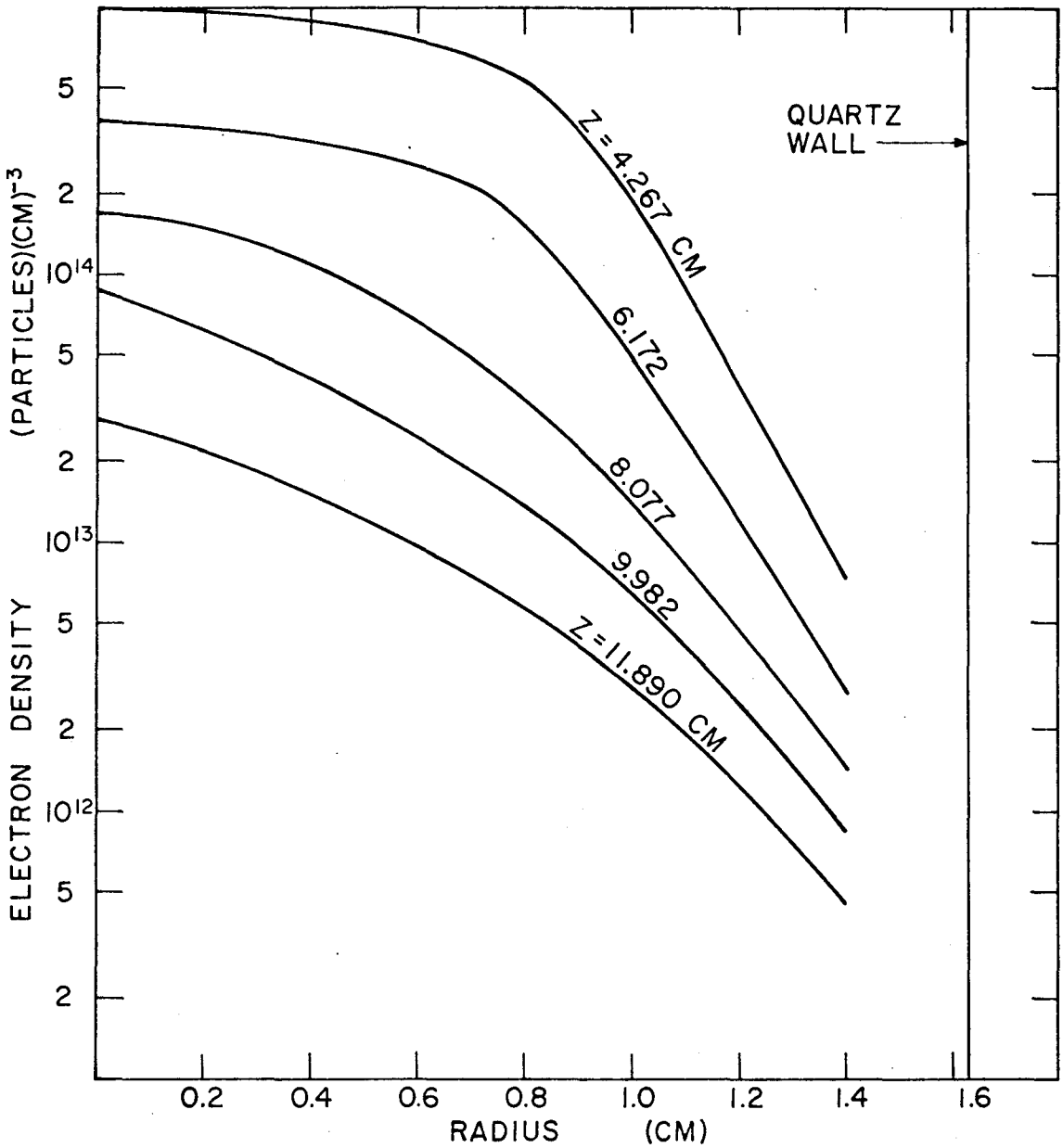

Fig. 3 Electron-Density Profiles in the Plasma Jet

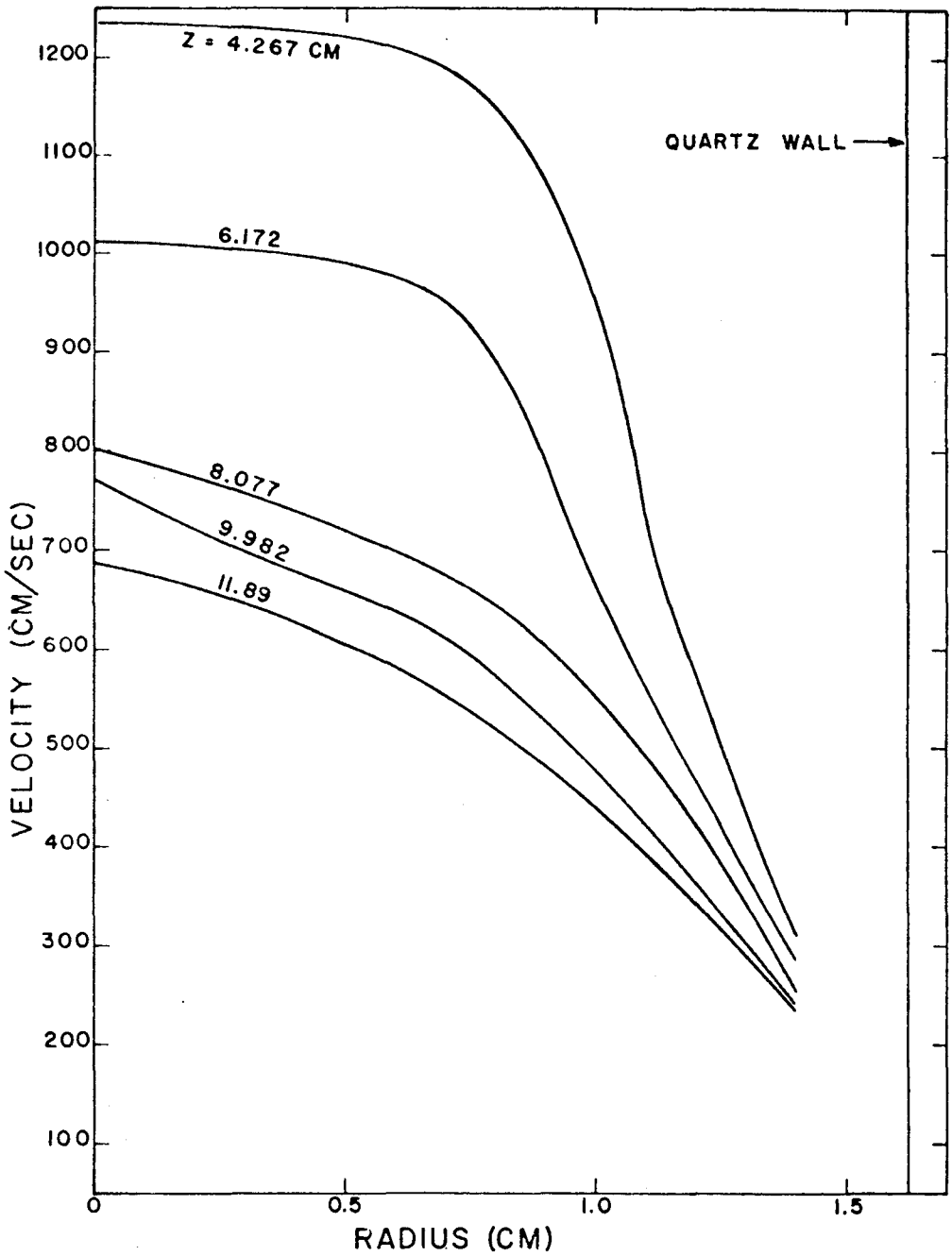

Fig 4. Velocity-Profiles in the Plasma jet

PROPOSITION P-1

The proposition describes the use of functional derivatives to test consistency of physical measurements.

One of the fundamental theorems in functional analysis which is related to the functional dependence of a set of variables is due to Jacobi. Functional dependence of a set of variables $f_1, f_2, f_3 \ldots\ldots f_n$ which are functions of another set of variables $x_1, x_2, x_3 \ldots\ldots x_n$ implies that there exists at least one relationship of the type $F(f_1, f_2 \ldots\ldots f_n) = 0$ which does not involve $x_1, x_2, x_3 \ldots\ldots x_n$ explicitly. When $f_1, f_2, f_3 \ldots\ldots f_n$ and all their first derivatives are continuous, the necessary and sufficient condition for their functional dependence is that the Jacobian should be identically zero:

$$J \equiv \frac{\partial(f_1, f_2 \ldots\ldots f_n)}{\partial(x_1, x_2 \ldots\ldots x_n)}$$

$$\equiv \begin{vmatrix} \frac{\partial f_1}{\partial x_1} & \frac{\partial f_1}{\partial x_2} & \ldots\ldots & \frac{\partial f_1}{\partial x_n} \\ \frac{\partial f_2}{\partial x_1} & \frac{\partial f_2}{\partial x_2} & \ldots\ldots & \frac{\partial f_2}{\partial x_n} \\ \ldots & \ldots & & \ldots \\ \frac{\partial f_n}{\partial x_1} & \frac{\partial f_n}{\partial x_2} & \ldots\ldots & \frac{\partial f_n}{\partial x_n} \end{vmatrix}$$

$$\equiv 0 \qquad \text{(P1-1)}$$

For the proof of above theorem, the reader is referred to reference (1).

Conversely, if J = 0 then it follows that there exists at least one relationship of the type:

$$F(f_1, f_2, \ldots\ldots f_n) = 0 \qquad \text{(P1-2)}$$

In many physical experiments, the physical quantities $f_1, f_2 \ldots\ldots f_n$ are evaluated as functions of some independent parameters $x_1, x_2, x_3 \ldots\ldots x_m$. If it is known that some of the measured quantities are related to each other, then one can test the consistency of their experimental measurement by applying condition (P1-1). On the other hand, one can determine if some of the measured quantities are related to each other or not by using condition (P1-2). One immediate result of the above theorem is that one should vary at least n number of parameters in order to test n number of observables in an experimental investigation, to be able to test consistency of their measurement.

The advantage of above method is that it can be applied pointwise. For example, if $f_1, f_2, \ldots\ldots f_n$ are measured in a certain field of $x_1, x_2, \ldots\ldots x_n$, then only the first derivatives of f_r are needed at a point to test if the data are consistent or not at that point.

Another great advantage is that the nature of the relationship between f_r need not be known to test the consistency of their measurement. The method can also be used

to fill up missing data or to correct the experimental values. It should be noted that equation (P1-1) may be easily written in a dimentionless form. Thus, only relative variations in the functions f_r are important, and absolute values are not needed. In many experiments, absolute quantities may be difficult to obtain, because of large systematic errors.

A useful criterion for the consistency of a set of measurements can be defined as the Jacobian error:

$$\sigma_J = \sqrt{\frac{\sum_{p=1}^{N} J_p^2}{N}} \qquad \text{(P1-3)}$$

Where J_p is the net value of the Jacobian evaluated at point p, and N is the total number of points in the set.

A few examples will illustrate the method. Suppose that an experiment consists of measuring the reaction rate constant k, which is assumed to be a function of temperature T only. The measurements are made in a tubular flow reactor and after solving material and energy-balance equations etc., the following functions are obtained:

$$k = k(r,z)$$

$$T = T(r,z)$$

These functions may be expressed as graphs, arrays of data, polynomial equations etc.. Now if $k = f(T)$ then from

condition (P1-1), one should obtain:

$$J = \begin{vmatrix} \frac{\partial k}{\partial r} & \frac{\partial k}{\partial z} \\ \frac{\partial T}{\partial r} & \frac{\partial T}{\partial z} \end{vmatrix} \equiv 0 \qquad \text{(P1-4)}$$

at every point in the reactor. The partial derivatives can be obtained from the functions $k = k(r,z)$ and $T = T(r,z)$ by numerical methods. In practice, one may find that $J \neq 0$ within the limits of error of the experiment and analysis of the data. Then the assumption $k = f(T)$ is not valid, and one must introduce another dependent variable like the concentration C of some reacting species such that the new quantity $k' = \Psi(k,C)$ will satisfy (P1-4) everywhere. Then it follows that $k' = \Phi(T)$. Note that introducing the third dependent variable $C(r,z)$ exceeds the available degrees of freedom. Hence the form of $\Psi(k,C)$ must be known (or guessed). However, the form of $\Phi(T)$ still need not be known for the purpose of testing the consistency of the data.

If condition (P1-4) is not satisfied only in restricted regions of the reactor, then it must be due to unexpected external purturbances, i. e. due to experimental errors.

Consider another experiment in which the composition of a planet's atmosphere is sought by measuring emissivity of the atmospheric gases. The emissivity expressed as energy radiated per unit time per gm. mole of the gas is

exclusively a function of the temperature of the radiating gas:

$$\mathcal{E} = \mathcal{E}(T)$$

The "Surveyor" mission has two probes which scan $\mathcal{E}(\theta,\Phi)$ and $T(\theta,\Phi)$ for a given height from the planet's surface, where θ and Φ are the spherical coordinates. In order to check if the temperature and emissivity data are consistent, one has to substitute the partial derivatives in the equation:

$$\begin{vmatrix} \frac{\partial \mathcal{E}}{\partial \theta} & \frac{\partial \mathcal{E}}{\partial \Phi} \\ \frac{\partial T}{\partial \theta} & \frac{\partial T}{\partial \Phi} \end{vmatrix} = 0$$

Again note that knowledge of the relationship $\mathcal{E} = \mathcal{E}(T)$ is not necessary for testing the consistency of measurements.

A concrete example will be given now, to demonstrate the usefulness of the criteria developed above. The velocities were expressed in a dimentionless form:

$$\nu = \frac{v}{v_{max}}$$

where v_{max} is the maximum velocity in the region of interest. The temperature distribution in the same region was measured spectroscopically (cf. Section I) and also expressed in a similar dimentionless form:

$$\theta = \frac{T}{T_{max}}$$

Function $\nu(r,z)$ and $\theta(r,z)$ are displayed in Tables P1-1 and P1-2 respectively. To check whether the velocity and temperature measurements are functionally related, the following Jacobian was evaluated numerically on IBM 7094 computer.

$$J = \frac{(\nu,\theta)}{(r,z)} = \begin{vmatrix} \frac{\partial \nu}{\partial r} & \frac{\partial \nu}{\partial z} \\ \frac{\partial \theta}{\partial r} & \frac{\partial \theta}{\partial z} \end{vmatrix} \qquad \text{(P1-5)}$$

The increments in r and z were taken as unity. The values of $J(r,z)$ are shown in Table P1-3. From the expected errors in measurements of the gradients, the error in J is expected to be $\pm 1.5 \times 10^{-3}$. Examination of Table P1-3 reveals that the Jacobian is in fact less than its expected numerical value, at most points of measurement. The Jacobian error defined by equation (P1-3) had a value of 1.3×10^{-3}, which is less than the expected experimental error of 1.5×10^{-3}. Hence one can conclude that a functional relationship of the type:

$$\nu = F(\theta) \qquad \text{(P1-6)}$$

exists between the velocity and the temperature. In Section I, a relationship between velocity and the temperature at a point was obtained from the equation of continuity as:

$$\nu = \Phi(r) \times \theta$$

where $\Phi(r)$ is the dimentionless radial distribution function. Figure V-11 shows that $\Phi(r)$ has almost constant value of unity over the region of interest, in which case, the explicit form of (P1-6) is

$$\nu = \theta$$

The above example was chosen from the main thesis for the purpose of illustration, but the principle developed above is perfectly general. Other applications of the above criteria include measurement of thermal conductivity, viscosity, diffusivity and other transport properties, P-V-T data, experimental fluid flow measurements and most experiments in which more than one parameters which may have functional dependence, are measured independently.

REFERENCE

1. R. P. Gillespie, "Partial Differentiation", p. 43, University Mathematical Text, Interscience, New York, (1951).

Dimentionless velocity distribution, temperature distribution and Jacobian evaluated as a point function. Radial distance increases horizontally and the axial distance increases vertically.

TABLE PI-1 $\nu(r,z)$

1.0000	1.0058	1.0067	0.9853	0.9602	0.9262	0.8839	0.8339	0.7769	0.7136	0.6446	0.5707	0.4923	0.4103
0.9176	0.9159	0.9090	0.8966	0.8783	0.8536	0.8222	0.7837	0.7375	0.6835	0.6210	0.5499	0.4695	0.3796
0.8620	0.8529	0.8430	0.8311	0.8161	0.7969	0.7724	0.7414	0.7028	0.6556	0.5985	0.5306	0.4506	0.3575
0.8268	0.8115	0.7980	0.7849	0.7706	0.7536	0.7326	0.7059	0.6721	0.6297	0.5772	0.5131	0.4359	0.3441
0.8061	0.7863	0.7695	0.7542	0.7387	0.7216	0.7013	0.6763	0.6449	0.6057	0.5571	0.4976	0.4255	0.3394
0.7939	0.7721	0.7530	0.7352	0.7175	0.6985	0.6769	0.6515	0.6208	0.5836	0.5386	0.4844	0.4198	0.3434
0.7840	0.7635	0.7439	0.7244	0.7040	0.6821	0.6579	0.6305	0.5992	0.5631	0.5216	0.4738	0.4198	0.3560
0.7703	0.7553	0.7378	0.7177	0.6952	0.6701	0.6424	0.6122	0.5795	0.5442	0.5063	0.4659	0.4229	0.3773

TABLE PI-2 $\theta(r,z)$

1.0000	0.9970	0.9919	0.9838	0.9767	0.9656	0.9464	0.9211	0.8765	0.7915	0.6538	0.5425	0.4555	0.3765
0.9246	0.9219	0.9198	0.9108	0.9023	0.8880	0.8616	0.8240	0.7655	0.6650	0.5522	0.4714	0.4066	0.3484
0.8441	0.8350	0.8259	0.8117	0.7966	0.7773	0.7490	0.7105	0.6559	0.5709	0.4858	0.4251	0.3735	0.3259
0.7663	0.7486	0.7289	0.7089	0.6859	0.6626	0.6350	0.6012	0.5574	0.4981	0.4392	0.3929	0.3497	0.3073
0.6943	0.6680	0.6377	0.6123	0.5830	0.5567	0.5314	0.5040	0.4727	0.4403	0.4049	0.3694	0.3320	0.2915
0.6589	0.6341	0.6059	0.5796	0.5503	0.5241	0.4970	0.4690	0.4365	0.4052	0.3734	0.3432	0.3108	0.2766
0.6377	0.6174	0.5951	0.5688	0.5415	0.5162	0.4858	0.4555	0.4180	0.3806	0.3462	0.3188	0.2905	0.2632
0.6051	0.5874	0.5672	0.5446	0.5188	0.4940	0.4650	0.4343	0.3994	0.3646	0.3307	0.3040	0.2799	0.2565

TABLE PI-3 $J(r,z)$

-0.0004	0.0001	0.0002	0.0009	0.0012	0.0015	0.0023	0.0031	0.0037	0.0041	0.0041	0.0031	0.0015	-0.0005
0.0001	0.0004	0.0004	0.0010	0.0014	0.0017	0.0022	0.0025	0.0023	0.0023	0.0024	0.0021	0.0015	0.0005
0.0005	0.0005	0.0005	0.0007	0.0011	0.0014	0.0019	0.0021	0.0018	0.0016	0.0016	0.0014	0.0013	0.0011
0.0008	0.0006	0.0007	0.0007	0.0010	0.0013	0.0017	0.0019	0.0017	0.0013	0.0011	0.0010	0.0012	0.0014
0.0004	0.0001	0.0001	-0.0000	0.0000	0.0001	0.0002	0.0003	0.0006	0.0009	0.0011	0.0013	0.0014	0.0015
0.0002	0.0000	-0.0001	-0.0002	-0.0002	-0.0003	-0.0003	-0.0002	0.0001	0.0005	0.0009	0.0012	0.0014	0.0014
0.0003	0.0004	0.0004	0.0003	0.0003	0.0001	0.0001	-0.0000	-0.0001	0.0000	0.0004	0.0006	0.0008	0.0012
0.0000	0.0002	0.0004	0.0004	0.0004	0.0003	0.0002	0.0000	-0.0001	-0.0002	0.0001	0.0004	0.0006	0.0012

PROPOSITION P-2

The following proposition illustrates how the size of a continuous stirred tank reactor may be chosen to obtain the maximum weight fraction of a polymer with some specified degree of polymerization.

Distribution of molecular weights plays a vital role in determining the physical properties of polymers. Control over the molecular weight distribution is highly desirable in the manufacturing processes. Polymerization reactions are quite commonly carried out in a continuously stirred tank (CST) reactor. One of the important properties of the CST reactor is the distribution of its residence time. It is proposed to evaluate the effect of the residence time distribution on the distribution of molecular weight of the polymer for a simple case.

The polymerization reactions are quite complex as they involve chain mechanism[1, 2]. The following discussion assumes linear polymerization, first order overall reaction and chain termination by chain transfer. Further, the principle of equal reactivity of the functional groups irrespective of the degree of polymerization is assumed[3].

If p is the probability that a given chain is continued, then $(1-p)$ is the probability that it is terminated. By our last assumption of equal reactivity, the apriori probability of bond formation remains the same for all

molecules at any instant. Then the apriori probability is also equal to the total number of bonds formed divided by the total number of possible bonds. It may be expressed as:

$$p = 1 - \frac{N}{N_o} \qquad \text{(P2-1)}$$

The probability that a molecule has exactly x recurring units (x-mer) is given by:

$$p^{x-1}(1-p)^2$$

Hence the total number of x-mers is given by:

$$N_x = N_o(1-p)^2 p^{x-1}$$

And the weight fraction of the x-mer is:

$$w_x = xN_x/N_o = x(1-p)^2 p^{x-1} \qquad \text{(P2-2)}$$

Now, for a first order reaction, the extent of the reaction is given by:

$$N = N_o e^{-kt} \qquad \text{(P2-3)}$$

where k is the first order rate constant. Substitution of (P2-3) in (P2-1) gives,

$$p = 1 - e^{-kt} \qquad \text{(P2-4)}$$

with this value of probability, the weight-fraction distribution at any instant is given by:

$$w_x = x(1 - e^{-kt})^{x-1} e^{-2kt} \qquad \text{(P2-5)}$$

It can be seen from equation (P2-5) that the distribution of molecular weights changes with the change in the age of the material inside the reactor. If different portions of the product stream emerging out of the reactor have different ages, then the overall distribution of the weight fractions will be governed by the residence-time-distribution function of the reactor as well as the kinetics of polymerization. For an ideal CST reactor, the residence-time-distribution function is given by[4]:

$$F(t) = 1 - e^{-t/\bar{t}}$$

In an actual CST reactor, the effects of imperfect mixing, hold-up volume and time-lag make the form of the residence-time-distribution function more complicated than the one shown above. A typical form of the function is shown in Figure P2-1.

The average-weight fraction of the x-mer in the product stream is given by:

$$\langle w_x \rangle = \int_{t=0}^{\infty} w_x \, dF(t)$$

Using the expression for the most probable weight-fraction distribution:

$$\langle w_x \rangle = \int_{0}^{\infty} x(1-e^{-kt})^{x-1} \, e^{-2kt} \, F' \, d(t/\bar{t}) \qquad \text{(P2-6)}$$

where F' is the slope of the residence-time-distribution

function. Equation (P2-6) was solved numerically on IBM 360 digital computer for different values of x and $k\bar{t}$ for the residence-time-distribution function shown in Figure P2-1. The solution is shown graphically in Figure P2-2 in which the average-weight fraction of the outlet stream is given as a function of the number of polymer units. It can be seen from the figure that the effect of a large average-residence time of the reactor is to increase the relative weight fraction of a polymer having a larger molecule. The effect of the spread in the residence time is manifested by the broadening of the weight-fraction distribution. At very low values of $k\bar{t}$, the unconverted monomer will be present predominantly, while at very large values of $k\bar{t}$, a uniform distribution of molecular weight will be obtained. In the industrial practice, it may be necessary to obtain the maximum weight fraction of a specified x-mer. One can choose the appropriate value of $k\bar{t}$ by the procedure outlined above, and can obtain the volume of the reactor from the following formula:

$$V_R = \frac{\dot{m}\bar{t}}{\rho}$$

Because of the effect of the spread in residence time, it will be desirable to connect a number of reactors of volume V_R chosen in the above manner, in parallel, rather than carrying out the reaction in a single large tank.

REFERENCES

1. P. J. Flory, "Principles of Polymer Chemistry", Chap. IV, Cornell Press, New York, (1953).
2. F. Bovey et al, "Emulsion Polymerization", Interscience, (1955).
3. M. Dole, "Introduction to Statistical Mechanics", pp. 26-31, Prentice-Hall, N. J. (1954).
4. H. Kramers and K. R. Westerterp, "Elements of Chemical Reactor Design", Chap. III, Section 2, Academic Press, New York, (1963).

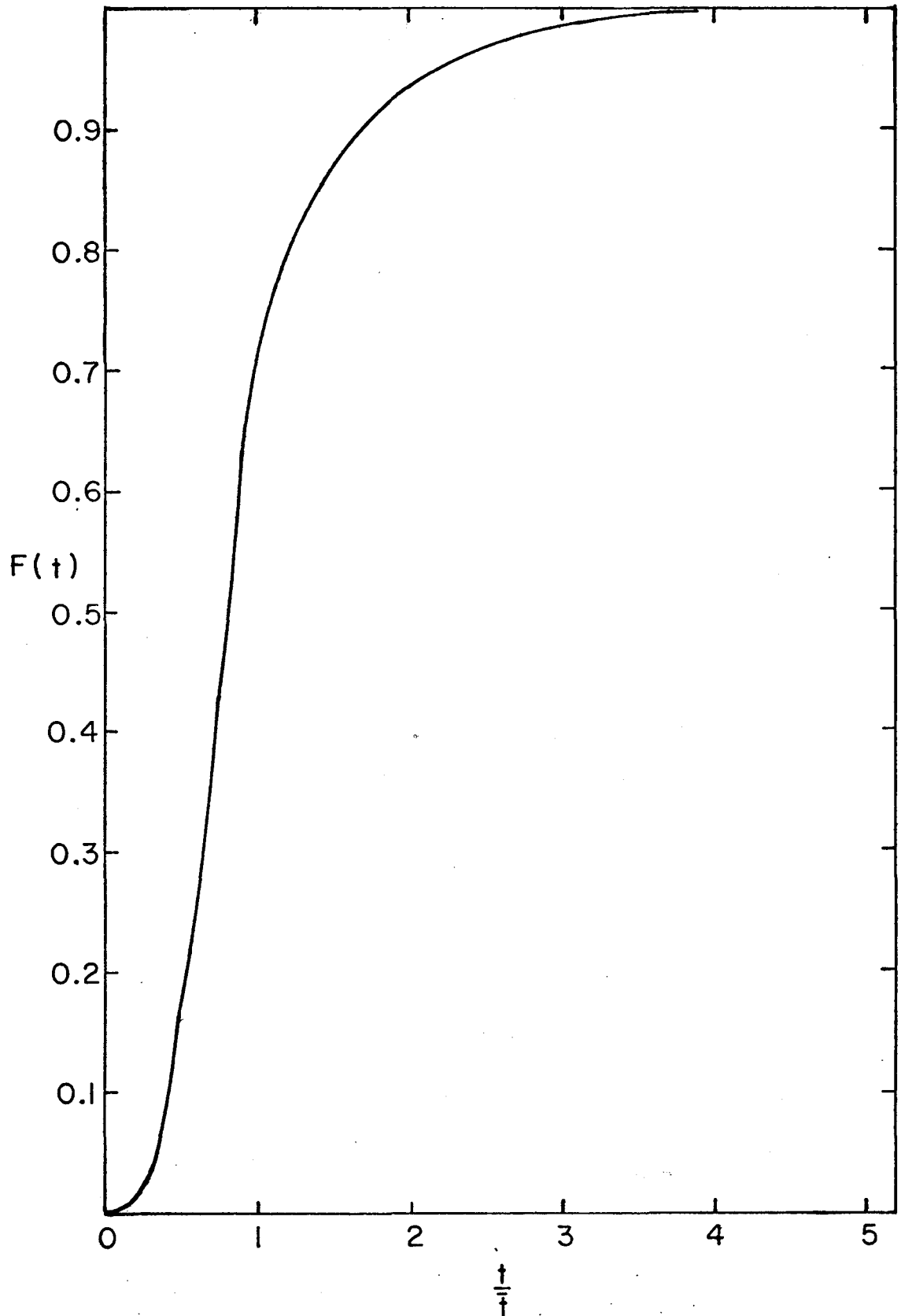

Figure P2-1 Residence-time distribution function

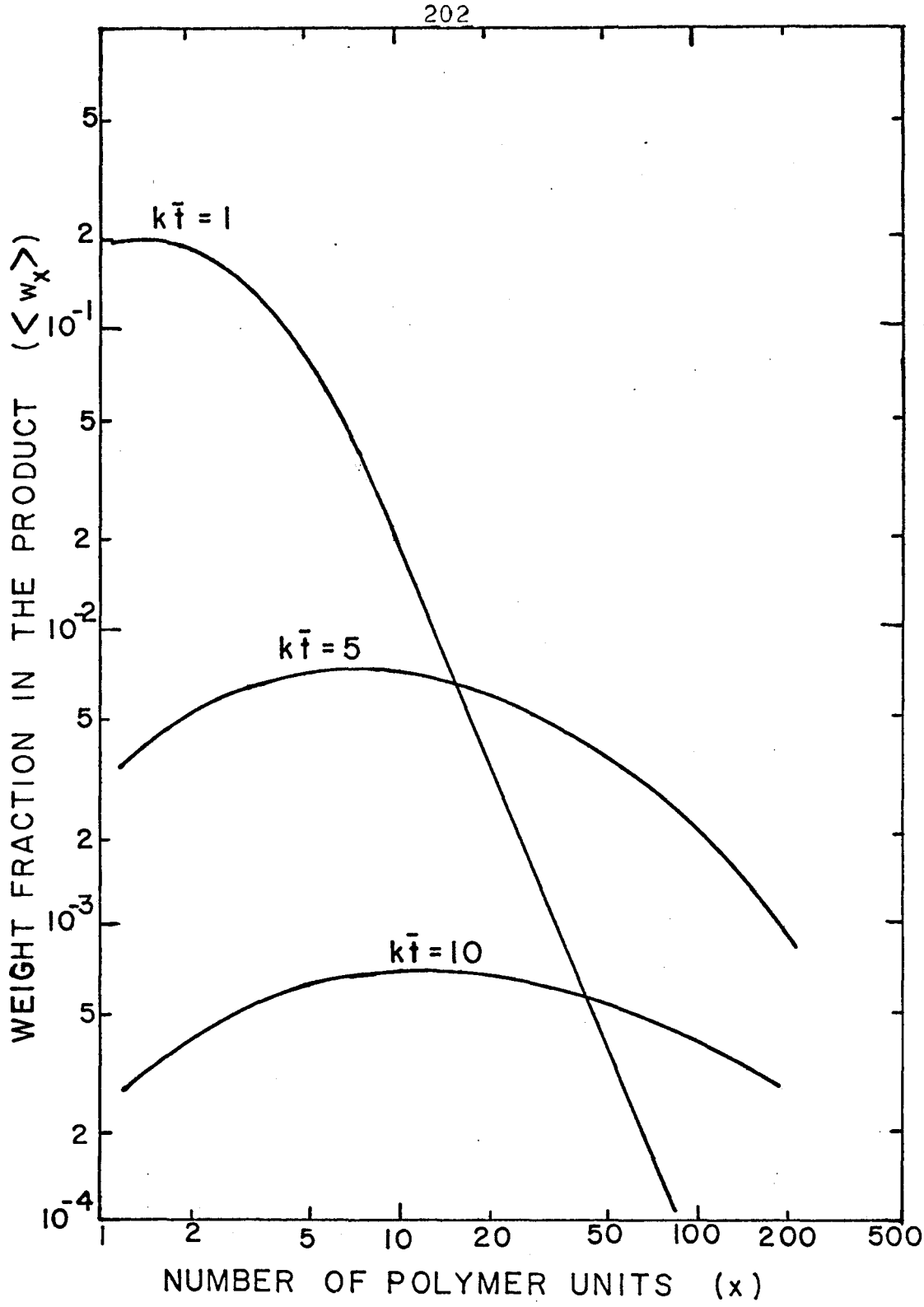

Figure P2-2 Distribution of weight fraction of a polymer in a continuously stirred tank reactor

PROPOSITION P-3

This proposition is a critique on the mechanism of oxidation of ethanol to acetaldehyde on a silver catalyst. An explanation is sought for the observations made by several workers regarding the overall rate, its temperature dependence, and dependence on the concentration of the reactants.

Partial oxidation of ethanol to acetaldehyde has been traditionally carried out at about 500°C on silver or copper catalysts in either pure or supported form[1, 2, 3, 4]. The stoichiometric equation for the reaction is:

$$C_2H_5OH + \frac{1}{2}O_2 \longrightarrow CH_3CHO + H_2O$$

$$\Delta H_f^\circ = -42 \text{ kcal/g mol}$$

(P3-1)

It should be pointed out that in absence of oxygen, dehydrogenation reaction takes place according to the equation

$$C_2H_5OH \longrightarrow H_2 + CH_3CHO$$

$$\Delta H_f^\circ = 11 \text{ kcal/g mol}$$

(P3-2)

The proposed mechanism says that the oxidation reaction shown in equation (P3-1) actually proceeds via two steps, the first step being reaction (P3-2) and the second step

being the reaction:

$$H_2 + \frac{1}{2}O_2 \longrightarrow H_2O \qquad \Delta H_f^\circ = -53 \text{ kcal/g mol} \qquad \text{(P3-3)}$$

Reaction (P3-3) being irreversible and faster compared with reaction (P3-2), the latter controls the rate of conversion of alcohol. The amount of oxidation taking place is then a function of the amount of oxygen reaching the reaction surface by diffusion. The maximum ratio of oxygen to ethanol molecules diffusing towards the reaction surface is $\frac{1}{2}$, which occurs when all the hydrogen liberated at the surface is oxidized. If the bulk concentration of oxygen is in excess of the value which will yield this maximum ratio, then the bulk phase concentration of oxygen will have no effect on the conversion of alcohol. In that case, a zeroth order dependence of conversion of ethanol with respect to oxygen can be expected.

The following observations recorded in the literature regarding the reaction in question support the above mechanism.

1. Higher pressure decreased the yield of acetaldehyde while higher temperature favored the yield[5].

   Application of Le Chatelier's principle suggests that reaction (P3-2) should be the rate controlling step, and that reaction (P3-2) should be independent

of reaction (P3-3).

2. The overall oxidation reaction was observed to be zeroth order with respect to the bulk concentration of oxygen[6]. Further, in a cognate reaction of butyl alcohol, not more than 13 per cent of the theoretical oxygen was consumed. Higher amount of oxygen favored further oxidation of the aldehyde[7].

It is possible that in the reaction of butyl alcohol, the critical value of the ratio of oxygen to alcohol molecules diffusing towards the surface was reached when 13% of the theoretical oxygen was used. To amplify this point, let the ratio of oxygen to ethanol molecules reaching the reaction surface be denoted by γ. Then

$$\gamma = \frac{\dot{m}_0}{\dot{m}_1} \approx \frac{D_0}{D_1} \frac{(p_0 - p_0^*)}{(p_1 - p_1^*)} \qquad \text{(P3-4)}$$

to the first approximation.

Since reaction (P3-3) is irreversible and fast, $p_0^* \approx 0$ and since reaction (P3-2) is quite slow, a small driving force for diffusion of alcohol molecules is sufficient. For the sake of estimation we will assume $p_1^* = 0.8p_1$. The ratio of diffusivities, according simple kinetic theory is approximately:

$$\frac{D_0}{D_1} = \sqrt{\frac{M_1}{M_0}} = 1.52$$

Then, from equation (P3-4) for $\nu = \frac{1}{2}$, $p_0/p_1 = 0.066$. The theoretical ratio being $p_0/p_1 = 0.5$. Hence the predicted ratio of $p_0/p_1 \approx 13\%$ of the theoretical value is in accord with the observation.

3. The observed rates of oxidation of ethanol on supported silver catalyst do follow the dehydrogenation kinetics.

Balandin et al have studied[8, 9] dehydrogenation of lower alcohols on copper catalyst and the reaction has been found to be a surface reaction controlled first order reaction[10] involving adsorption equilibrium. The rate of decomposition of ethanol can be represented as:

$$r = \frac{dx}{dt} = \frac{k_0 p_1 e^{-\frac{E}{RT}}}{p_1 + p_2 + 0.4p_3} \qquad \text{(P3-5)}$$

From the similarity of structure between copper and silver, it may be assumed that the form of equation (P3-5) holds good for a silver catalyst.

Day studied oxidation of ethanol on silver catalyst supported on pumice in a tubular flow reactor[11]. The catalyst was 2.7928 g of silver deposited on 9 ml of pumice stone in 12 mesh size. The feed gas was heated to 105°C. One set of his data is analysed below, on the basis of dehydrogenation mechanism.

The material balance for an integral flow reactor is given by

$$\frac{W}{F} = \int_0^x \frac{dx}{r} \qquad \text{(P3-6)}$$

The stoichiometry of the reaction gives:

$$\frac{p_1}{1 - x} = \frac{p_2}{x} = \frac{p_3}{x} \qquad \text{(P3-7)}$$

substituting (P3-5) and (P3-7) in (P3-6) one obtains:

$$\frac{W}{F} = \int_0^x \frac{1 + 1.4x}{k_0 x} e^{\frac{E}{RT}} dx \qquad \text{(P3-8)}$$

The temperature within the reactor will be assumed constant for a given run. Then equation (P3-8) can be integrated to give

$$\frac{W}{F} \times \frac{1}{1.4 \times \ln\left(\frac{1}{1-x}\right) - 0.4x} = \frac{1}{k_o} e^{\frac{E}{RT}}$$

Using the following variable

$$Y = \ln\frac{W}{F} - \ln\left(1.4 \ln\frac{1}{1 - x} - 0.4x\right)$$

a straight line should be obtained between Y and $\frac{1}{T}$ in the form:

$$Y = \frac{E}{RT} - \ln k_0$$

Table p3-1 gives the feed, temperature and conversion reported by Day and the corresponding values of Y and $\frac{1}{T}$. Figure p3-1 is the resulting plot between Y and $\frac{1}{T}$ which can be seen to be quite close to a straight line. A least squares analysis gave the following results:

$$k_o = 4.1 \times 10^{-4}$$

$$E = 2860 \text{ kcal/g mol}$$

The value of activation energy for silver determined above is much smaller than the value of 12 kcal/g mol for copper [9], which may explain why silver is a more efficient catalyst for this reaction.

Understanding of the physical and chemical steps involved in a reaction is highly desirable for the design of a reactor for industrial-scale operation [12].

REFERENCES

1. W. L. Faith and D. B. Keyes, I. & E. C., 23, 1250, (1931).
   W. L. Faith and D. B. Keyes, I. & E. C., 24, 924, (1932).
2. L. R. Michels and D. B. Keyes, I. & E. C., 34, 138, (1942).
3. Chem. Abstracts, 48, 1408(b), (1954).
   Chem. Abstracts, 46, 425(g), (1952).
4. Thorpe's Dictionary of App. Chem., 4th ed., vol. I, p. 15, Longman's Green & Co., London, (1937).
5. J. A. Patterson Jr. and A. R. Day, I. & E. C., 26, 1276, (1934).
6. Chem. Abstracts, 52, 14303(i), (1958).
7. R. R. Davies and H. H. Hodgson, J. Chem. Soc., p. 282, (1943).
8. Chem. Abstracts, 45, 4541(d), (1951).
   Chem. Abstracts, 53, 835(c), (1959).
9. A. A. Balandin in "Advances in Catalysis", vol. X, p. 96, Academic Press, New York, (1958).
10. A. C. Neish, Can. J. Research, 23B, 49, (1945).
11. A. R. Day, J. Phys. Chem., 35, 3272, (1931).

Table P3-1

Analysis of A. R. Day's Data on Ethanol Oxidation over Silver Catalyst

Run No.	F = Feed Rate of Alcohol in g mol/sec x 10^4	Feed Rate of Air g mol/sec x 10^4	$\frac{O_2}{E_tOH}$ =	Reaction Temperature °K	Conversion of Alcohol x	Y =	$\frac{1}{T}$ x 10^3
1	2.73	6.4	0.495	744	0.806	9.723	1.345
2	2.68	6.4	0.503	742	0.807	9.743	1.349
3	2.25	5.25	0.492	701	0.822	9.863	1.427
4	2.20	5.25	0.501	695	0.824	9.878	1.440
5	1.715	4.09	0.501	642	0.856	10.018	1.559
6	1.685	4.09	0.509	649	0.854	10.018	1.540

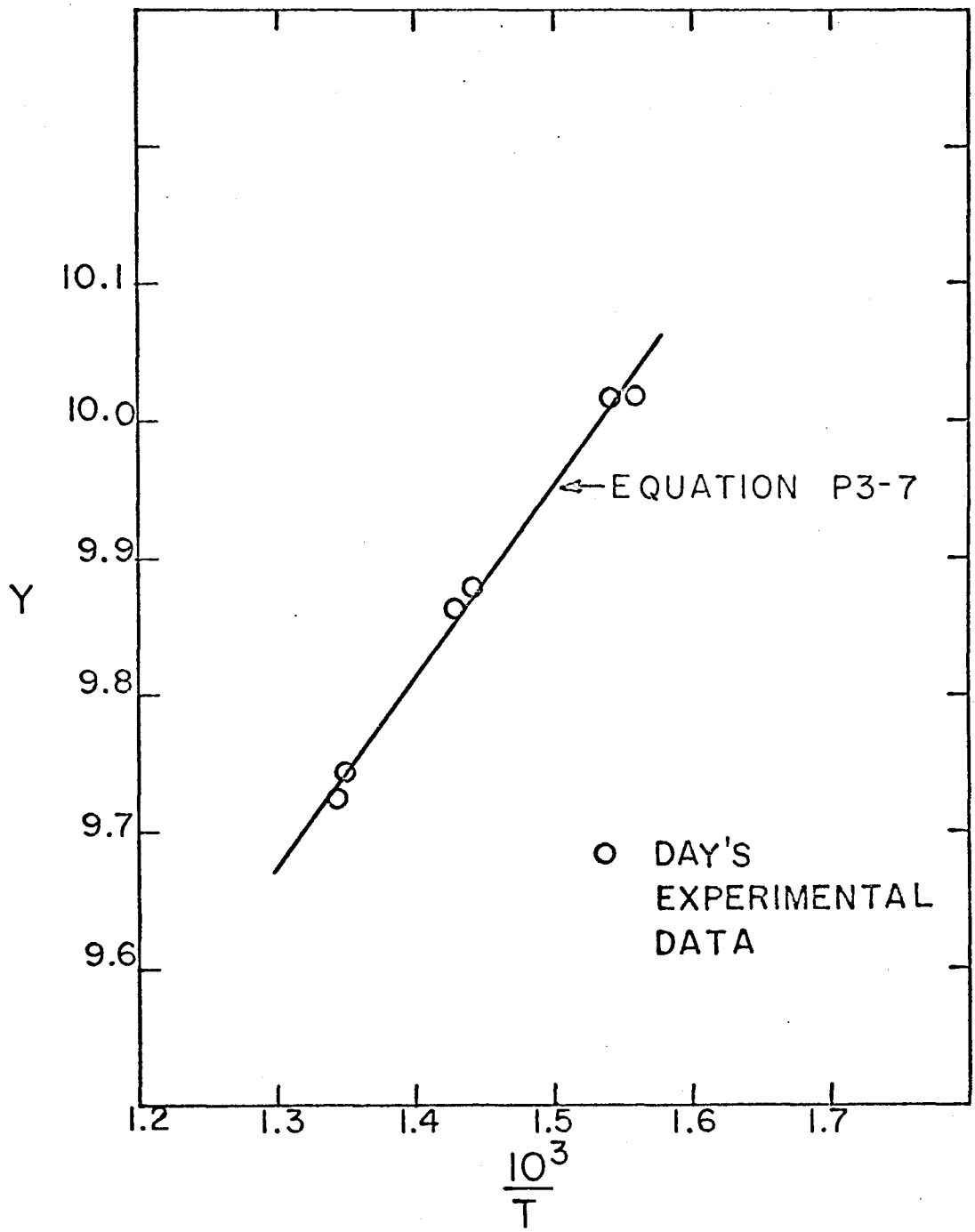

Figure P3-1

Comparison of the proposed mechanism for catalytic partial oxidation of ethanol with the experimental data of A. R. Day. Y represents the rate constant parameter as defined in the text.

NOMENCLATURE

A_{nm}	Einstein transition probability for radiation from energy level n to m	$(sec)^{-1}$
A(p)	argon atom in the p^{th} excited state, p=1 for ground state p=2 for metastable state etc.	
A*	argon atom in some excited state	
A_2^*	excited molecular intermediate of argon	
c	velocity of light in vacuum	$(cm)(sec)^{-1}$
C	an instrument constant	
C_1, C_2	Planck's first and second radiation constants	
C_p	heat capacity at constant pressure	$(cal)(g\ mol)^{-1}(°K)^{-1}$
D	Fick diffusivity	$(cm)^2(sec)^{-1}$
D_a	ambipolar diffusivity	$(cm)^2(sec)^{-1}$
E	activation energy	$(cal)(g\ mol)^{-1}$
E(p)	excitation energy of the p^{th} excited state	$(cm)^{-1}$ or eV

E^+	ionization energy of argon	$(cm)^{-1}$ or eV
E^z	ionization energy of the z fold ionized atom	$(cm)^{-1}$ or eV
f_{nm}	absorption oscillator strength	
F	feed rate of alcohol	$(g\ mol)/(sec)^{-1}$
F(t)	residence time distribution function	
g(p)	statistical weight of the p^{th} excited level	
G_λ	wavelength response as defined	
h	Planck's constant	(erg)(sec)
I	intensity of radiation	$(watts)(cm)^{-3}$
I'	incident intensity of radiation	
I'_λ	intensity of radiation per unit wavelength	$(watts)(cm)^{-3}(ster)^{-1}$
I'_ν	intensity of radiation per unit frequency	$(watts)(sec)(cm)^{-3}(ster)^{-1}$
I_{nm}	intensity of line radiation	$(watts)(cm)^{-3}$
$I_{nm}(r)$	intensity calculated at a radial position r	$(watts)(cm)^{-3}$

$I_{nm}(x)$	intensity measured in the line of sight at transverse position x	(watts)(cm)$^{-2}$
J(p)	Jacobian as defined, a function of point p	
k	Boltzmann constant	(cm)$^{-1}$(°K)$^{-1}$
k_1, k_2, k_3	specific reaction rate constants for forward reactions	(cm)^3(g mol)$^{-1}$(sec)$^{-1}$ or similar units
k_{-1}, k_{-2}, k_{-3}	specific reaction rate constants for reverse reactions	(cm)^3(g mol)$^{-1}$(sec)$^{-1}$ or similar units
k_o	frequency factor in Arrhenius expression for rate constant	
K	thermal conductivity	(watts)(cm)$^{-1}$(°K)$^{-1}$
m	mass of argon atom	g
m_e	mass of electron	g
$\dot{m}$	mass flow rate	(g)(sec)$^{-1}$
M	molecular weight, also third body in a reaction	
n(p)	population density of the p^{th} excitation level	(particles)(cm)$^{-3}$

$n_E(p)$	equilibrium population density	(particles)(cm)$^{-3}$
$\bar{n}(p)$	average population density of the p^{th} excited level	(particles)(cm)$^{-3}$
$n_r(p)$	population density of the p^{th} excited state at radial position r	(particles)(cm)$^{-3}$
n_A	population density of neutral atoms of argon	(particles)(cm)$^{-3}$
n_+	population density of argon ions	(particles)(cm)$^{-3}$
n_e	population density of electrons	(particles)(cm)$^{-3}$
n_t	total number of particles per unit volume	(particles)(cm)$^{-3}$
n_z	population density of z^{th} ions	(particles)(cm)$^{-3}$
N	total number of molecules present at time t	
N_o	total number of monomer units intially present	
N_r, N_z	molar flux of reactant in in radial and axial directions respectively	(g mol)(cm)$^{-2}$(sec)$^{-1}$ or (particles)(cm)$^{-2}$(sec)$^{-1}$

N^*	excited nitrogen atom	
p	partial pressure, also denotes principal quantum nember of excitation level	(atm)
p^*	partial pressure of the gas at catalyst surface	(atm)
P	total pressure	(atm)
$\underline{q}$	heat flux (vector)	$(watts)(cm)^{-2}$
r	radial position, also designation of temperature cell, also reaction rate based on unit weight of the catalyst	$(g\ mol)(g)^{-1}(sec)^{-1}$
r_o	radius of the boundary of the plasma jet	(cm)
R	gas-law constant	$(atm)(cm)^3(°K)^{-1}(g\ mol)^{-1}$
R_e	rate of recombination of electrons with ions	$(particles)(cm)^{-3}(sec)^{-1}$
s	total number of isothermal cells in the strip under observation	
S	ionization coefficient	$(cm)^3(particles)^{-1}(sec)^{-1}$
t	time	(sec)
$\bar{t}$	average residence time	(min)

T	absolute temperature	(°K)
$\bar{T}(p)$	space-average temperature of the p^{th} excitation level	(°K)
$\underline{v}$	velocity (vector)	$(cm)(sec)^{-1}$
v_z	velocity in the axial direction	$(cm)(sec)^{-1}$
V	volume	$(cm)^3$
$\dot{V}$	volumetic flow rate	$(cm)^3(sec)^{-1}$
w_x	weight fraction of a given x-mer	
$\langle w_x \rangle$	average weight fraction of a given x-mer	
W	weight of catalyst	(g)
x	fractional conversion of a alcohol, also number of monomer units, also transverse position	(cm)
x_{N_2}, x_{NO}	mole fraction of the gas denoted by subscript	
Y	rate constant parameter as defined	
z	axial position in the plasma jet also nuclear charge	(cm)

Z	partition function of neutral argon	
Z_m	partition function of metastable argon	
Z^+	partition function of singly ionized argon	
Z^n	partition function of n fold ionized atom	

Greek Symbols

α	recombination coefficient for electrons	$(cm)^3(particles)^{-1}(sec)^{-1}$
γ	decay coefficient	$(cm)^3(particles)^{-1}(sec)^{-1}$
ν	frequency	$(sec)^{-1}$
δ	critical collision distance	$(\mathring{A})$
σ	Stefan's radiation constant,	$(watts)(°K)^{-4}$
	also collision radius	$(\mathring{A})$
σ_j	Jacobian error as defined	
ρ	molar density	$(g\ mol)(cm)^{-3}$
$\rho(p)$	fractional departure from equilibrium of the p^{th} excited state as defined	
ϵ_T	total emissivity	

$\epsilon_{\lambda T}$	monochromatic emissivity for a given temperature and wavelength	
λ	wavelength of radiation	(cm) or (Å)
λ_{nm}	wavelength of radiation arising from a transition from level n to m	(cm) or (Å)
Φ	steric factor	
$\mathscr{E}$	radiated power	$(watts)(cm)^{-3}$
Γ	gamma function	

Special Notation

ΔH_f°	standard heat of reaction	$(cal)(g\ mol)^{-1}$
(NO), (N_2)	parentheses indicate concentration of the reactant gas	$(g\ mol)(cm)^{-3}$

Special Subscripts		Special Subscripts	
0	oxygen	e	electron
1	alcohol	m, n	refers to the excited level
2	hydrogen		
3	aldehyde		
A	argon		